DYNAMIC ANALYSIS OF TENSION LEG PLATFORMS

a report

from the Texas A & M
RESEARCH FOUNDATION
College Station, Texas

by

James R. Morgan

and

Dia Malaeb

January 1982

50272-101

REPORT DOCUMENTATION PAGE	1. REPORT NO. NSF/CEE-82033	2.	3. Recipient's Accession No. PB83-100982
4. Title and Subtitle Dynamic Analysis of Tension Leg Platforms, 1982 Final Report			**5. Report Date** January 1982
			6.
7. Author(s) J.R. Morgan, D. Malaeb			**8. Performing Organization Rept. No.**
9. Performing Organization Name and Address University of Houston Texas A & M Research Foundation Houston, TX 77004			**10. Project/Task/Work Unit No.**
			11. Contract(C) or Grant(G) No. (C) (G) PFR8006467
12. Sponsoring Organization Name and Address Directorate for Engineering (ENG) National Science Foundation 1800 G Street, N.W. Washington, DC 20550			**13. Type of Report & Period Covered**
			14.

15. Supplementary Notes

Submitted by: Communications Program (OPRM)
National Science Foundation
Washington, DC 20550

16. Abstract (Limit: 200 words)

A deterministic approach for the dynamic analysis of tension-leg platforms subjected to wave forces and ground motion is described. A mathematical model is developed based on a set of coupled nonlinear differential equations for sway, surge, heave, pitch, roll, and yaw motions. A time domain analysis is selected for investigating the dynamic characteristics of the anchored structure. The time domain analysis model is capable of obtaining time histories of displacement response in the direction of all degrees of freedom when the platform is subjected to wave loading and/or ground motion. It can also obtain response spectra for all degrees of freedom, the effects of variations in several parameters, and response to dynamic loading. Several enhancements, including the use of higher wave theories and random sea states would allow the model to be applied to a wider range of problems.

17. Document Analysis a. Descriptors

Mathematical models
Stresses
Dynamic loads
Nonlinear differential equations

Platforms
Displacement
Dynamic structural analysis

b. Identifiers/Open-Ended Terms

Ground motion

J.R. Morgan, /PI
D. Malaeb, /PI

c. COSATI Field/Group

18. Availability Statement NTIS	19. Security Class (This Report)	21. No. of Pages
	20. Security Class (This Page)	22. Price

(See ANSI-Z39.18)   See Instructions on Reverse

OPTIONAL FORM 272 (4-77)
(Formerly NTIS-35)
Department of Commerce

DYNAMIC ANALYSIS OF
TENSION-LEG PLATFORMS

A Final Report
for
NSF Research Initiation
Project PFR-8006467

"SEISMIC CONSIDERATIONS FOR
COMPLIANT OFFSHORE STRUCTURES"

by

James R. Morgan
and
Dia Malaeb

January 1982

ACKNOWLEDGEMENT

TABLE OF CONTENTS

TABLE OF CONTENTS
(Continued)

LIST OF TABLES

LIST OF FIGURES

LIST OF FIGURES (continued)

LIST OF FIGURES (continued)

LIST OF FIGURES (continued)

LIST OF FIGURES (continued)

NOTATION

a,b:	spacing between corner and middle columns in the x and y directions, respectively
a',b':	lengths of hulls and cross braces
c:	wave speed or celerity
d:	water depth
D_i:	diameter of ith column
d.o.f.:	degree of freedom
E:	depth of centerline of hulls below mean water surface
e:	eccentricity of buoyancy forces
{F}:	vector of forcing functions
F_B:	buoyancy force
ΔF_B:	change in buoyancy force
F_{cv}:	total vertical force of dynamic pressure on corner column bases
F_{I_i}:	horizontal inertia force on ith column
F_{D_i}:	horizontal drag force on ith column
$F_v, \bar{F}_v$:	total vertical inertia and drag forces on hulls
F_x, F_y:	x and y components of inertia forces on the hulls, respectively
$\bar{F}_x, \bar{F}_y$:	x and y components of drag forces on the hulls, respectively
F_{x_T}, F_{y_T}:	total horizontal forces on columns and hulls in the x and y directions, respectively
F_{z_T}:	total vertical forces
G:	center of gravity of platform
g:	acceleration of gravity

h_0:	platform depth in water
h:	distance from the center of gravity to base of the hulls
$\tilde{h}_i$:	distance from instantaneous water level to base of ith column
H:	wave height
k:	wave number = $2\pi/L$
k_c:	leg stiffness (longitudinal)
$[K]$:	stiffness matrix
k_{ij}:	stiffness coefficients
$\{K\}$:	stiffness force vector
l:	cable length
L:	wave length
$[M]$:	matrix of structural plus added masses
M_{P_x}, M_{P_y}:	moments of dynamic pressure on corner column bases about x-axis and y-axis, respectively
M_{V_x}, M_{H_x}:	moments about the x-axis of vertical and horizontal forces on the hulls
M_{V_y}, M_{H_y}:	moments about the y-axis of vertical and horizontal forces on the hulls
$M_{x_T}, M_{y_T}, M_{z_T}$:	total moments about x-, y-, and z-axes
M_{I_i}:	moment of the inertia forces on columns
M_{D_i}:	moment of the drag forces on columns
t:	time
T:	wave period
T_0:	cable tension
TLP:	tension-leg platform
ΔT_i:	change in cable tension

u: fluid particle velocity

$\dot{u}$:   fluid particle acceleration

U_{rel}:   relative velocity between structure and fluid particle

W: weight of platform

x,y,z: coordinate axes

x_i, y_i: coordinates of ith column measured in direction of and perpendicular to wave propagation, respectively

$\{x\}, \{\dot{x}\}, \{\ddot{x}\}$:   vectors of structural displacements, velocities, and accelerations, respectively

$\{\ddot{x}_g\}$:   vector of ground accelerations

$\{x_r\}$:   vector of structural displacements with respect to ground motion

$\bar{z}$:   distance between center of gravity and mean water level

α: direction of wave propagation measured from the x-axis

β: used in Newmark β-method solution procedure

β', β'':   used in force calculations as $\cos\alpha$ and $\sin\alpha$, respectively

γ: used in β-method equation

γ', γ'':   used in force calculations as $(b\sin\alpha)$ and $(a\cos\alpha)$, respectively

ρ: fluid density

I. INTRODUCTION

A. Objective

Offshore production platforms have been manufactured predominantly as fixed steel template jackets or concrete gravity structures for operations in water depths up to 200 meters. Manufacturing, installation, and maintenance costs of fixed platforms rise rapidly as water depths increase. Recently, however, attention has been focused on the design of tension-leg platforms. Relatively small increases in manufacturing and installation costs with added water depth make the tension-leg platform an attractive alternative.

The design of tension-leg production platforms requires an understanding of the dynamic behavior of the structure during storm waves, wind, ground motion conditions, etc. In order to design a reliable structure, it is necessary for the engineer to take into account the effect of platform motion on personnel, equipment, and operations. It is also necessary to take into account the anchoring system and the forces in the mooring legs produced by wave actions and platform motions.

The primary objective of this research is to develop a complete and accurate deterministic approach for the dynamic analysis of tension-leg platforms (TLP's) subjected to wave forces and ground motion. A mathematical model is developed based on a set of coupled nonlinear differential equations for sway, surge, heave, pitch, roll, and yaw motions. The nonlinearity of the coupled differential equations of motion makes a power spectral analysis in the frequency domain infeasible. Thus, a time domain analysis was selected for investigating the dynamic characteristics of the

anchored structure. The advantage of this approach is that nonlinear functional relationships, which require approximations in the spectral models, can be handled exactly in the time domain.

The time domain dynamic analysis model developed herein is capable of obtaining the following:

1) Time histories of displacement response in the direction of all degrees of freedom (surge, sway, heave, pitch, roll, and yaw) when the platform is subjected to wave loading and/or ground motion.

2) Response spectra (i.e., variation of response amplitudes with respect to wave period) for all degrees of freedom.

3) Effects of variations in several different parameters.

4) Effects of coupling and nonlinearities.

B. Research Plan

In order to accomplish the objectives set forth in this project, the following research plan was developed and undertaken:

1) Literature search and choice of the most appropriate dynamic analysis of TLP's.

2) The development of a deterministic dynamic analysis model.

3) Verification of mathematical model.

4) Parametric studies to identify design criteria.

Few attempts have been made in the literature to simulate, or calculate, the dynamic response of tension-leg platforms. A review of previous work was undertaken with the objective of sorting out the important parameters influencing the structure's behavior. The previous attempts to model the response of tension-leg platforms have neglected either coupling or nonlinearities or both, and none have addressed the possible effects of ground motion.
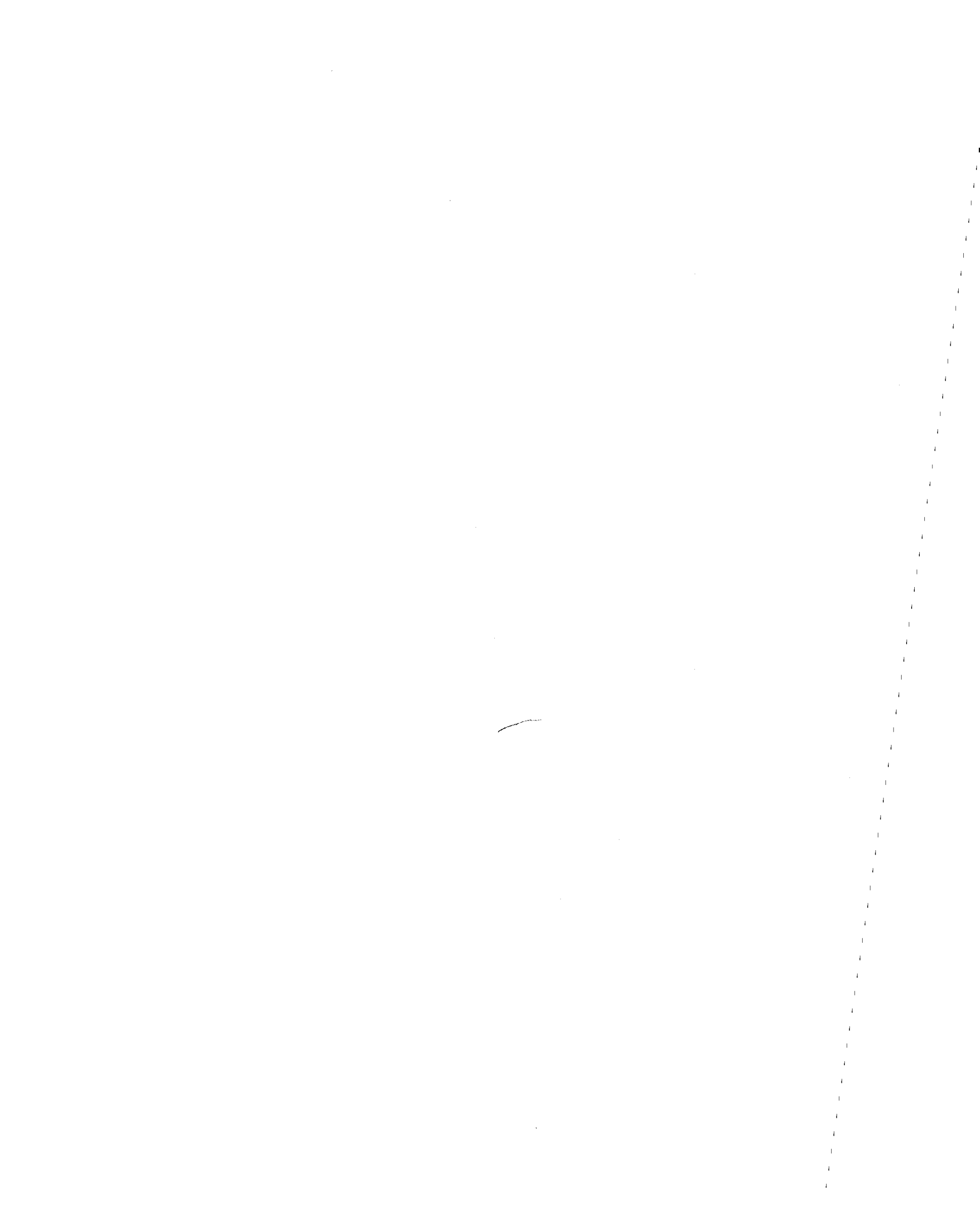
The development of a complete deterministic dynamic analysis model involves the formulation of a nonlinear stiffness matrix, selection of a suitable wave theory, derivation of complete forcing functions, selection of an efficient numerical method capable of carrying out the solution of nonlinear coupled differential equations in the time domain, and development of an appropriate computer code to perform the dynamic response calculations.

Wave forces and ground motion are two of the environmental loadings which could be applied to the offshore structure. Time histories of the complete response of the model to these environmental forces are generated. A parametric study is carried out in an effort to determine the significant design parameters that need to be considered in the design and analysis of tension-leg platforms.

C. Review of Previous Research

Various methods of dynamic analysis of offshore structures subjected to wave loading have been presented in recent technical literature (see for example references 1-11). Linear or piecewise linear mathematical models to analyze response in the frequency domain have been employed by many researchers (Refs. 1,2,4,5,8, and 10); whereas nonlinear time domain analyses were performed by other researchers (Refs. 3,6,7, and 9).

Frequency domain or spectral analysis models are based on a linear formulation of the dynamic problem. Nonlinear terms inherent in the forcing function, and the relative displacement, velocity, and acceleration between the structure and the fluid particles are neglected. It is also assumed that coupling between degrees of freedom is neglected. Moreover, spectral models are capable only of finding maximum response amplitudes,

and not time histories of the response as is the case in time domain analyses. Nonlinear and coupling effects are important and can have significant effects on the structure's dynamic behavior. Time domain (or deterministic) models are capable of handling all kinds of nonlinearities. The benefits of time domain analysis include the ability to incorporate any type of nonlinearaity in force which can be adequately described, and the availability of response time histories to aid in assessment of the effects of coupling between degrees of freedom. Such nonlinear and coupling effects cannot be easily included in a frequency domain even with approximations such as equivalent linearization.

Previous nonlinear deterministic models did not account for all types of nonlinearity and coupling. Typically they included a numerical integration of wave force equations along each segment of the platform at each iteration for every time step. Some also included a nonlinear finite element formulation to describe the nonlinear stiffness of the anchor lines. These analyses are generally very expensive. The current model attempts to eliminate or minimize the effects of the following assumptions which are common to most published analyses:

1) Equivalent linearization of nonlinear terms in the anchoring stiffness and fluid drag forces (some deterministic and all frequency domain models).

2) Neglecting coupling effects between degrees of freedom (both frequency domain and time domain models).

3) Numerical integration of wave forces at every time step.

4) Omission of ground motion in the forcing functions.

Frequency domain analysis is inexpensive and may be adequate for a preliminary look at the dynamics of the problem but it is not sufficient for a complete and accurate prediction of a coupled nonlinear response of the structure. Hence, a deterministic approach is needed to account for the nonlinear and coupled behavior involved in the problem. The complete deterministic model presented in this research attempts to satisfy the requirements listed above and to include the effects of ground motion as well as water waves.

II. DEVELOPMENT OF DYNAMIC ANALYSIS MODEL

A. General

A review of previous work related to dynamic analysis of TLP's indicates a need for a complete nonlinear deterministic analysis. The development of such a model involves the formulation of a nonlinear stiffness matrix which describes the behavior of the anchoring cables and buoyant forces. The selection of a wave theory yielding a reasonable representation of the water waves in terms of particle velocity and acceleration, and in terms of wave forces, and yet simple is also involved. Once a wave theory is selected, a force calculation method which utilizes the fluid particle velocities and accelerations derived from the wave theory can be chosen to yield wave forces that agree with experimental results and best represent the actual forces produced by the waves. After formulating the nonlinear stiffness matrix and the wave forces on the structure, provided the structure properties and dimensions are known, an efficient time domain numerical method that is capable of handling all kinds of nonlinearities and coupling is employed to integrate the equations of motion and obain time histories of the response.

The structure considered in this research consists of four corner columns which are linked to vertical tethers, four middle columns, two main hulls, and two cross bracings (see Figure 1). Specifications of the structure dimensions, masses, mass moments of inertia, added masses, added mass moments of inertia, center of gravity, water depth and draft are required to complete the description of the TLP. The complex structure is assembled from a group of simpler bodies whose individual hydrodynamic properties are

known. The total hydrodynamic force on the assembled structure is assumed to be equal to the sum of the forces on the component bodies.

The model developed herein utilizes nonlinear stiffness coefficients based on derived stiffness-displacement relationships which are functions of the instantaneous position of the structure rather than a more expensive finite element approach. These stiffness functions are coupled as well as nonlinear. Coupling effects are ignored or neglected in frequency domain models and in most time domain analyses. The effect of including coupling effects in the stiffness matrix will be shown to be significant and, if neglected, misleading results can be obtained.

The linear wave theory (Ref. 12) (sometimes called Airy wave theory) has been found to give wave forces close to those obtained using higher order wave theories, provided a proper method of calculating wave forces is used with a suitable choice of the fluid added mass and drag coefficients (Refs. 6,7, and 10). Linear wave theory provides good solutions in deep water, i.e., for water-depth-to-wave length ratio greater or equal to 0.5 (Ref. 13). Airy linear wave theory is used in this model because it is practical, easy to apply, and reliable over a large segment of the whole wave regime (Ref. 14).

The forces on the structure are classified as hydrostatic (arising from buoyancy), anchoring (restoring stiffness), hydrodynamic (inertia and drag due to waves), and inertial (arising from ground motion). The hydro-dynamic forces are computed with the Morison equation (Ref. 15), with velo-cities and accelerations based on relative motion between structure and water. Earthquake excitation consists of horizontal and vertical base accelerations based on ground motion records.

The structure is represented by a mathematical model which can be reduced to a system of coupled nonlinear differential equations that are solved by direct numerical integration on a digital computer. The equations of motion are integrated in a stepwise manner using the Newmark β-method (Ref. 15).

The equations of motion are represented by Equation 1 in matrix form as

$$[M]\{\ddot{x}\} + [K]\{x\} = \{F(x,\dot{x},\ddot{x},t)\} \tag{1}$$

where [M] is the mass matrix for all six degrees of freedom,

[K] is a 6 x 6 nonlinear stiffness matrix,

{F} is the vector of forcing functions,

{x} is the structural displacement vector,

{$\dot{x}$} is the structural velocity vector,

{$\ddot{x}$} is the structural acceleration vector, and

t is the time.

This chapter presents details of the development of a complete nonlinear coupled dynamic analysis model.

B. Derivation of Nonlinear Stiffness

1. Degrees of Freedom

Since the structure is considered as a rigid body, the motion will consist of six degrees of freedom -- three translational and three rotational. The coordinate axes and the degrees of freedom used in the analysis are presented in Fig. 2. Surge, sway, and heave are defined as the

horizontal motion along the x-axis, the horizontal motion along the y-axis, and the vertical motion along the z-axis, respectively. Pitch, roll, and yaw are defined as the rotational motion about the y-axis, the rotational motion about the x-axis, and the rotational motion about the z-axis, respectively. The degrees of freedom are numbered as follows:

Surge: d.o.f. No. 1

Sway: d.o.f. No. 2

Heave: d.o.f. No. 3

Pitch: d.o.f. No. 4

Roll: d.o.f. No. 5

Yaw: d.o.f. No. 6

2. Derivation of Stiffness Coefficients

A nonlinear stiffness matrix [K] including all six degrees of freedom is formulated, where k_{ij} is the force in degree of freedom "i" due to an arbitrary displacement in the direction of degree of freedom "j", with all other degrees of freedom restrained. To derive the nonlinear stiffness coefficients, each degree of freedom is given an arbitrary displacement and the forces developed constitute the coefficients in the corresponding column of the stiffness matrix. The coefficients of the first column of the stiffness matrix are found by giving the structure an arbitrary displacement x in the surge direction as shown in Figure 3. The static equilibrium forces exerted on the structure at its original position are shown in Figure 4. The static equilibrium forces are the weight of the structure, W, the buoyancy force, F , and the initial tension (or pretensioning force), $4T_0$. Through summation of forces in the vertical direction one obtains:

$$+\uparrow \Sigma F_z = 0$$
$$F_B - 4T_0 - W = 0 \tag{2}$$

The forces acting on the structure with a displacement, x, in the direction of surge are shown in Figure 5. A sum of forces in the x-direction yields:

$$\overset{+}{\rightarrow} \quad \Sigma F_x = 0$$

$$k_{11} - 2[2(T_0 + \Delta T_1)_x] = 0$$

$$k_{11} = 4(T_0 + \Delta T_1)\sin \gamma_x \tag{3}$$

where T_0 is the value of the initial tension in each leg, ΔT_1, is the increase in tension in each leg from the x-displacement, and γ_x is the angle of inclination of the legs with respect to the vertical, and it is given by:

$$\sin \gamma_x = \frac{x}{\ell'} = \frac{x}{\sqrt{\ell^2 + x^2}}$$

The elongation in the chain length is

$$\Delta \ell_1 = \ell' - \ell = \sqrt{\ell^2 + x^2} - \ell,$$

hence

$$\Delta T_1 = k_c \, \Delta \ell_1,$$

where k_c is the stiffness of the chain for each leg.

Now, summing the forces in the vertical direction gives:

$$+\uparrow \Sigma F_z = 0$$

$$k_{31} + F_B - W - 2 \, 2(T_0 + \Delta T_1)_z = 0$$

$$k_{31} + (F_B - W) - 4(T_0 + \Delta T_1) \cos \gamma_x = 0$$

where

$$\cos \gamma_x = \frac{1}{\ell'} = \frac{1}{\sqrt{\ell^2 + x^2}}$$

Recalling Equation (2), $F_B - W = 4T_0$,

$$k_{31} = 4T_0(\cos \gamma_x - 1) + 4 \, \Delta T_1 \cos \gamma_x \tag{4}$$

In summing the moments about the y-axis vertical forces produce no moment, therefore only horizontal components of the tension in the chain are considered:

$$\zeta + M_G = 0$$

$$k_{41} + 4(T_0 + \Delta T_1)_x \, (\bar{h}) = 0$$

$$k_{41} = -4(T_0 + \Delta T_1) \sin \gamma_x \, (\bar{h})$$

Combining this with Equation (3) yields:

$$k_{41} = -\bar{h} k_{11} \tag{5}$$

The coefficients of the second column of the stiffness matrix are found by giving the structure an arbitrary displacement in the sway direction with all other degrees of freedom (d.o.f.'s) restrained. The coefficients are identical to those of the first column with change in notations as follows:

$$k_{22} = 4(T_0 + \Delta T_2) \sin \gamma_y \tag{6}$$

$$k_{32} = 4T_0(\cos \gamma_y - 1) + \Delta T_2 \cos \gamma_y \tag{7}$$

$$k_{52} = + \bar{h} \, k_{22} \tag{8}$$

where

$$\sin \gamma_y = \frac{y}{\sqrt{\ell^2 + y^2}} \, ,$$

$$\cos \gamma_y = \frac{1}{\sqrt{\ell^2 + y^2}} \, ,$$

and

$$\Delta_T = k_c \, (\sqrt{\ell^2 + y^2} - \ell)$$

The coefficients of the third column of the stiffness matrix are found by giving the structure an arbitrary displacement in the heave direction, keeping all other d.o.f.'s restrained. The corresponding forces acting on the structure are shown in Figure 6. A sum of forces in the z-direction yields:

$$+\uparrow \Sigma F_z = 0$$

$$k_{33} - W - 4(T_o + \Delta T_3) + (F_B - \Delta F_B) = 0$$

$$k_{33} + (F_B - W - T_0) - \Delta F_B - 4\Delta T_3 = 0;$$

However, $(F_B - W - 4T_0) = 0$ from Equation (2); therefore,

$$k_{33} = \Delta F_B + 4\Delta T_3 , \tag{9}$$

where $\Delta F_B = \rho g \Delta V$, ρ is the mass density of water, g is the acceleration of gravity, ΔV is the change in submerged volume, and ΔT_3 is the change in tension in each leg arising from heave.

The coefficients of the fourth column of the stiffness matrix are found by giving the structure an arbitrary rotation about the y-axis with all other d.o.f.'s restrained. Figure 7 shows the corresponding forces acting on the structure. Summing the moments about the y-axis gives:

$$\zeta +\Sigma M_G = 0$$

$$k_{44} - F_B e_4 - 2(T_0 + \Delta T_4) r + 2(T_0 - \Delta T_4') s = 0$$

which can be written:

$$k_{44} = F_B e_4 + 2 \Delta T_4 r + 2 \Delta T_4' + 2 T (r-s), \tag{10}$$

where e_4 is the eccentricity of the buoyancy force calculated according to the formula $e_4 = \dfrac{I_y}{V}$, where I_y is the moment of inertia of the cross section of the structure intersecting the water surface, about the y-axis, and V is the volume of the submerged portion of the structure. From geometry (see Figure 7) d, r, s, ψ_1, ΔL_4, and $\Delta L_4'$ are calculated as follows:

$$d_1 = \sqrt{\bar{h}^2 + a^2} ,$$

$$r = d_1 \cos(\psi - \alpha_y) ,$$

$$s = d_1 \cos(\psi + \alpha_y) ,$$

$$\psi_1 = \tan^{-1}(\bar{h}/a) ,$$

and

$$\Delta L_4 = \bar{h} - d_1 \sin(\psi - \alpha_y) ,$$

$$\Delta L_4' = d_1 \sin(\psi + \alpha_y) - \bar{h} .$$

Summing the forces in the vertical direction gives:

$$+\uparrow F_z = 0$$

$$k_{34} + F_B - 2(T + \Delta T_4) - 2(T - \Delta T_4') - W = 0$$

$$k_{34} + (F_B - 4T - W) - 2\Delta T_4 + 2\Delta T_4' = 0$$

$$k_{34} = 2 \, \Delta T_4 - 2 \, \Delta T_4'$$

where $\Delta T_4 = k_c \, \Delta L_4$ and $\Delta T_4' = k_c \, \Delta L_4'$

The coefficients of the fifth column of the stiffness matrix are found by imposing an arbitrary rotation about the x-axis, keeping all other d.o.f.'s restrained. The resulting coefficients are identical to those of the fourth column with a change in notation as follows:

$$k_{55} = F_B \, e_5 + 2 \, \Delta T_5 \, u + 2 \, \Delta T_5' \, v + 2T(u - v) \tag{12}$$

$$k_{35} = 2 \, \Delta T_5 - 2 \, \Delta T_5' \tag{13}$$

where

$$d_2 = \sqrt{\bar{h}^2 + b^2} \ ,$$

$$u = d_2 \cos(\psi_2 + \alpha_x) \ ,$$

$$v = d_2 \cos(\psi_2 - \alpha_x) \ ,$$

$$\psi_2 = \tan^{-1}(\bar{h}/b) \ ,$$

$$\Delta L_5 = \bar{h} - d_2 \sin(\psi_2 - \alpha_x) \ ,$$

$$\Delta L_5' = d_2 \sin(\psi_2 + \alpha_x) - \bar{h} \ ,$$

$$\Delta T_5 = k_c \, \Delta L_5 \ ,$$

and

$$\Delta T_5' = k_c \, \Delta L_5'$$

The coefficients of the sixth column of the stiffness matrix are found by giving the structure a rotation about the z-axis with all other d.o.f.'s restrained. The forces acting on the structure arising from yaw rotation are depicted in Figure 8.

A sum of the moments about the z-axis gives:

$$+\Sigma M_z = 0$$

$$k_{66} - 4(T + \Delta T_6)_\phi \sqrt{a^2 + b^2} = 0$$

$$k_{66} = 4(T + \Delta T_6) \ \frac{\phi(a^2 + b^2)}{\sqrt{2 + \phi^2(a^2 + b^2)}} \tag{14}$$

where

$$\frac{\phi \sqrt{a^2 + b^2}}{1^2 + \phi^2(a^2 + b^2)} = \sin \phi' , \text{ and}$$

$$\Delta T_6 = k_c \left(\sqrt{1^2 + \phi^2 (a^2 + b^2)} - 1 \right)$$

A summation of forces in the vertical direction gives:

$$\uparrow + \Sigma F_z = 0$$

$$k_{36} + F_B - W - 4(T + \Delta T_6) \cos \phi' = 0$$

but, $F_B - W = 4T_0$; therefore,

$$k_{36} = 4T (\cos \phi' - 1) + 4 \Delta T_6 \cos \phi' \tag{15}$$

where

$$\cos \phi' = \frac{1}{\sqrt{1^2 + \phi^2(a^2 + b^2)}} \qquad \text{(see Figure 9)}$$

3. Discussion

Two significant aspects can be noted concerning the derived stiffness coefficients: coupling and nonlinearity. Coupling terms are the nondiagonal coefficients of the stiffness matrix. Heave is coupled to surge, sway, pitch, roll, and yaw, respectively (Equations (4), (7), (11), (13), and (15)). Further, pitch is coupled to surge, (Equation (5)), and roll is coupled to sway (Equation (8)).

The stiffness matrix, including all of the coupling terms detailed above, is:

$$
\begin{array}{c}
\text{Surge} \\
\text{Sway} \\
\text{Heave} \\
\text{Pitch} \\
\text{Roll} \\
\text{Yaw}
\end{array}
\begin{bmatrix}
k_{11} & 0 & 0 & 0 & 0 & 0 \\
0 & k_{22} & 0 & 0 & 0 & 0 \\
k_{31} & k_{32} & k_{33} & k_{34} & k_{35} & k_{36} \\
k_{41} & 0 & 0 & k_{44} & 0 & 0 \\
0 & k_{52} & 0 & 0 & k_{55} & 0 \\
0 & 0 & 0 & 0 & 0 & k_{66}
\end{bmatrix}
$$

As will be shown later in this report, coupling has a significant effect on the calculated response of the structure. Coupled equations of motion are intractable in Frequency Domain models, and nonlinear time domain analysis published in the literature generally neglected coupling effects.

As shown above, the stiffness matrix is asymmetric. This implies that some degrees of freedom are coupled to other degrees of freedom, but not vice versa. For example, this is apparent in the heave degree of freedom (third row and third column of the stiffness matrix). The heave row contains only nonzero terms; i.e., heave is coupled to surge, sway, pitch, roll, and yaw. However, the heave column contains only one nonzero term (k_{33}); i.e., as the structure moves in the vertical direction (heaves), there is no required motion in the other directions. By the same argument, pitch is coupled to surge, and roll is coupled to sway, but not vice versa. Moreover, other types of coupling occur between degrees of freedom as can be seen later in the derivation of the forcing functions.

Another significant aspect of the stiffness matrix is the nonlinearity of its coefficients. For example, sine and cosine terms and square and square root terms contribute to the nonlinearities of the stiffness coefficients (see Equations (2) through (15)). Since each coefficient k_{ij} is equal to the stiffness force at degree of freedom "i" due to an <u>arbitrary</u> (and <u>not</u> a unit) displacement in the direction of degree of freedom "j", the sum of coefficients in each row of the stiffness matrix will give the total stiffness force "K_i" of that particular degree of freedom. Hence,

$$K_i = \sum_{j=1}^{6} k_{ij} \qquad (16)$$

C. Derivation of Wave Forces

1. Selection of Wave Theory

Theoretical simulation of water waves, and of sea motion in general, involves rigorous mathematical analysis. The basic hydrodynamic equations that govern the wave kinematics are the equation of continuity (Laplace's equation) and the equation of momentum (Bernoulli's equation). The form and solution of these equations vary, depending on the intended appliction of wave kinematics. However, in general, all solutions assume incompressible, inviscid, and irrotational fluid particles. The simplest solution of the hydrodynamic equations involves a further assumption, that the waves are of small amplitude (H/2) compared to the water depth (d) and the wavelength (L). This solution was introduced by Airy (Reference 12), and became known as the linear wave theory.

Higher order wave theories are not based on the assumption of small amplitude to solve the hydrodynamic equations. Instead, they include

higher order terms (terms higher than first order) in the solution. Stokes (Ref. 17) developed equations for waves of finite amplitude by accounting for higher order terms. The Stokes wave theories have been developed for terms up to fifth order. The successfully higher order theories give wave surface profiles that are steeper in the crests and flatter in the trough than those given by the linear wave theory. Dean (Ref. 18) developed the stream function wave theory. This theory, which is a numerical one, has demonstrated good agreement with experimental wave channel test results for a wide range of H/T^2 ratios (Ref. 19). Many other analytical and numerical wave theories have been developed and can be found in the literature (see for example Refs. 20 - 23).

The relative ranges of application for some of the prominent wave theories are shown in Fig. 10 (see Ref. 24). It can be seen that, for d/T^2 ratio of greater than about 1.0 (ft/s^2), and for H/T^2 ratio of less than about .035, the linear wave theory applies. In this study, water depths start at 200 m. Therefore, from the d/T^2 = 1.0 ratio, the maximum wave period that can be used with the linear wave theory is $\sqrt{200 \times 3.3}$ = 25.6 sec, which is large enough to cover the range of wave periods used in this study. The maximum wave height that can be used is $H = 0.035T^2$. For large values of wave period, say T = 25 sec, the wave height could be as large as 22 ft (6.7 m). It should be noted that, while wave heights greater than those just described also were used in this study, the response is linear with wave height over the range between the maximum wave height used and those within the above guidelines. Further, it has been shown that the predominant wave height for a 17 sec wave is approximately 15 m (Ref. 10) and that surge and sway response are not significantly affected by wave steepness and agree well with linear wave theory predictions (Ref. 9).

Therefore, the linear wave theory is sufficient to obtain the kinematics of the waves to be used in the dynamic analysis of tension-leg platforms in deep water.

A schematic diagram of an elementary, sinusoidal progressive wave is presented in Fig. 11 (Ref. 14). The velocity and acceleration of the fluid particle at depth z below the mean water level are respectively given by the linear wave theory as:

$$u = \frac{\pi H}{T} e^{-kz} \cos [k(\bar{X} - ct)] \tag{16}$$

and

$$\dot{u} = \frac{2\pi^2 H}{T^2} e^{-kz} \sin [k(\bar{X} - ct)] \tag{17}$$

where H, T, and c are the wave height, period, and celerity, respectively, and k = 2 π/wavelength.

2. Justifications for using Morison's Equation

Experimental studies by Morison, et al. (Ref. 15), led to the formulation of a wave force equation that became known as Morison's equation. This equation has been widely used for more than two decades in the calculation of wave forces on offshore structures. The equation consists of a drag term, as in the case of flow of constant velocity, and an inertia term due to the acceleration of the fluid particle.

The original form of Morison's equation is:

$$F = 0.5 \, \rho C_d D \, |U|U + C_m \, \rho\pi \, D^2/4 \, \frac{dU}{dt} \tag{18}$$

where F is the force per unit length experienced by a cylinder; U and dU/dt represent the undisturbed velocity and acceleration of the fluid, respectively; and C_d and C_m are the drag and inertia coefficients.

Morison's equation has been widely accepted for force computations because of good correlation with experimental results in a large number of practical cases. However, the use of Morison's equation gave rise to a great deal of discussion on what values of the two coefficients should be used. Experimental results by different researchers were scattered and divergent. However, the force transfer coefficients C_d and C_m, for one-dimensional flow over a circular cylinder, have been well studied by Sarpkaya (Ref. 25) and Garrison (Ref. 13), and their experimental results have produced a very promising approach for the systematic analysis of test data.

Morison's equation provided a hypothesis that expresses the force both as a function of time and other independent parameters, for the case where the wave slope and associated pressure gradient are roughly constant across the diameter of the cylinder and the wave scattering is negligible. Morison also assumes that in the region near the cylinder the kinematics of the undisturbed flow do not change in the incident wave direction. However, since the kinematics of the flow do vary with distance (as shown in Fig. 12), the above assumptions restrict the D/L ratio to a small value. Sarpkaya (Ref. 26) and Leonard, et al. (Ref. 19), suggested that the application of Morison's equation be limited to D/L values of less than 0.2. They also suggested that in cases where D/L is larger than 0.2, wave diffraction occurs. In the diffraction dominated region (see Fig. 13) the total inertial force results from the sum of two components (Ref. 26): the

force from the pressure field of the undisturbed fluid (the incident wave), and that from the disturbances caused by the presence of the body (scattered wave).

Diffraction forces arise from the scattering of incident waves by structure. These forces become significant when the structural member dimensions reach a substantial fraction of the wave length. Models for describing the force arising from diffraction have been developed by McCamy and Fuchs (Ref. 27) and others, generally by the use of potential theory with finite elements or finite difference methods. Significant contributions to the computation of hydrodynamic forces and moments on large gravity-type platforms have been made by Hogben and Standing (Ref. 28), Garrison, et al. (Ref. 29), Mei (Ref. 30) and others, using diffracion theory.

In conclusion, the use of Morison's equation in wave force calculations is justified if the following conditions are met:

1) For D/L to be less than 0.2, with the largest diameter of 16 meters used in the analysis, the wave length should be larger than 5D, i.e., 80 meters.

2) For a maximum diameter of 16 meters, the wave height should be greater than 5 meters to avoid the diffraction dominated region (see Fig. 14).

3) The original form of the equation should be modified in order to account for the relative velocity and acceleration between the oscillating structure and the fluid particles.

4) Reasonable values of the force transfer coefficients C_d and C_m may be obtained from the literature (e.g., recommendations of Garrison (Ref. 13) and Sarpkaya (Ref. 26)).
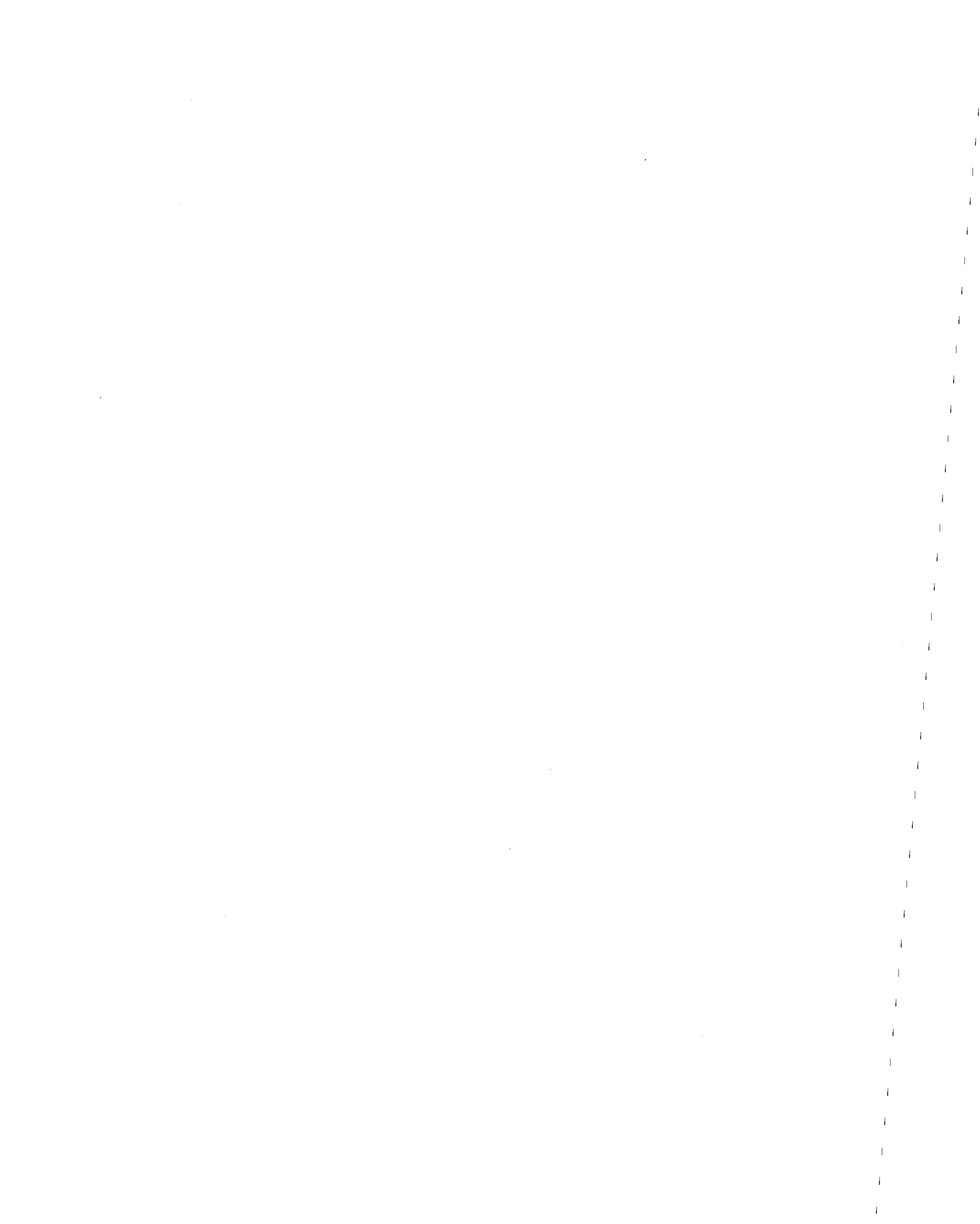
3. Procedure for Wave Force Calculation

In order to properly describe the dynamic response of the TLP, the wave forces must be accurately calculated. The conditions listed in the previous section for using Morison's equation in wave force calculations all have been met in this study. Hence, the wave forces are calculated from a modified version of Morison's equation and include the relative velocity and acceleration between the structure and the fluid particle. Equation (18) is modified to account for the relative motion between the structure and the fluid particle, and separated into drag and inertia terms. The drag and inertia forces on an element dz along the length of the cylinder become:

$$\delta F_d = \frac{\rho}{2} C_D D \ U_{rel} \ U_{rel} \ dz \tag{19}$$

and

$$\delta F_I = \rho \frac{\pi D^2}{4} [C_m \dot{U} - (C_m - 1) \ddot{x}] \ dz \tag{20}$$

where ρ is the mass density of the fluid, D is the diameter of the cylinder, U_{rel} is the relative velocity given by

$$U_{rel} = u - [\dot{x} - (z - \bar{z})\dot{\alpha} + \frac{1}{2} x_i \dot{\alpha}^2] \tag{21}$$

and

$$\ddot{x} = \ddot{x} - (z - \bar{z}) \ddot{\alpha} + \frac{1}{2} x_i \ddot{\alpha}^2 \tag{22}$$

Equations (21) and (22) are derived based on Figure 14 where $\dot{x}$, $\ddot{x}$, $\dot{\alpha}$, $\ddot{\alpha}$ are the velocity, acceleration, angular velocity, and angular acceleration of
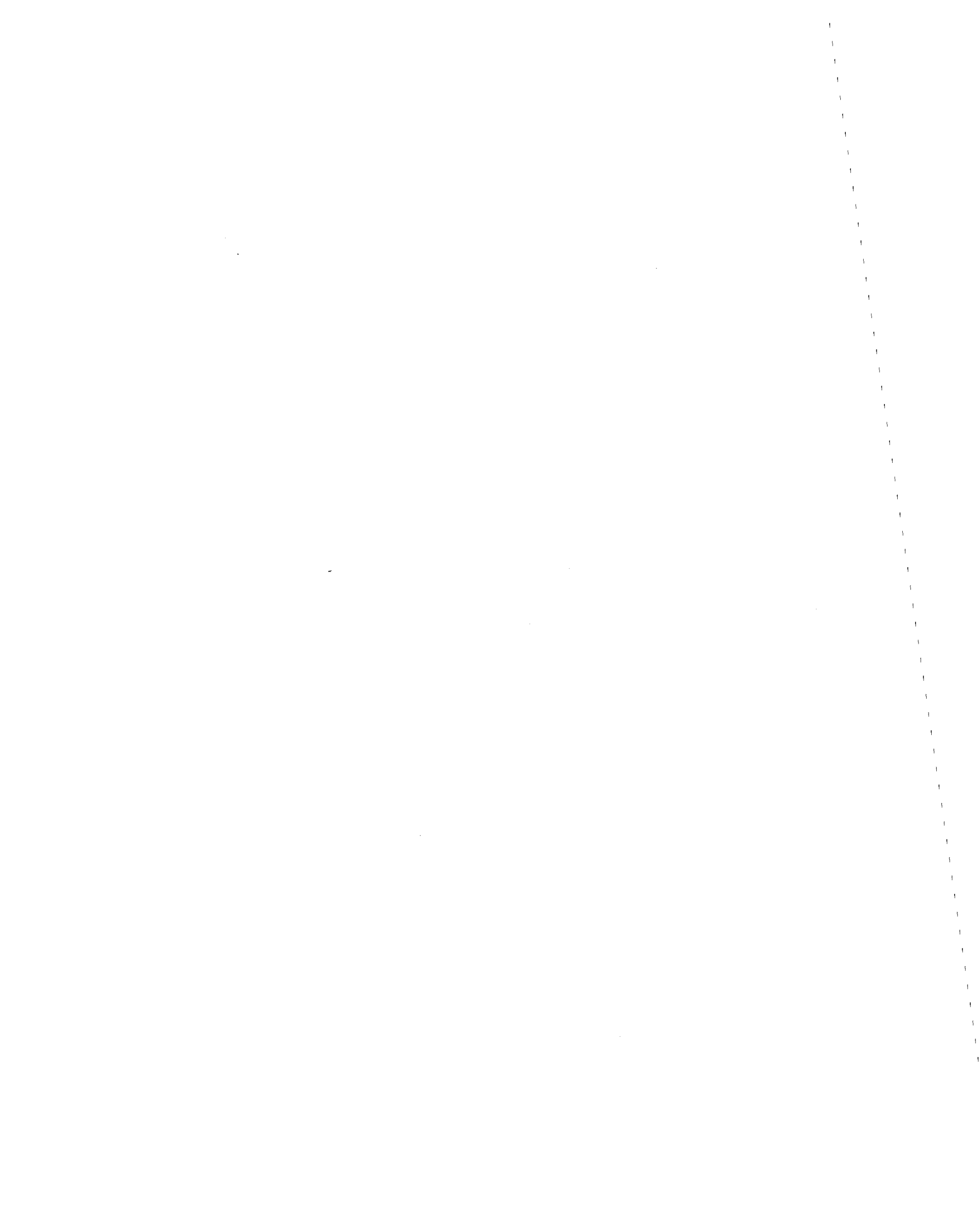
the center of gravity (in this case the center of rotation) of the structure, respectively, and x is the relative velocity of element dz of the cylinder with respect to the water.

Substituting Equations (21) and (22) into Equations (19) and (20), respectively, yields:

$$\delta F_d = \frac{\rho}{2} C_d \ D|u-[\dot{x}-(z-\bar{z})\ \dot{\alpha}+\frac{1}{2}\ x_i\dot{\alpha}^2]|\{u-[\dot{x}-(z-\bar{z})\ \dot{\alpha}+\frac{1}{2}\ x_i\dot{\alpha}^2]\}dz \qquad (23)$$

and

$$\delta F_I = \rho\frac{\pi D^2}{4} \ [C_m \ \dot{u} \ - \ (C_m-1) \ \{\ddot{x}-(z-\bar{z})\ \ddot{\alpha}+\frac{1}{2}\ x_i\ddot{\alpha}^2\}]dz \qquad (24)$$

These two equations are integrated along the length of each column and hull to obtain the total instantaneous force on the structure.

The moments of these forces about the axes of rotation are found by multiplying the force equations by the appropriate moment arms and then integrating over the length of each cylinder to obtain the total moments. It should be noted that despite the nonlinearity of the drag force and moment equations and the coupling of pitch and surge or roll and sway in both the inertia and drag equations, a closed form integration can be carried out by hand, thereby avoiding the need for time consuming numerical integration. This method of force calculation is the major contributor to the efficiency of the mathematical model and computer program developed in this study.

A force calculation method similar to that of Kirk and Etok (Ref. 10) is used with the following major changes:

1 - Inclusion of drag forces

2 - Incorporation of relative motion between structure and fluid particles

3 - Accounting for instantaneous position of structure

4 - Inclusion of coupling terms in wave force derivation

The following outline contains a complete description of the wave force equations which must be derived:

1) Horizontal forces

    a) Inertia forces on columns

    b) Drag forces on columns

    c) Inertia forces on hulls and cross braces

    d) Drag forces on hulls and cross braces

2) Vertical forces

    a) Vertical inertia forces on hulls

    b) Vertical drag forces on hulls

    c) Dynamic pressure on corner column bases

3) Moments of forces about x, y, and z axes

    a) Moments due to inertia forces on columns

    b) Moments due to drag forces on columns

    c) Moments due to horizontal inertia forces on hulls

    d) Moments due to horizontal drag forces on hulls

    e) Moments due to vertical inertia forces on hulls

    f) Moments due to vertical drag forces on hulls

    g) Moments due to dynamic pressure on corner column bases

4. Summary of Wave Forces

Details of the complete derivation of wave forces and moments are presented in Appendix I. A summary of the resulting force equations is given below:

Horizontal forces

Surge (x-axis):
$$F_{x_T} = \sum_{i=5}^{12} (F_{I_i} + F_{D_i}) \cos \alpha + F_x + \bar{F}_x \qquad (25)$$

Sway (y-axis):
$$F_{y_T} = \sum_{i=5}^{12} (F_{I_i} + F_{D_i}) \sin \alpha + F_y + \bar{F}_y \qquad (26)$$

Vertical forces

Heave (z-axis):
$$F_{z_T} = F_v + \bar{F}_v + F_{cv} \qquad (27)$$

Moments

Pitch (about y-axis):

$$M_{y_T} = \sum_{i=5}^{12} (M_{I_i} + M_{D_i}) \cos \alpha + M_{v_y} + M_{H_y} + M_{P_y} \qquad (28)$$

Roll (about x-axis):

$$M_{x_T} = \sum_{i=5}^{12} - (M_{I_i} + M_{D_i}) \sin \alpha + M_{v_x} + M_{H_x} + M_{P_x} \qquad (29)$$

Yaw (about z-axis):
$$M_{z_T} = \sum_{i=5}^{12} (F_{I_i} + F_{D_i}) y_i \qquad (30)$$

where $\sum_{i=5}^{12}$ is the summation over the corner columns (5-8) and the middle columns (9-12), α is the orientation angle or angle of wave incidence, F_x and $\bar{F}_x$ are the x-components of the total horizontal inertia and drag forces on the hulls, F_y and $\bar{F}_y$ are the y-components of the total horizontal inertia and drag forces on the hulls, F_v and $\bar{F}_v$ are the total vertical inertia

and drag forces on the hulls, F_{CV} is the total vertical dynamic pressure force on the bases of the corner columns, M_I and M_D are the moments of the horizontal forces on the columns about an axis perpendicular to the wave direction, M_{V_y} and M_{H_y} are the moments of the vertical and horizontal hull forces about the y-axis, M_{P_y} is the moment of the dynamic pressure on the bases of the corner columns about the y-axis, M_{V_x} and M_{H_x} are the moments of the vertical and horizontal hull forces about the x-axis, M_{P_x} is the moment of the dynamic pressure on the bases of the corner columns about the x-axis, and y_i is the moment arm, of column i, for moments about the z-axis.

D. Earthquake Forces

Platform motions are excited by an earthquake through the horizontal and/or vertical translation of the ground where the legs are anchored. The equations of motion are written with structural displacements $\{x_r\}$ relative to the ground motion. This provides an earthquake forcing function that is equal to the mass of the structure times the ground acceleration. The effect of interaction of the structure with either calm water or waves is also included. The equations of motion can be written as

$$[M]\{\ddot{x}_r\} + [K]\{x_r\} = \{f(t,\dot{x},\ddot{x})\} - [M]\{\ddot{x}_g\} \qquad (31)$$

where $\{\ddot{x}_g\}$ is the ground acceleration vector. The inertial force vector due to ground acceleration, on the right-hand side of the equation of motion, consists of all six degrees of freedom included in the analysis. This means that the model is capable of handling not only horizontal ground motion, but also vertical as well as rocking and torsional ground motions.

The derivation of the force vector arising from the interaction between the structure and the fluid particles is listed in detail in Appendix II.

E. Mathematical Model

1. Equations of Motion

Now that the nonlinear stiffness equations have been derived and the wave and earthquake forces are formulated, a set of coupled nonlinear differential equations can be formed. These equations of motion form the basis for a mathematical model that performs the dynamic analysis of tension-leg platforms. The equations of motion (written in matrix form in Equation (1)) are rewritten here in vector form as

$$\{m_i \ddot{x}_i\} + \{K_i\} = \{F_i(x,\dot{x},\ddot{x},t)\} \tag{32}$$

where $\{m_i \ddot{x}_i\}$ is the inertial force vector in which m_i is the structural -- plus added -- mass of degree of freedom "i", and $\ddot{x}_i$ is the acceleration of the structure in the direction of degree of freedom "i", $\{K_i\}$ is the coupled nonlinear stiffness force vector developed in section (B) (see Equation 16), and $\{F_i(x,\dot{x},\ddot{x},t)\}$ is the vector of nonlinear external forces (waves or earthquakes) developed in sections (C) and (D). The equations of motion generally describe the dynamic equilibrium between the inertia, the restoring, and the exciting forces.

The structure used in the analysis is represented schematically in Figure 3. The center of gravity of the platform is assumed to be located a distance z from the mean water level and a coordinate system is attached at its origin to the equilibrium position of the center of gravity. The center of rotation (pitch, roll, yaw) is assumed to be located at the center of gravity. The platform is modeled as a rigid body free to translate in three directions (surge, sway, heave) and rotate in three directions

(pitch, roll, yaw), with restoring forces that model the legs (cables or chains) and buoyant forces.

2. Solution Procedure

The equations of motion are both coupled and nonlinear. Hence a time domain analysis method is required, as mentioned earlier in the report, to calculate the response of the structure to various types of loading. The general approach to solving nonlinear equations of motion is through an integration of the acceleration and velocity curves in the time domain.

Two well known methods of integration have been widely used for time domain dynamic analysis of fixed, or floating, offshore structures. The first one is the Newmark-Beta method, and the second one is the Newton-Raphson technique. The latter does not work well for heave, roll, or pitch (see Ref. 7). The Newmark-Beta method is more general and is used as a standard against which other methods are compared. The Beta method has been used in time domain models for dynamic analyses of fixed offshore structures, with good results (Ref. 3).

The Newmark-Beta method is used in this model to integrate, in a step-wise manner, the equations of motion and to obtain time histories of the structure's response in an iterative manner. The iterative method can be used to determine the accelerations, velocities, and displacements of the structure at time t_{n+1} based on corresponding values at time t_n and the accelerations at t_{n+1}. The equations have the following form:

$$\dot{x}_i(t_{n+1}) = \dot{x}_i(t_n) + (1-\gamma)\Delta t\, \ddot{x}_i(t_n) + \gamma\Delta t\, \ddot{x}_i(t_{n+1}) , \qquad (33)$$

and

$$x_i(t_{n+1}) = x_i(t_n) + \Delta t\, \dot{x}_i(t_n) + (\tfrac{1}{2} - \beta)\Delta t^2\, \ddot{x}_i(t_n) + \beta\Delta t^2\, \ddot{x}_i(t_{n+1}) \qquad (34)$$

The value of γ is usually set to 1/2 by damping considerations and the value of β is chosen in the range of 1/8 to 1/4 for reasons of convergence. Values of γ and β of 1/2 and 1/6, respectively, are used in this model. The vector of accelerations at time t_{n+1} are found by substituting the vectors of velocities and displacements into the equations of motion as follows:

$$\{\ddot{x}_i\} = \frac{1}{m_i} [\{F(x_i(t_{n+1}), \dot{x}_i(t_{n+1}), \ddot{x}_i(t_{n+1}), t_{n+1}\}$$

$$- \{K_i(x_i(t_{n+1}))\}] \tag{35}$$

Equations (33), (34), and (35) are solved in an iterative manner. An assumed value of x_i at t_{n+1} is usually chosen equal to the value at the previous time step. New values of x_i and $\dot{x}_i$ at t_{n+1} are then calculated from Equations (33) and (34), and a new value of $\ddot{x}_i$ is computed from Equation (35). This process is repeated until the assumed and the calculated values of acceleration converge within a predetermined tolerance. The value of the tolerance is established through compromise between accuracy and cost. The β-method accepts both continuous forcing functions (as in case of waves) and discrete forcing functions (as in case of earthquakes), and is extended for the purpose of this study to three dimensions and six degrees of freedom.

3. Computer Code

A compact and inexpensive computer program has been developed to perform the numerical calculations of the motion of anchored as well as floating structures subjected to the action of waves, currents, and earthquakes. A flow chart of the computer program is depicted in Figure 19.

The structural geometry, material properties, wave properties and ground acceleration are input to the program. The displacement, velocity

and acceleration vectors are initialized and an assumption for the acceleration vector is made for the next time step. New displacement and velocity vectors are then calculated based on the assumed acceleration. The forces and stiffnesses corresponding to these values of displacements, velocities, and accelerations are then calculated. Finally, using the equations of motion a new value of the acceleration is calculated and compared with the assumed value. The process is repeated until the difference between the calculated value and the assumed value of the acceleration is less than a predetermined convergence factor. Once the equations of motion are satisfied, the final acceleration value for this time step becomes the assumed value of the acceleration for the next time step, and the whole process is repeated.

At each time step the program calculates:

- The six components of motion (surge, sway, heave, pitch, roll, and yaw) together with velocities and accelerations.
- The total forces and moments due to waves or earthquake.
- The stiffness vector (restoring forces).
- The tension and tension variation of each leg.

At the end of the analysis the program calculates the maximum values of the displacements, velocities, and accelerations of the structure, and the maximum tension and tension variation of each of the four legs. If plots are desired, the variables of interest can be scaled with respect to their maximum values and plotted versus time.

4. Data Used for Evaluation of Platform Motion

To provide a convenient comparison of results for the mathematical model developed for the analysis of platform motion, the following data taken from Kirk and Etok (Ref. 10) were used for the AKER TPP-41:

- Buoyancy = weight of displaced fluid = 436,810kN

- Water depth = 160 meters

- Draft = depth of submerged portion of the structure = 35 m

- Mass of deck equipment = 18,000 tons

- Mass of one main hull + ballast = 2,000 tons

- Total mass of TPP in air = 31,200 tons

- Structural and fluid added mass in heave = 56,000 tons

- Strucural and fluid added mass in sway = 82,700 tons

- Structural and fluid added mass moment of inertia in roll = 1.49 x 10^8 ton-meter square (tm^2)

- Structural and fluid added mass moment of inertia in pitch = 9.68 x 10^7 tm^2

- Diameter of corner columns = 16 m

- Diameter of middle columns = 3.5 m

- Diameter of cross braces = 6 m

- Depth and width of main hulls = 13 x 9.5 m

- Spacing of corner columns = 70 m

- Height of platform center of gravity = 41.7 m

- Number of cables per leg = 3

- Number of wires per cable = 400

- Diameter of each wire = 7 mm

- Area of wire per leg = 46,180 mm^2

- Cable length = 125 m, 200 m

- Initial tension per leg = 25,000 kN

Some of the above data are modified to meet the objectives of this research. Such modifications include water depth, hull sizes, and masses.

F. Summary of Dynamic Analysis Model

A complete nonlinear deterministic dynamic analysis model has been developed in this chapter. The model is based on a set of coupled nonlinear differential equations integrated in the time domain using Newmark's Beta Method. Wave kinematics are calculated from the linear wave theory, and wave forces are calculated from a modified form of Morison's equation. The coupling and nonlinearities of the equations of motion are contributed by both the stiffness and the forcing functions.

A computer program is written to perform the numerical solution and obtain time histories of the response in all degrees of freedom. The tension forces in the anchoring legs can be calculated from displacement time histories of the different degrees of freedom, and time histories of these forces can be generated.

Data used in the computer program are taken from one of the selected references with slight changes in some cases for the sake of a complete and meaningful testing of the model.
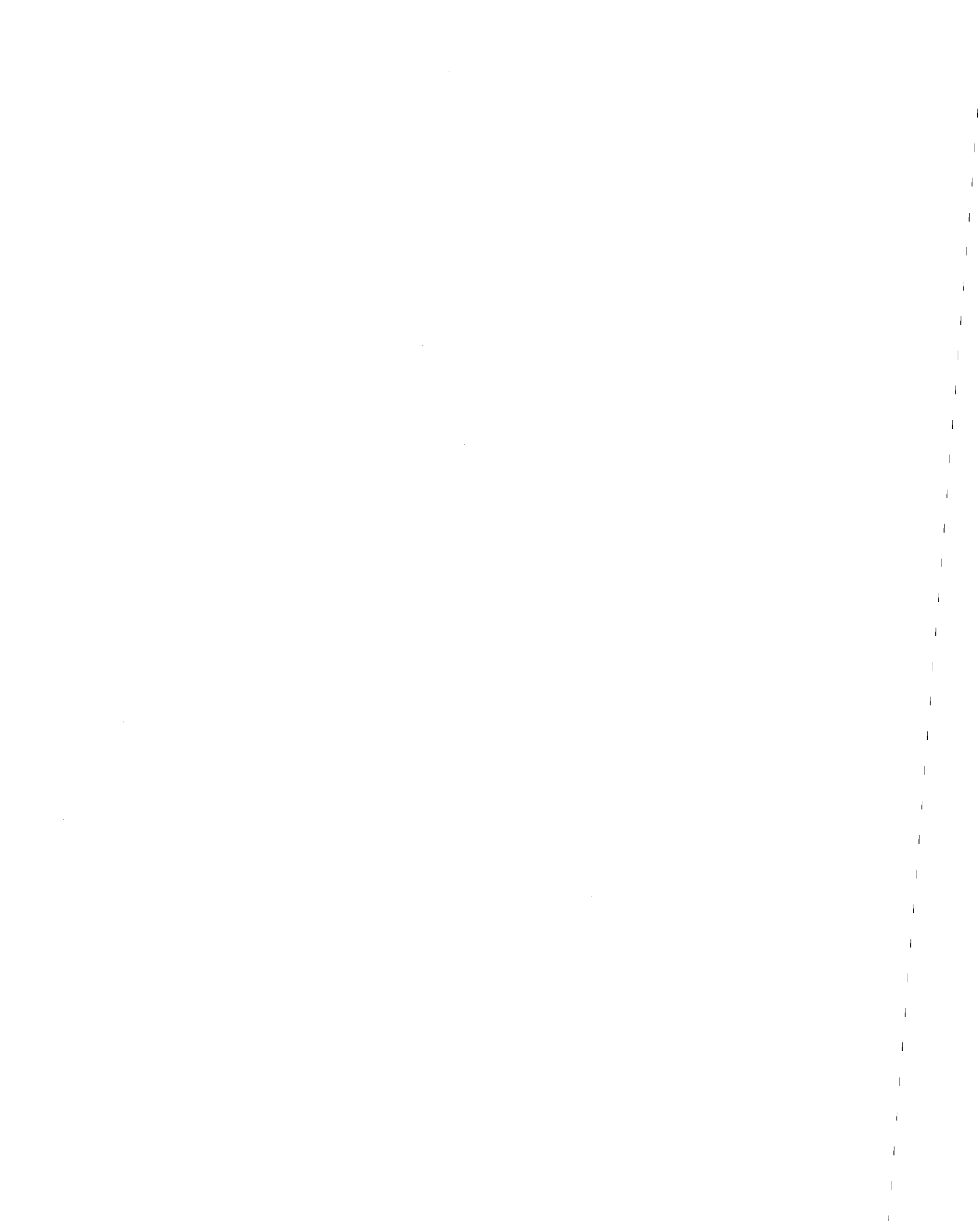
III. RESPONSE OF THE MODEL

A. General

The major objective of the dynamic analysis model presented herein is to simulate the response of tension-leg platforms to ocean-environment loading. In this chapter, the model is tested by the application of wave loading and earthquake forces. Time histories of surge, sway, heave, pitch, roll, and yaw are calculated by the model. The relative importance of design variables for tension-leg platforms is found through a parametric analysis. Some of these parameters studied are:

1) Wave period (Response Spectra)

2) Wave height

3) Water depth

4) Cable stiffness

5) Initial tension

6) Direction of wave propagation

The importance of coupling and nonlinearity is demonstrated through comparison of the response of the coupled system to that of the uncoupled, and the response including nonlinear terms to that by existing linear models. The effect of earthquakes on the motion of the platform is also studied.

B. Response to Wave Forces

The platform data described in Chapter II were used to test the mathematical model developed herein. A coefficient of inertia (C_m) of 1.5 and a coefficient of drag (C_d) of 1.0 were used in the wave force calculations of Chapter II, and assumed to be constant throughout the analysis. A wave height of 15.0 meters and a wave period of 17 seconds were chosen to
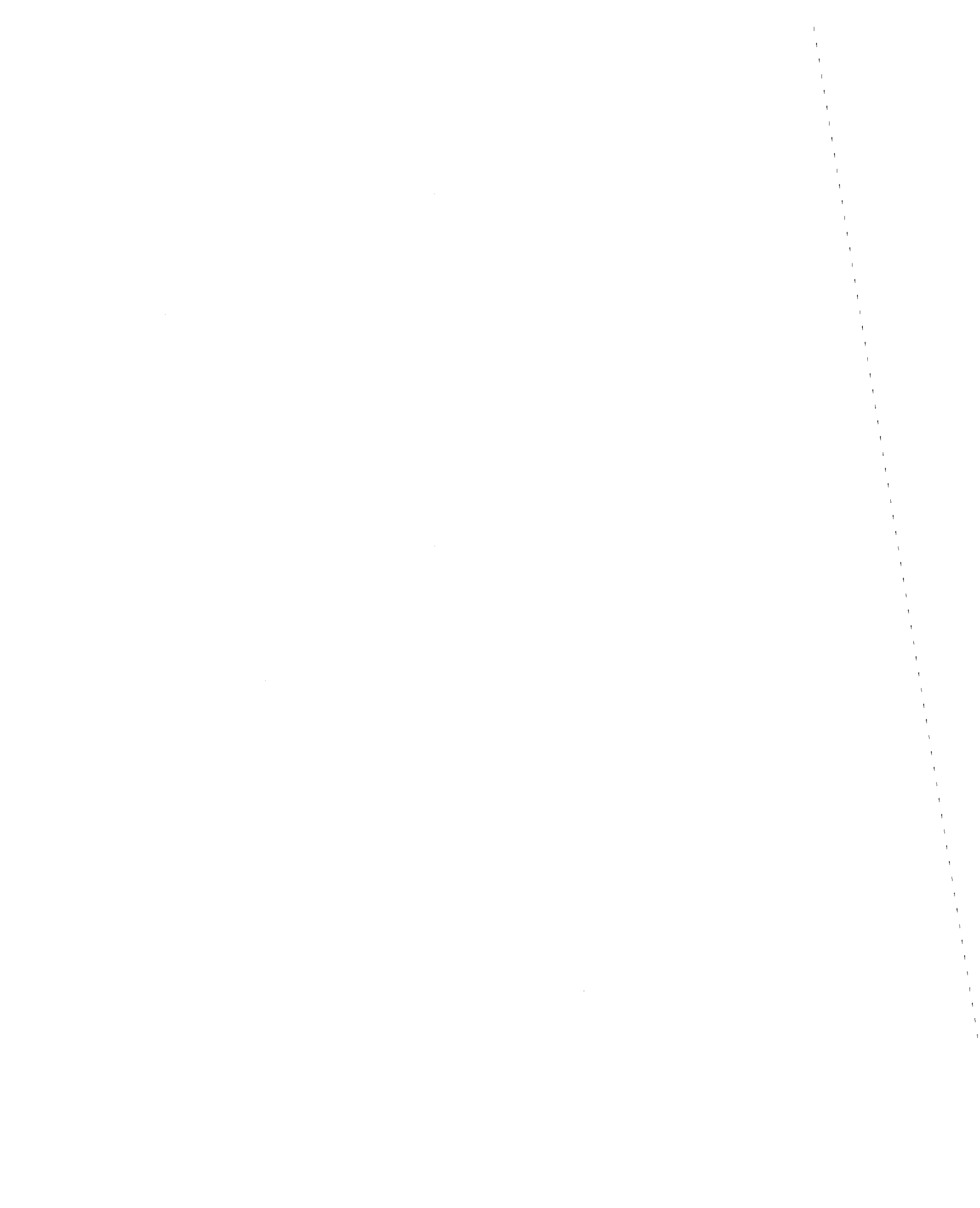
describe a "significant wave" to be used in the rest of the analysis. Simulation of various sea states of interest was done by varying the wave height and the wave period.

1. Time Histories

Time histories of response in the direction of each of the six degrees of freedom were obtained. Time histories of surge, sway, heave, pitch, roll, and yaw, respectively, for the significant wave described above and for a wave propagation angle of 35 degrees from the x-axis are depicted in Figures 20-25. Responses for all six degrees of freedom, with inertia and without drag, are presented in Figures 26-31 for the same sea state. Comparisons between the responses including drag forces and those that exclude drag show that the nonlinear drag forces (sometimes called interaction forces) contribute a significant amount of damping to the displacement response. The periods of vibration for all six degrees of freedom of the structure for the sea state described above are shown in Table 1. Also shown in Table 1 are the response amplitudes (or maximum values) of the structure's six degrees of freedom for both cases (including drag and excluding drag).

Velocity response time histories for all six degrees of freedom are shown in Figures 32-37 for the significant sea state (with drag forces included). Time histories of acceleration responses are also calculated and shown in Figures 38-43. Table 2 includes the maximum values of these velocities and accelerations. The time histories of the motion (displacements, velocities, and accelerations) are important input for analysis of the tension in the anchor legs, as well as in analyzing the stresses in the various members of the structure caused by hydrodynamic and earthquake forces.

2. Response Spectra

Plots of maximum amplitude of vibration versus wave period (or wave frequency) will be referred to as response spectra. Two cases were studied in order to develop response spectra for the six degrees of freedom of the platform. Case 1 includes only fluid inertia forces (i.e., excluding drag forces), and case 2 includes both intertial and drag forces.

The response spectra for surge ($\alpha = 0^0$) and sway ($\alpha = 90^0$) are shown in Figures 44 and 45, respectively. It can be seen that both surge and sway amplitudes reach a peak at a wave period of approximately 5 seconds and another peak at a period near 7 seconds. Zero response amplitudes, corresponding to zero resultant wave forces, occur at wave periods of 5.5 and 9.5 seconds at which the wave lengths are 47 and 140 meters, respectively. This arises from a "force cancellation" caused by spacing of middle and corner columns. For wave periods greater than 9.5 seconds the response amplitudes increase consistently (but not necessarily linearly) as seen in the figures. The dashed lines in Figures 44 and 45 indicate the response of surge and sway for case 1 (inertia forces only), whereas the solid lines show the response spectra for case 2 (inertial and drag forces). It is clear that drag forces result in a decreased response amplitude throughout the range of wave periods. For example, for T = 16 seconds the surge response amplitude is approximately 11 meters for case 1 and 10 meters for case 2; i.e., drag accounts for a response reduction of about 10 percent. For a wave period of 8 seconds, however, the response amplitude is 8.6 meters for case 1 and 5.5 meters for case 2; i.e., drag accounts for a reduction of more than 35 percent in response. Therefore, a significant overestimation of the response amplitude can result from neglecting drag.

The response spectra of heave for $\alpha = 0^0$ and $\alpha = 90^0$, respectively, are illustrated in Figures 46 and 47. It can be seen that heave response spectra show similar trends to those of surge and sway. This arises from a strong coupling of heave and surge ($\alpha = 0^0$) and heave and sway ($\alpha = 90^0$) in the stiffness equations as described in Chapter II. The calculations of the cable tensions caused by the platform displacements in six degrees of freedom can give misleading results if heave coupling to sway and surge is ignored. The time histories for coupled and uncoupled heave response for $T = 17$ seconds and $H = 15$ meters are shown in Figures 48 and 49, respectively. Based on a comparison of these dramatically different curves, the authors conclude that coupling effects should not be neglected.

The results of response amplitude calculations for pitch and roll (Figures 50 and 51) indicate that at low wave periods the response for pitch and roll reaches its maximum value. Pitch and roll also exhibit the "force cancellation" phenomenon described for sway and surge. The effect of drag on pitch and roll also can be seen in the figures, but the percentage of reduction in response amplitudes is small.

The response spectrum for yaw at $\alpha = 35^0$ is given in Figure 52. A sharp peak in yaw response amplitude occurs at a wave period of 6 seconds. The response amplitude decreases rapidly for periods larger than 6 seconds and is negligible for periods larger than 10 seconds.

3. Parametric Study

a) Wave Height

Wave heights were varied in the range 0-30 meters for a constant wave period of 17 seconds. Response amplitude versus wave height plots for surge, heave, and pitch are given in Figures 53-55. The plots indicate a relationship that is essentially linear for small wave heights (i.e., for

wave heights smaller than about 15 meters). For large wave heights, however, this linearity does not hold true. For example, in Figure 56 there is a significant shift in slope for wave heights greater than about 19 meters. Attempts to normalize response spectra with respect to wave height, therefore, must consider only the range of wave heights where linear relationships are applicable.

b) Water Depth

Water depths were varied in the range 100-1000 meters for the significant sea state used in the rest of the analysis. Figures 56-58 illustrate the variation of response amplitudes of sway, heave, and roll, respectively, with water depth. As can be seen in the above plots, the roll response amplitude increases linearly with water depth. The sway response amplitude, however, does not vary linearly with water depth; i.e., the rate of increase of surge is not constant with water depth. While sway and roll amplitudes increase (linearly or otherwise) with water depth, that of heave decreases sharply in the range 100-400 meters and then it starts to increase slowly for depths greater than 400 meters (see Figure 57). Decrease in heave for deeper water arises from the decrease in cable stiffness (k = AE/L) corresponding to an increase in cable length. The less stiff the cables, the smaller is the effect of coupling between heave and surge or between heave and sway. Therefore, as the platform surges or sways in increasing water depths, the heave is less dependent on sway or surge; hence heave response amplitudes are smaller.

Surge and pitch response amplitude variations with water depth are similar to those of sway and roll, respectively. Yaw response amplitude variation with water depth was found to be small and hence can be neglected.
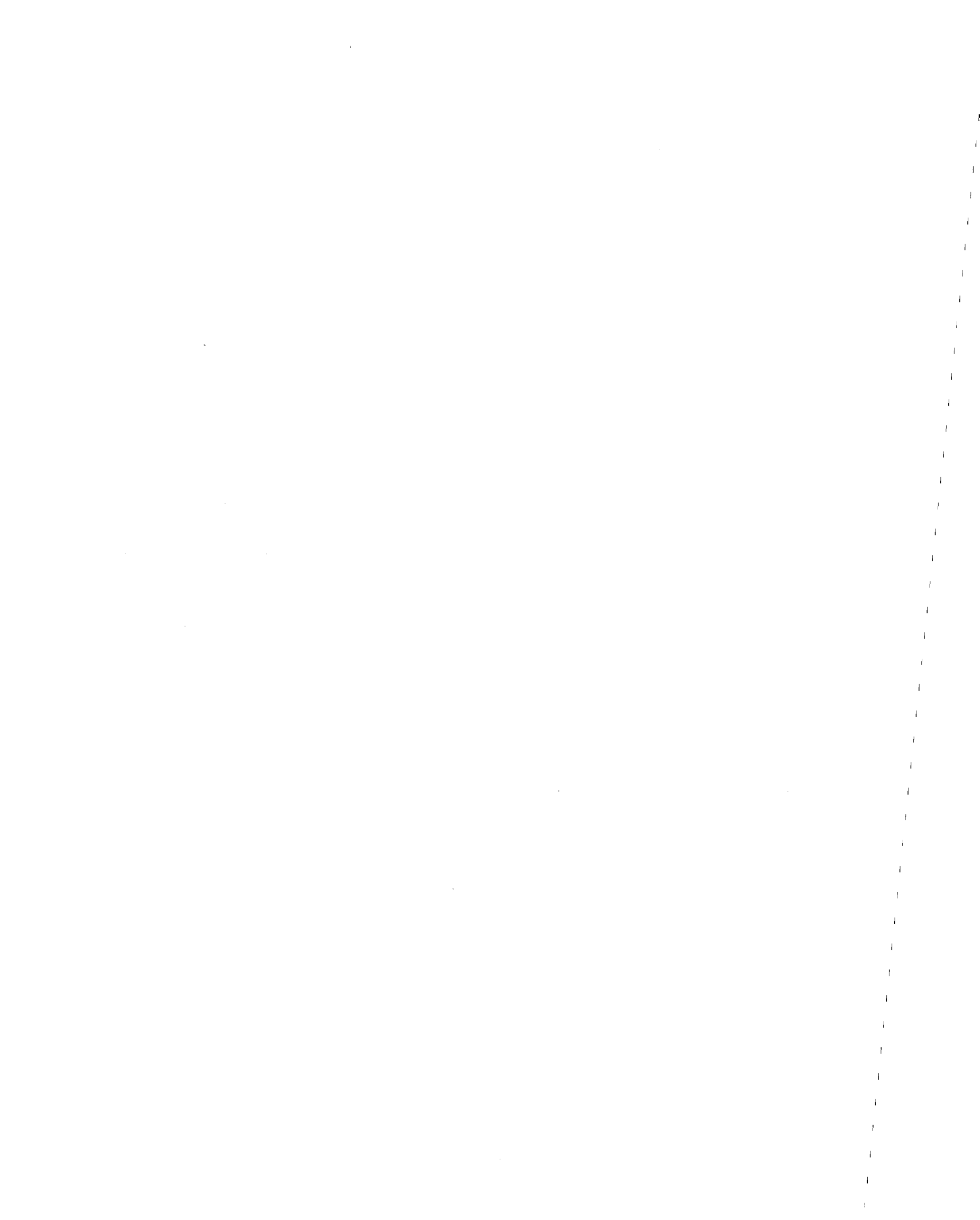
c) Cable Stiffness

The stiffness of the tension legs may be varied by increasing the number of chains per leg, the cross-sectional area, or the elastic modulus of the chains. The variation of response amplitudes of surge, heave, and pitch, respectively, with respect to cable stiffness, at a constant water depth of 125 meters are shown in Figures 59-61. The plots show that the response of the structure drops sharply with an increase in cable stiffness up to about 20,000 kN for pitch and 12,000 kN for surge and heave. The effect of additional stiffness decreases rapidly as seen in the figures.

d) Initial Tension

Changing the initial tension involves changes in other variables such as buoyancy, added mass, draft (depth of submerged portion of platform), and cable length. Since for a constant water depth the cable length plus the draft should be equal to the water depth, the buoyancy, added mass, and cable tension are calculated for different cable length-draft combinations. The variables involved were changed in a manner such that the variation in cable tension ranged from zero to 100,000 kN per leg. Cable stiffness was kept constant at 73,888 kN/m, and water depth was 160 meters.

Response amplitudes for sway, heave, and roll, respectively, versus initial cable tension are depicted in Figures 62-64 for a 90° wave incidence angle. A significant decrease in response can be seen for initial tensions of up to 45,000 kN/leg in the case of sway and heave, and 35,000 kN/leg in the case of roll. As the initial tension is increased further, the response amplitudes start to increase until they reach a peak and then decrease again. While one would expect a continuous decrease in response from an increase in initial tension, the results obtained here show that this is not always the case. For the range of initial tensions where the

response amplitudes increase, the structure's stiffness changes and the natural periods of vibration reach a range where the forcing function can cause resonance (see Figure 64).

e) Direction of Wave Propagation

In order to gain a better understanding of the effects of change in direction of wave propagation on the response of the structure, the platform properties and member dimensions were modified slightly such that the structure becomes symmetric. The angle of wave propagation (α) was varied in the range between zero and 90°. Figure 65 shows the response of surge and sway to direction of wave propagation. The shapes of the curves are close to parabolic and, as is expected, symmetric about and with peak response at $\alpha = 45^o$.

The variation of heave response amplitude with respect to angle of wave propagation is illustrated in Figure 66. The heave response is minimum at both $\alpha = 0^o$ and $\alpha = 90^o$, maximum at $\alpha = 45^o$ and symmetric about $\alpha = 45^o$. This plot is similar to a combined surge-sway plot because of the coupling of heave to both surge and sway. The variation of pitch and roll response amplitudes is presented in Figure 67. As shown in the plots, pitch varies nearly parabolically for $\alpha < 45^o$ and linearly for $\alpha > 45^o$, and roll varies linearly for $\alpha < 45^o$ and parabolically for $\alpha > 45^o$. Pitch and roll curves also are symmetric about $\alpha = 45^o$.

The yaw response variation with respect to   is shown in Figure 68. Zero yaw occurs at $\alpha = 0^o$, $\alpha = 90^o$, and $\alpha = 45^o$ (since the structure is made symmetric). Maximum yaw occurs at $\alpha = 20^o$ and $\alpha = 70^o$ and the yaw curve is symmetric about $\alpha = 45^o$.

4. Illustrations of Nonlinearity and Coupling

Drag terms have been shown to reduce maximum displacement response

amplitudes by as much as 35 percent. Nonlinearities in the stiffness relationships also are significant. The variation of leg stiffnesses with respect to surge displacement is shown in Figure 69. It can be seen that the force-displacement relationship may be considered linear for surge displacements of up to 5 meters without appreciable error. However, for larger displacements the computed forces differ significantly from those projected by an assumed linear stiffness.

The effect of coupling is apparent from a comparison of the responses computed assuming coupled and uncoupled degrees of freedom, respectively. A force-pitch displacement curve is presented in Figure 70. Whereas the curve obtained assuming coupled pitch and surge exhibits a hysteretic characteristic, the straight line represents the results if no coupling is assumed. A similar comparison for heave displacement response is presented in Figure 71. In both cases there is substantial difference between the uncoupled and coupled to surge response.

5. Summary of Response to Waves

The dynamic analysis model developed as part of this research was thoroughly tested for response to water waves. A parametric analysis study was performed in an effort to emphasize the relative importance of each individual parameter to the behavior of tension-leg platforms. The dynamic response in all of the structures six degrees of freedom were plotted versus each parameter. Important concepts can be obtained from these plots in order to optimize the design of TLP's. In comparison with Ref. 10, the general trends of the response amplitudes are found to be in agreement. However, since the authors of Ref. 10 normalized their response amplitudes with respect to the wave height, no attempt is made to compare numerical values of response amplitudes for specific wave periods.

C. Response to Earthquake Forces

The dynamic analysis model presented in this report was tested for wave forces, and a parametric analysis was performed. The results obtained show that the model successfully simulates the dynamic behavior of tension-leg platforms subjected to ocean waves. In this section, the response behavior of the platform subjected to ground motion is studied using the above model.

Two cases were studied: case 1 for earthquakes occurring in a calm sea, and case 2 for earthquakes and waves occurring simultaneously. The derivation of earthquake forces and corresponding fluid drag and inertial forces arising from relative motion between structure and fluid particles for a calm sea (case 1) is given elsewhere in the report. The forces for case 2 are easily obtained by superimposing the inertial forces from ground motion onto forces developed for waves only. The correctness of the forces derived in case 1 was checked by comparing the response obtained from case 1 with that obtained from case 2 (setting wave height equal to zero to simulate a calm sea).

1. Time Histories

Earthquake excitation consists of horizontal and vertical base accelerations based on ground motion records. The primary earthquake record used in the analysis was the El Centro earthquake of 1940. Figure 72 shows the time history of the east-west component of the El Centro earthquake. Other ground motion records used include Pacoima Dam and Kern County earthquakes.

Response time histories of surge, heave, and pitch for El Centro earthquake occurring in a calm sea are shown in Figures 73-75. Surge response during the 30-second duration of the earthquake reaches a maximum

of 2 meters. At the end of the 30 seconds the structure attains some velocity and displacement that act as initial values for the free vibration of the platform. The surge response reaches a maximum of about 3.5 meters in the free vibration region. Heave and pitch arise from the coupling effects that associate them with surge, but their magnitudes are found to be small.Also, a time history of surge response to Pacoima Dam earthquake is shown in Figure 76. The maximum surge in this case was about 0.6 meters.

Earthquakes may also occur simultaneously with waves. Figure 77 illustrates the time history response of surge to a combined loading of El Centro (EW) earthquake and a 17-second wave. The response is dominated by the wave forces rather than by the earthquake. While the effect of earthquakes on the displacement time history of surge is small for combined waves and earthquakes, the effect on the acceleration time history is significant. The maximum acceleration caused by the wave only is 0.7 m/sec^2 and that from the earthquake and wave combined is 2.0 m/sec^2. In this case the increase of surge acceleration caused by the earthquake is found to be as much as 300%.

2. Initial Conditions

Initial conditions for the combined earthquake and wave loading are of two types: (1) initial displacement and velocity of the earthquake time history, and (2) initial displacement, velocity, and acceleration of the structure. The initial velocity and displacement for the ground motion record are on the order of few centimeters and centimeters per second, respectively. The structure's initial displacement and velocity arising from wave action just before the earthquake occurs, however, are on the order of meters and meters per second, respectively. Therefore any initial conditions for the earthquake time history are negligible compared to those
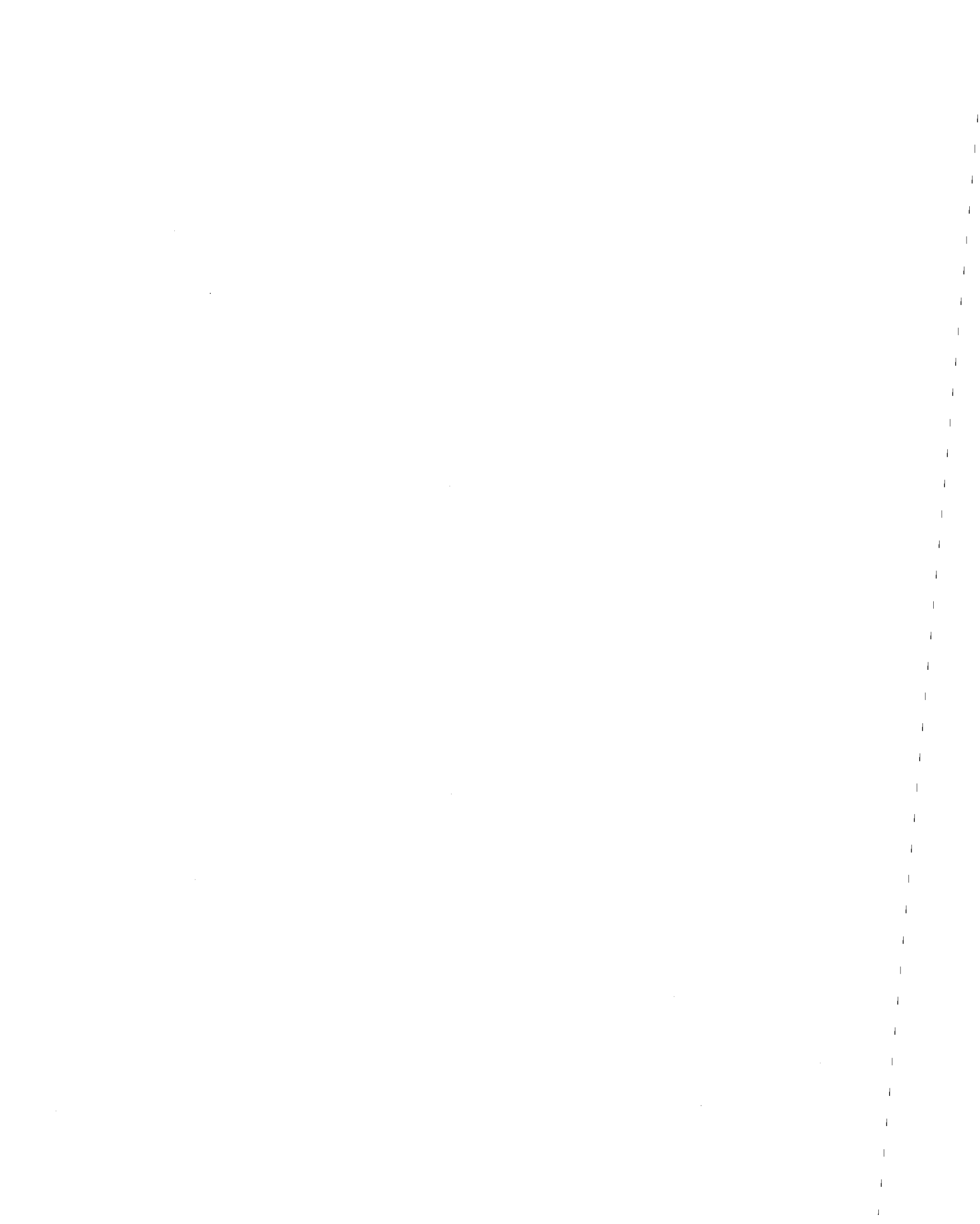
of the structure just before the earthquake occurs. Therefore, for sim-
plicity's sake, zero initial conditions were assumed for the ground.

To emphasize the effect of initial conditions on the time history of
surge, first the wave was started and then the earthquake was introduced
some time after the wave loading had started. The surge time history re-
sponses for a 17-second wave with El Centro (EW) earthquake introduced at
t = 7 seconds and at t = 16 seconds, after the onset of the wave, is shown
in Figure 78. It can be seen that the time histories are affected by the
initial conditions of the structure at the time of the earthquake. How-
ever, this does not seem to have a significant effect on the displacement
time histories because of the dominance of wave induced displacements.

3. Water Depth

The effect of variations in water depth for both earthquake and com-
bined wave and earthquake loading was studied. A time history of surge re-
sponse to only earthquake motion for a water depth of 1000 meters is pre-
sented in Figure 79. The maximum surge attained is 8.5 meters at the peri-
od of 170 seconds, while that for a 200-meter water depth (see Figure 72)
was 3.5 meters at a period of 75 seconds. Hence, both amplitude and period
of surge response increase with water depth. Surge response amplitudes are
plotted versus water depth for three cases (Figure 80): earthquake only,
wave only, and wave and earthquake combined. It can be seen that the re-
sponse amplitude varies nonlinearly with water depth for all three cases.
A similar plot for heave response amplitude versus water depth is presented
in Figure 81.

4. Comparison

A comparison of the time histories and response amplitudes for the

above three cases is presented in order to evaluate the effect of earthquakes on the motion of the platform. Time histories of surge response to waves and combined wave and earthquake forces in a water depth of 1000 meters are shown in Figure 82. The increase in response amplitude caused by the inclusion of the earthquake is as much as 10 percent for this case. The same percentage of increase as above can be seen in Figure 83 for a 200-meter water depth with the earthquake introduced at t = 200 seconds (i.e., in the steady state region of the vibration).

Referring to Figures 80 and 81, it can be seen that to predict the response amplitude for combined wave and earthquake loading, one cannot simply superpose the maximum response amplitude arising from only earthquake forces to that arising from only wave forces. For example, at a water depth of 1000 meters the maximum surge response amplitude caused by earthquake motion alone is 8.5 meters; that from wave action alone is 26.5 meters; and that associated with the combined loading is 29.0 meters. Therefore, it would be too conservative to design for 35.0 meters (26.5 + 8.5) instead of for 29.0 meters. The reason that superposition does not apply in this case is that the peak responses from earthquake forces are out of phase with those caused by wave forces. Similarly, the maximum heave respose cannot be obtained from a superposition of the separate loadings; however, in some cases the sum of maximum heave response to individual loadings is less than the value obtained for the combined loading (see 800-meter water depth). This phenomena is another illustration of the importance of coupling between heave and surge responses.

5. Summary

Time histories of response to earthquake loading and to combined wave and earthquake forces were obtained. The displacement response from
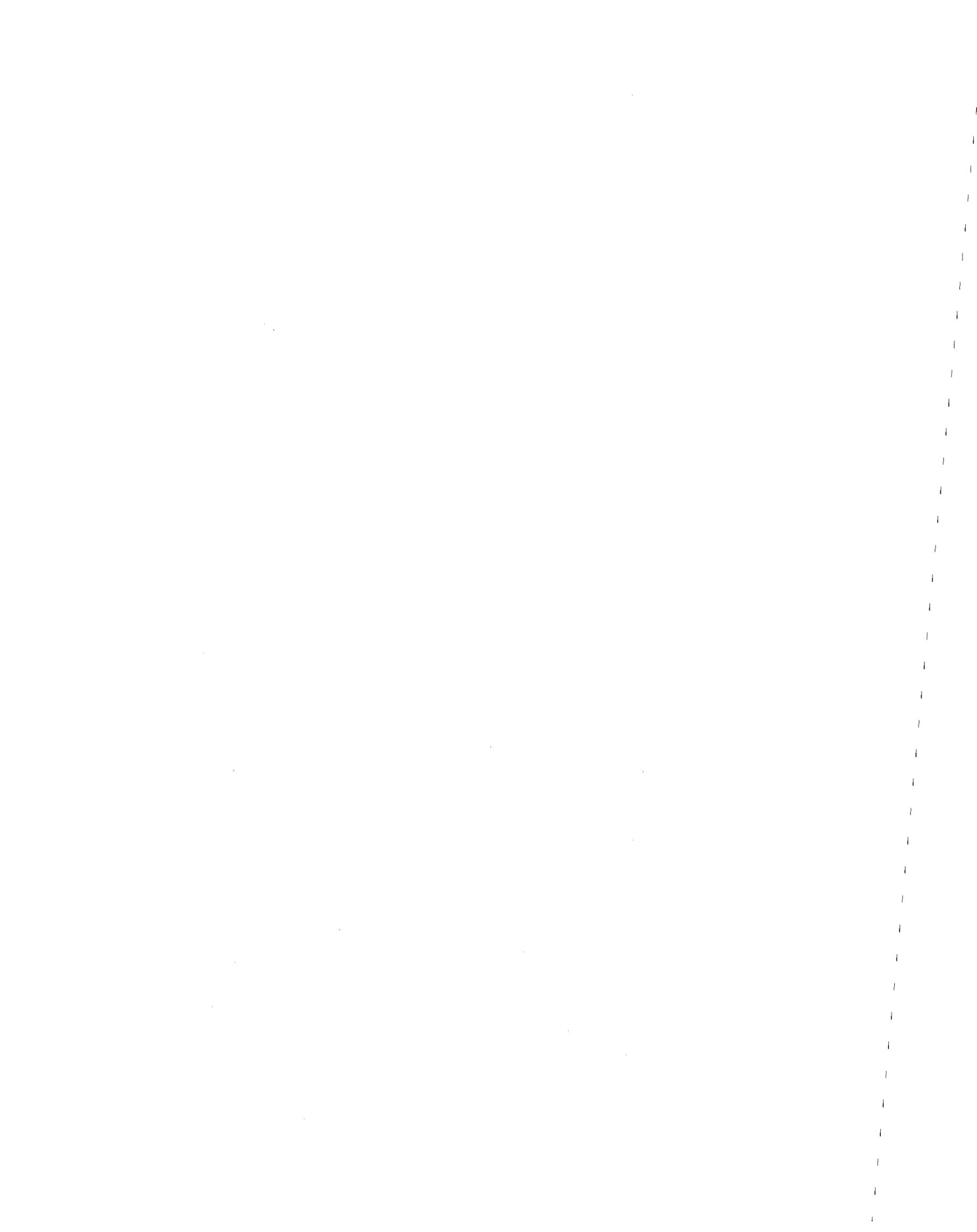
combined loading was found to be dominated by the wave. However, the accelerations were significantly affected by the earthquake. The maximum acceleration was found to be up to three times that caused by waves alone. The earthquake was introduced at different time spacings measured from the starting time of the wave in order to cover as many different initial conditions as possible. Water depth was varied and its effect on the response amplitudes was studied. An increase of about 10% in displacement response amplitudes due to earthquake forces was noticed throughout the range of water depths used in the analysis.

IV. SUMMARY, CONCLUSIONS

AND RECOMMENDATIONS

A. Summary

In this study, a complete nonlinear deterministic dynamic analysis model for tension-leg platforms has been developed and response of the platforms to wave and earthquake loadings have been studied. The accomplishments in the development of the dynamic analysis model include:

1) The formulation of closed form nonlinear coupled stiffness coefficients and the formation of a stiffness force vector.

2) Derivation of closed form forcing functions for waves and earthquakes using Morison's equation (modified to include relative motion between structure and fluid particles). Both inertial and drag components of the forcing functions were included, and wave kinematics were obtained from the linear wave theory. Integration of the force equations along the length of each submerged member of the platform was carried out manually, thereby reducing the total cost of dynamic analysis significantly.

3) Development of a mathematical model based on a set of coupled nonlinear differential equations whose solution yields the dynamic response of the platform.

4) Development of a compact and inexpensive computer code to perform the numerical calculations of the motion of tension-leg platforms. The computer progam employs Newmark's Beta method to integrate the equations of motion sequentially in time and obtain time histories of the response.

B. Conclusions

Response time histories for each of the six degrees of freedom of the platform were obtained. A parametric analysis was carried out in order to identify the important parameters involved in the behavior of tension-leg platforms. The following conclusions can be made with regard to the platform behavior and response to dynamic loading:

1) Coupling can significantly affect the behavior of the structure. The strongest coupling exists between heave and sway and between heave and surge. The coupled heave response amplitude is several times larger than the uncoupled amplitude. Therefore, neglecting coupling can result in a significant underestimation of response.

2) Two types of nonlinearities are inherent in the analysis: (1) nonlinearity of stiffness force vector arising from large displacements, and (2) nonlinearity of the forcing function arising from the square of velocity terms in the drag force calculations. The stiffness nonlinearity is found to be insignificant if surge and sway are less than approximately 5 meters. However, for large sway and surge, neglecting stiffness nonlinearity can lead to an overestimation of the response amplitudes. Nonlinearity in drag forces is found to be significant in that it represents the fluid damping arising from the relative motion between the structure and fluid particles and therefore leads to response reduction with time.

3) Variation of wave period shows that surge, sway, and heave are most significant for high wave periods (i.e., periods greater than 15 seconds) and pitch and roll are most significant for periods around 5 seconds.

4) Variation of wave height shows linear relationships for wave heights less than about 15 meters and becomes nonlinear for larger wave heights.

5) Increasing the leg stiffness tends to decrease response; however, for leg stiffness larger than 20,000 kN, little effect on response was noticed.

6) Increasing water depth results in an increase in surge, sway, pitch, and roll response and a decrease in heave response.

7) Higher initial tensions tend to make the structure stiffer, hence it reduces the response. However, as the stiffness increases, the period of vibration decreases; and as it approaches that of the wave, higher response amplitudes are observed.

8) Coupling between pitch or roll and surge or sway has been shown to have a significant effect on computed responses. The extent of this coupling is dependent on the location of the center of rotation, which can be expected to migrate with the level of response. Most results reported herein are based on rotations centered at the base of the hulls, which minimizes the interaction between pitch and surge. Further research is needed to establish an appropriate location for the center of rotation or to determine the expected variations of its location.

9) The displacement response to combined wave and earthquake loading was found to be dominated by the wave. A uniform increase in response of approximately 10% arising from the inclusion of earthquakes was observed. The accelerations, however, were significantly affected by the earthquake. The maximum acceleration was found to be three times that caused by waves alone.

C. Recommendations

The model developed herein is adapted to the response of tension-leg platforms; however, the wave force section could be easily applied to any problem. Several enhancements would allow the model to be adapted to a wider range of problems (i.e., shallower water, larger members, larger wave heights, etc.). These enhancements include:

1) Application of higher order wave theories.

2) Employing the diffraction theory for computing wave forces on large members at low wave periods.

3) Aplication of a random sea state.

4) Varying coefficients of added mass and damping with respect to time.

5) Variations in location of the center of rotation.

REFERENCES

1. Burke, B. G., "The Analysis of Motions of Semi-Submersible Drilling Vessels in Waves," Proceedings of 1st Annual Offshore Technology Conference, 1969, paper OTC 1024.

2. Pauling, J. R. and E. E. Horton, "Analysis of the Tension-Leg Stable Platform," Proceedings of 2nd Annual Offshore Technology Conference, 1970, paper OTC 1263.

3. Burke, B. G. and J. T. Tighe, "A Time Series Model for Dynamic Behavior of Offshore Structures," Proceedings of the 3rd Annual Offshore Technology Conference, 1971, paper OTC 1403.

4. Garrison, C. J., "Dynamic Response of Floating Bodies," Proceedings of 6th Annual Technology Conference, 1974, paper OTC 2067.

5. McDonald, R. D., "Design and Field Testing of the Triton Tension Leg Fixed Platforms," OTC 2104, 1974.

6. Kirk, C. L. and R. K. Jain, "Wave Induced Oscillations of Tension-Leg Single Buoy Mooring Systems," Proceedings of 8th Annual Offshore Technolgy Conference, 1976, paper OTC 2494.

7. Natvig, G. J. and J. W. Pendered, "Nonlinear Motion Response of Floating Structures to Wave Excitation," Proceedings of 9th Annual Offshore Technology Conference, 1977, paper OTC 2796.

8. Albrecht, H. G., D. Koenig, "Non-Linear Dynamic Analysis of Tension-Leg Platforms, for Medium and Greater Depths," Proceedings of 10th Annual Offshore Technology Conference, 1978, paper OTC 3044.

9. Denise, J. P. F. and N. J. Heaf, "A Comparison Between Linear and Non-Linear Response of a Proposed Tension-Leg Production Platform," Proceedings of 11th Annual Offshore Technology Conference, 1979, paper OTC 3555.

10. Kirk, C. L. and E. U. Etok, "Dynamic Response of Tethered Production Platforms in a Random Sea State," Second International Conference on Behavior of Offshore Structures, London, August 1979.

11. Jeffrys, E. R. and Patel, M. H., "Dynamic Analysis Models of Tension Leg Platforms," Proceedings of 13th Annual OTC, 1981, paper OTC 4075.

12. Airy, G. B., "On Tides and Waves," Encyclopedia Metropolitania, London, 1845.

13. Garrison, C. J., "Drag and Inertia Coefficients in Oscillatory Flow about Cylinders," ASCE National Water Resources and Ocean Engineering Convention, 1976.

14. U. S. Army Coastal Engineering Research Center, Offshore Protection Manual, Dept. of the Army Corps of Engineers, Fort Belvoir, Va., 1977.

15. Morison, J. R., O'Brien, M. P., Johnson, J. W. and Shaaf, S. A., "The Forces Exerted by Surface Waves on Piles," Petroleum Transaction, 1950, AIME, Vol. 189.

16. Newmark, N. M., "A Method of Computation for Structural Dynamics," Transactions, ASCE, Vol. 127, pp. 1406-1435, 1962.

17. Stokes, G. G., "On the Theory of Oscillatory Waves," Transactions Camb. Phil. Soc. 8, pp. 441, 455, 1847.

18. Dean, R. G., "Stream Function Representation of Nonlinear Ocean Waves," Journal of Geophysical Research, Vol. 70, No. 18, Sept. 1965, pp. 4561-4572.

19. Leonard, J. W., Garrison, C. J. and Hudspeth, R. T., "Deterministic Fluid Forces on Structures: A Review," Journal of Structural Division, ASCE, Vol. 107, No. ST6, June 1981.

20. Cokelet, E. D., "Steep Gravity Waves in Water of Arbitrary Uniform Depth," Institute of Oceanographical Sciences, pp. 183-230, 1977.

21. Chappelear, J. E., "Direct Numerical Calculations of Wave Properties," Journal of Geophysical Research, Vol. 66, No. 2, Feb. 1961, pp. 501-508.

22. Korteweg, D. J. and DeVries, G., "On the Change of Form of Long Waves Advancing in a Rectangular Canal, and on a New Type of Long Stationary Waves," Philosophical Magazine, 5th Series, 1895, pp. 422-443.

23. Munk, W. H., "The Solitary Wave Theory and its Application to Surf Problems," Annals of the New York Academy of Sciences, Vol. 51, 1949, pp. 376-462.

24. LeMehaute, B., An Introduction to Hydrodynamics of Water Waves, Water Wave Theories, Vol. II, TR EREL118-POL-3-2, U.S. Dept. Comm., ESSA, Washington, D.C., 1969.

25. Sarpkaya, T., "In-Line and Transverse Forces on Cylinders in Oscillatory Flow at High Reynolds Numbers," OTC Paper No. 2533, 1976.

26. Sarpkaya, T., "Hydrodynamic Drag-Wave Forces-Response of Structures to Wave Induced Loads," Lecture at University of Houston, Houston, Texas, 1979.

27. MacCamy, R. C. and Fuchs, R. A., "Wave Forces on Piles: A Diffraction Theory," U.S. Army, Beach Erosion Board, Tech. Memo No. 69, 1954.

28. Hogben, N. and Stading, R. G., "Experience in Computing Wave Loads on Large Bodies," OTC Paper No. 2189, 1975.

29. Garrison, C. J. and Stacy, R., "Wave Loads on North Sea Gravity Platforms: A Comparison of Theory and Experiment," OTC Paper No. 2794, 1977.

30. Mei, C. C., "Numerical Methods in Water Waves Diffraction and Radiation," Annual Reviews Fluid Mechanics, Vol. 0, pp. 393-416, 1978.

TABLE 1. PERIODS OF VIBRATION AND
RESPONSE AMPLITUDES*

Degree of Freedom	Period (sec)	Response Amplitude	
		Undamped	Damped
Surge	70	16.45 m	14.17 m
Sway	70	14.00 m	10.41 m
Heave	5	.97 m	.70 m
Pitch	6	.22^0	.21^0
Roll	6	.15^0	.146^0
Yaw	6	.18^0	.16^0

*T = 17 sec

H = 15 meters

= 35 degrees

TABLE 2. MAXIMUM VALUES OF VELOCITY
AND ACCELERATION*

Degree of Freedom	Maximum Velocity	Maximum Acceleration
Surge	2.51 m/s	.722 m/s^2
Sway	1.95 m/s	.520 m/s^2
Heave	.173 m/s	.076 m/s^2
Pitch	.139°/s	.119°/s^2
Roll	.095°/s	.082°/s^2
Yaw	.032°/s	.011°/s^2

*T = 17 seconds

H = 15 meters

= 35 degrees
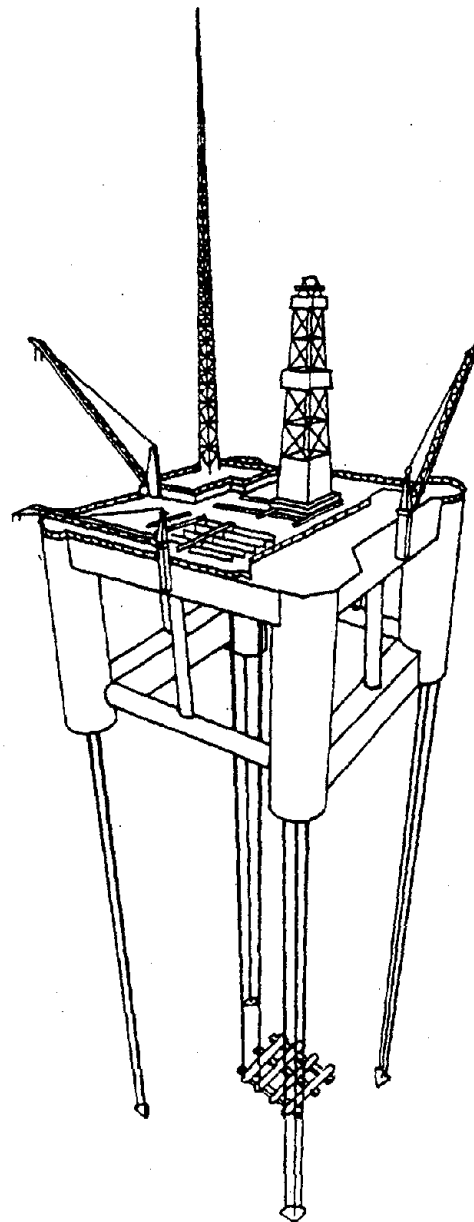
Corner Column - 16 m

Middle Column - 3.5 m

Hulls   - 13 x 9.5 m

Cross Braces   - 16 m

Figure 1. Typical Tension-Leg Platform
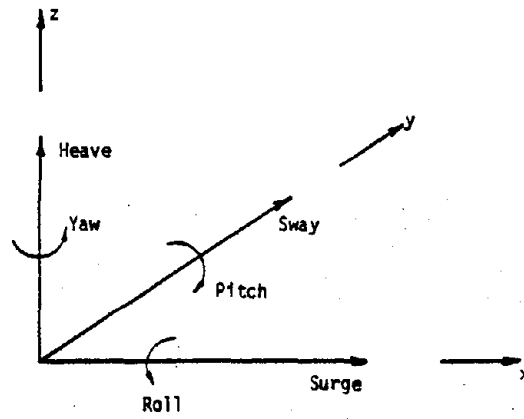
Figure 2. Coordinate System and Structural Degrees of Freedom
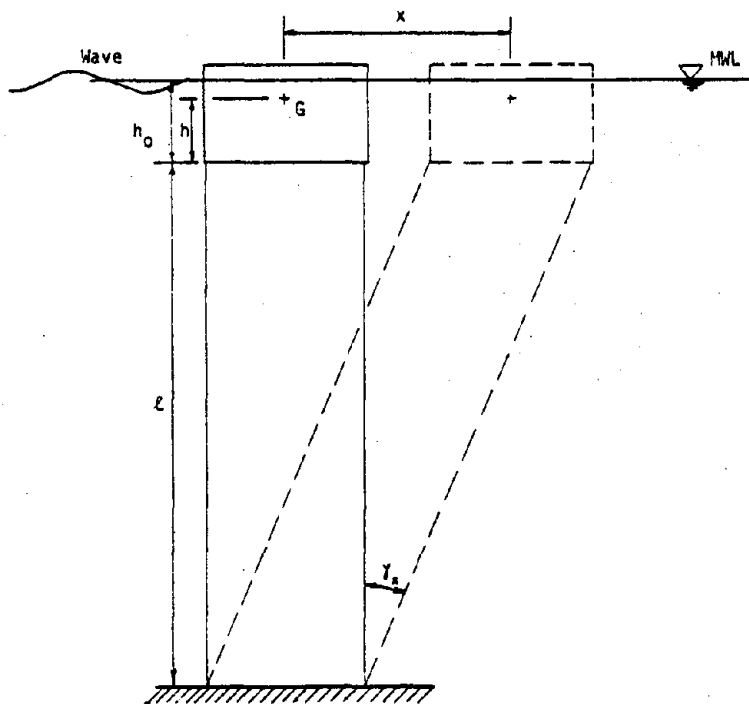
Figure 3. Buoy with a Unit Displacement in the Surge Direction
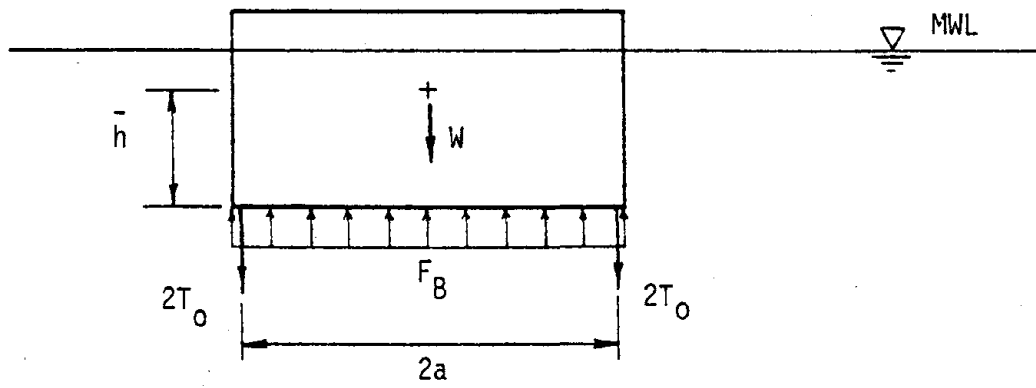
Figure 4 Static Equilibrium Forces
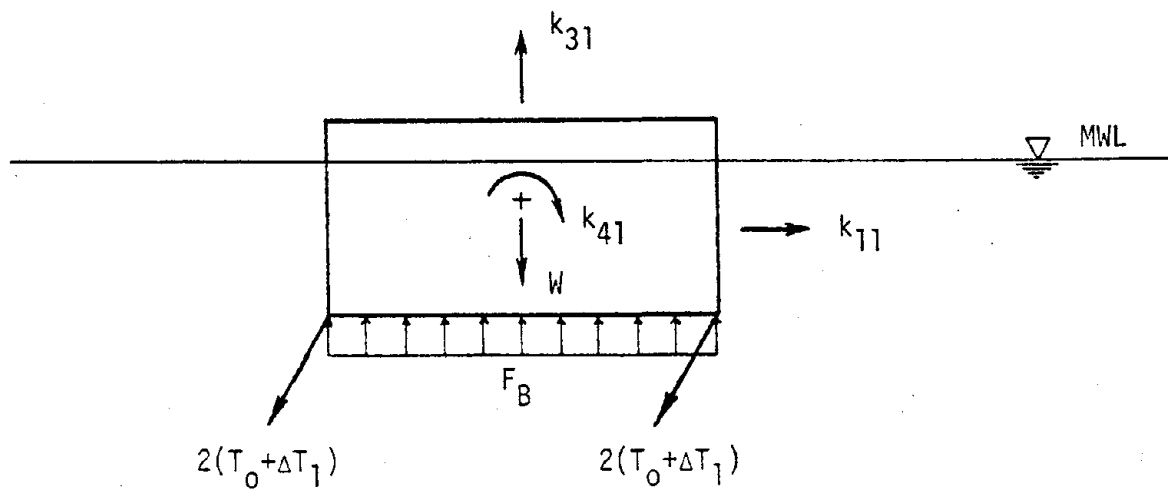
Figure 5. Forces Resulting from a Surge Displacement
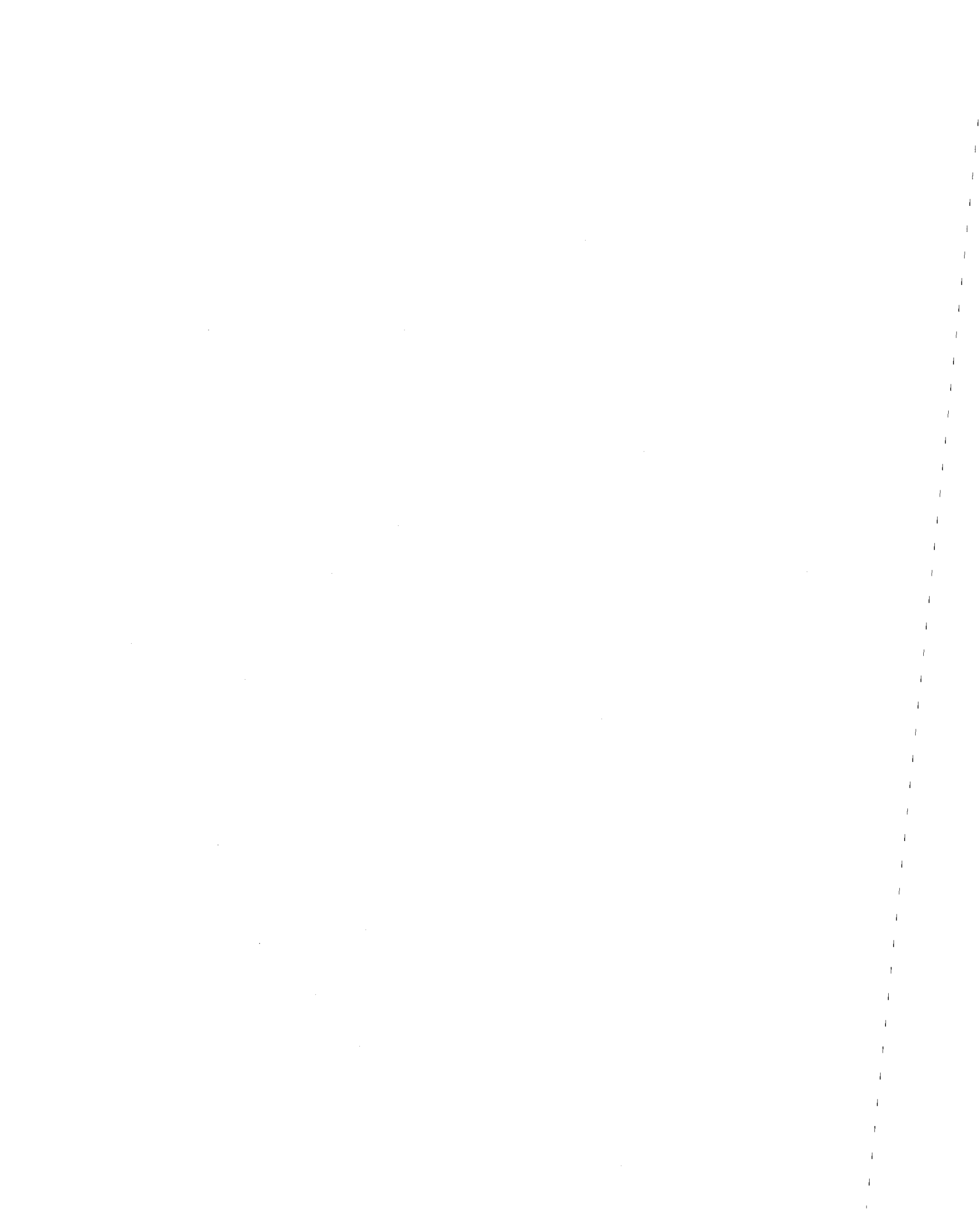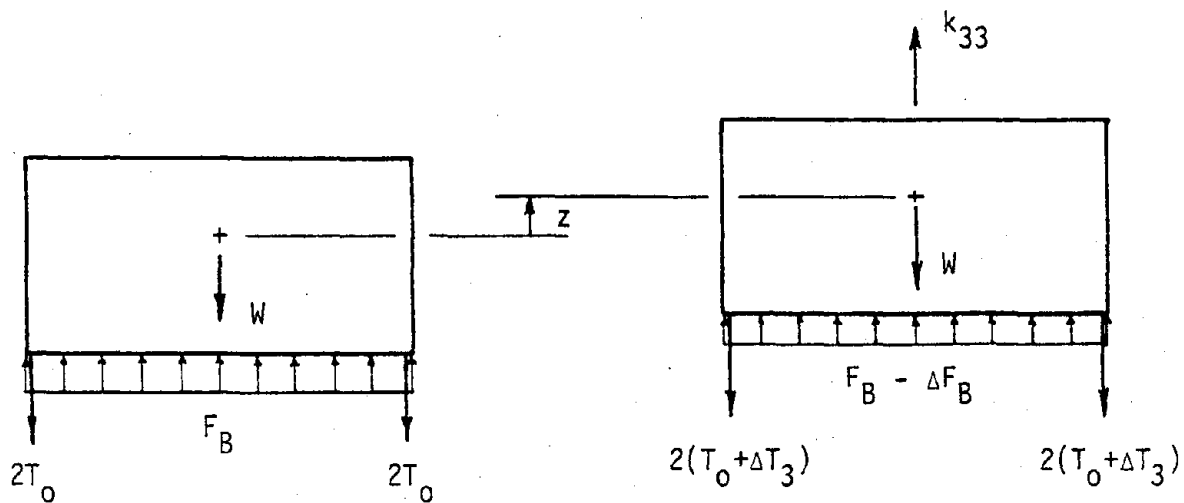
Figure 6. Restoring Forces: a) at Equilibrium Position
                         b) after Heave Displacement
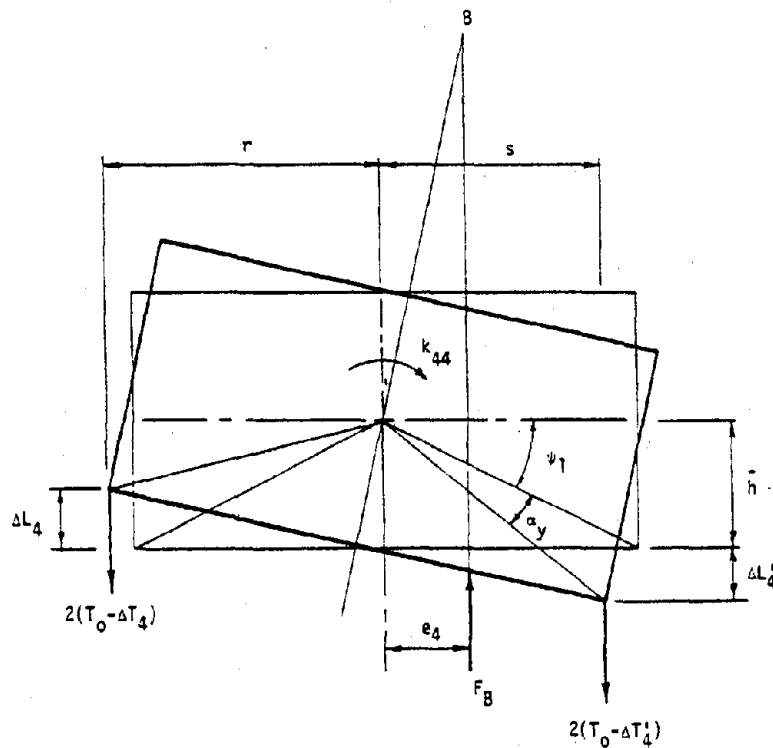
Figure 7. Restoring Forces Corresponding to a Pitch Rotation
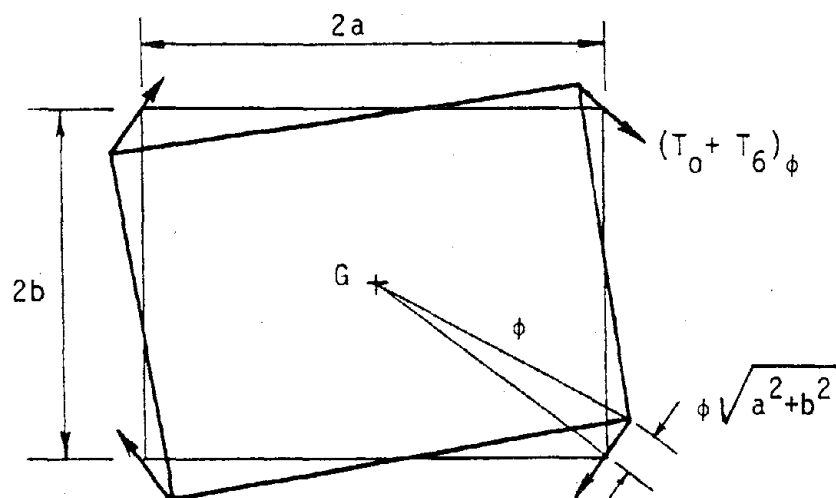
Figure 8. Horizontal Restoring Forces Corresponding to a Yaw
Rotation
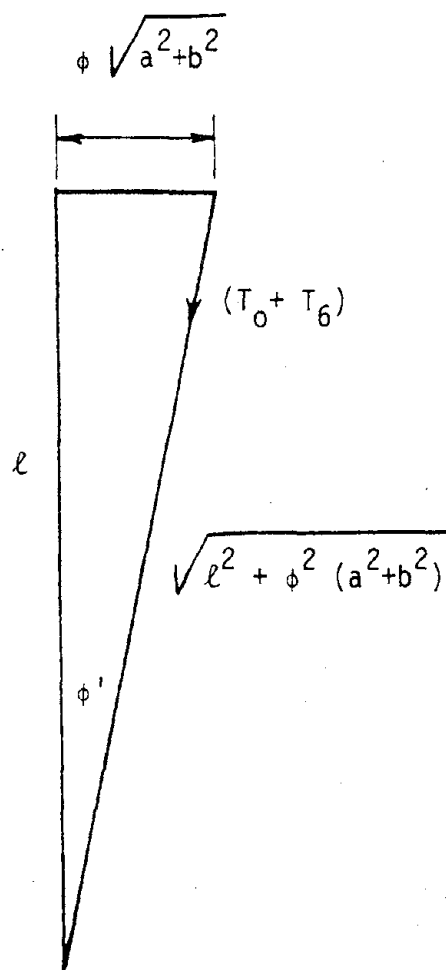
Figure 9. Leg Forces Resulting from a Yaw Rotation
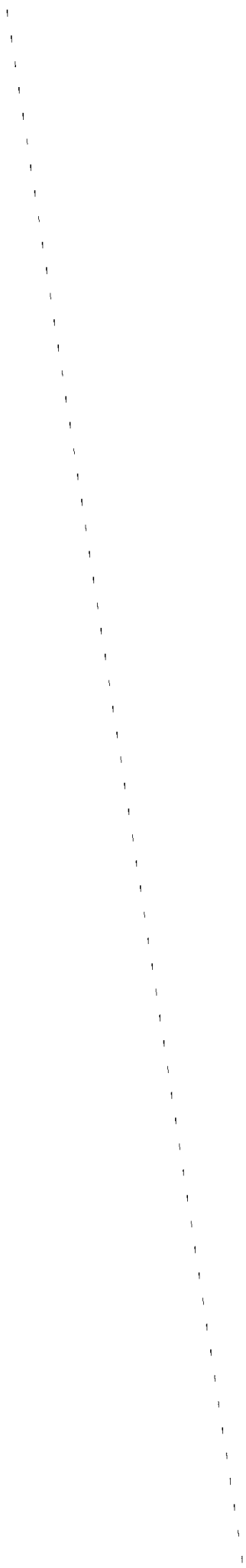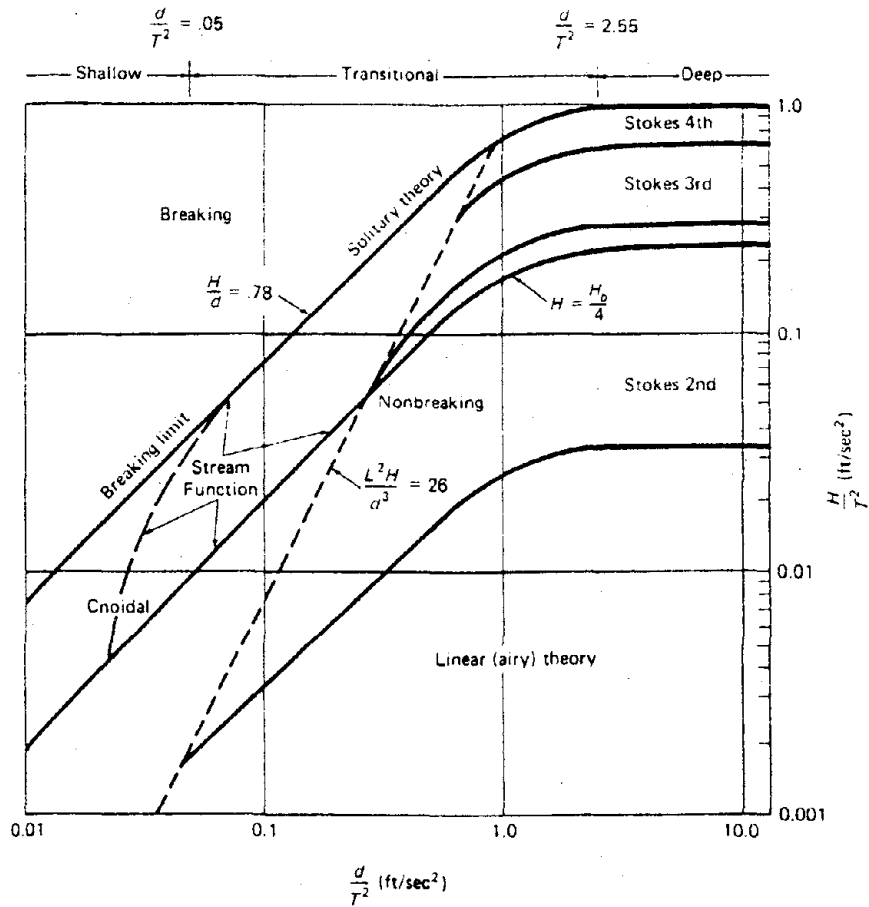
Figure 10. Regions of Validity for Various Wave Theories
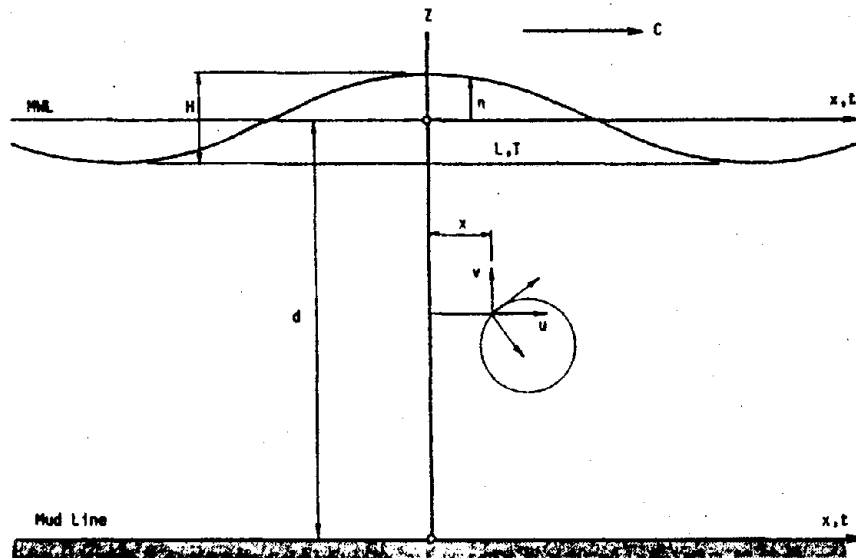
Figure 11. Schematic Diagram of Elementary, Sinusoidal Progressive
Waves
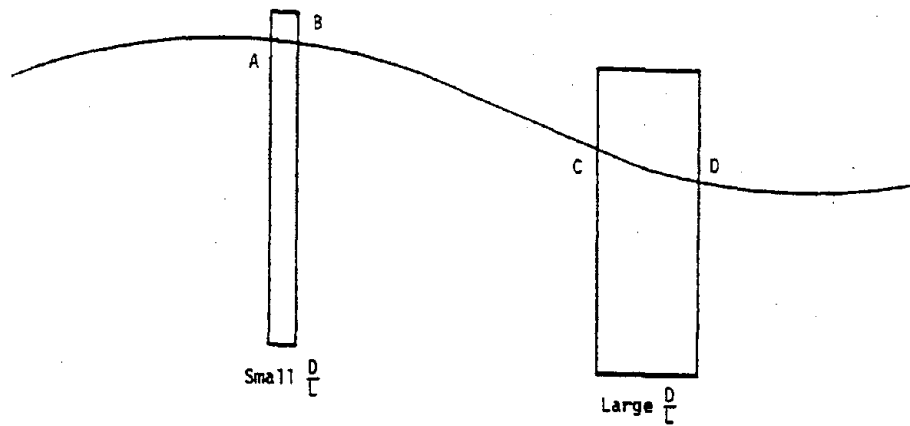
Figure 12. Variations of Wave Kinematics with Respect to Member
Diameters
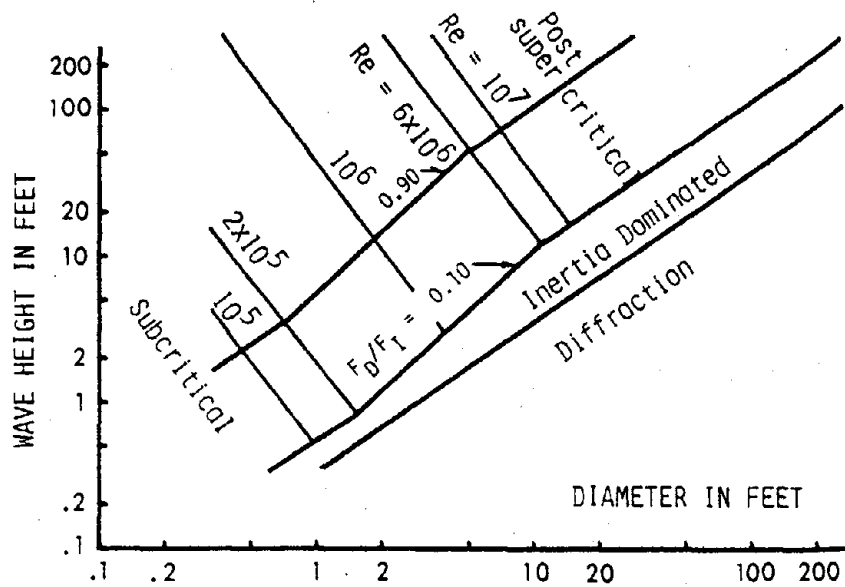
Figure 13. Classification of Various Loading Regimes
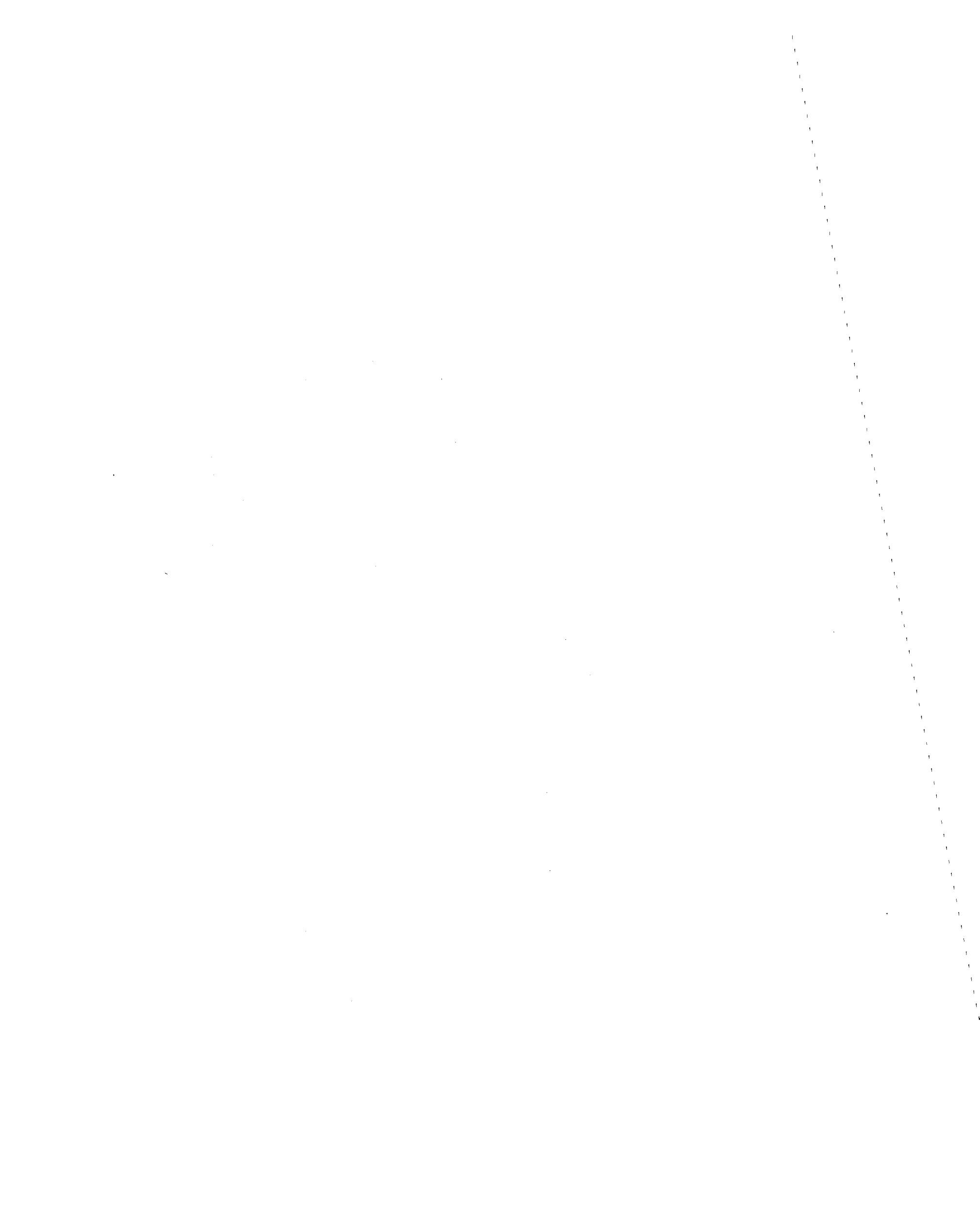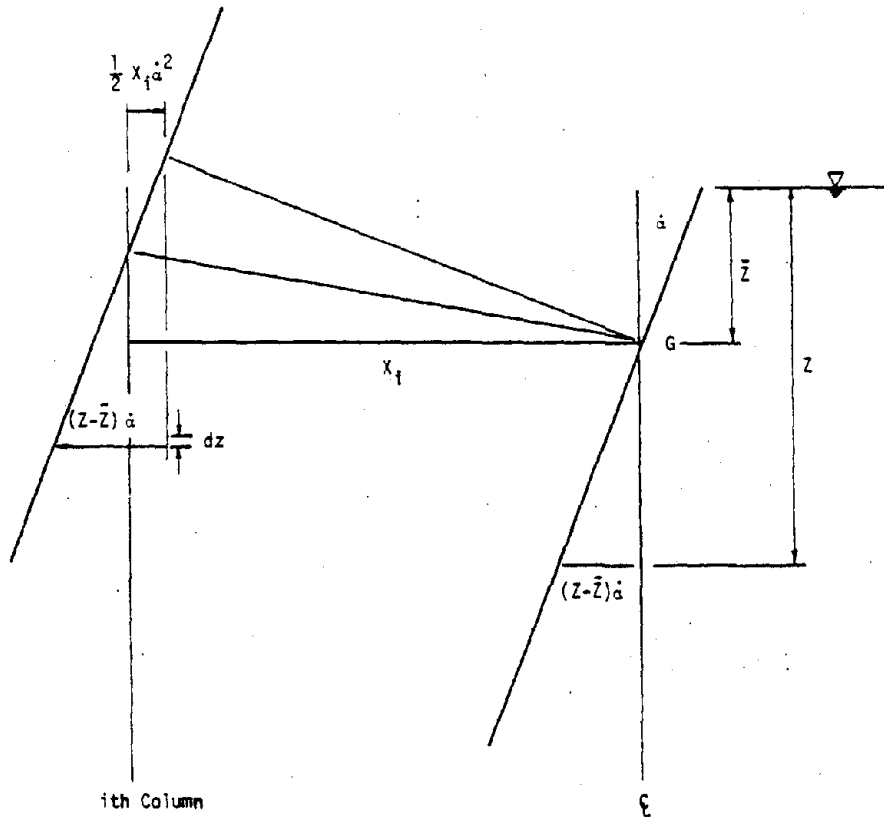
Figure 14. Velocity of Element dz Along ith Column Arising from
Pitch or Roll
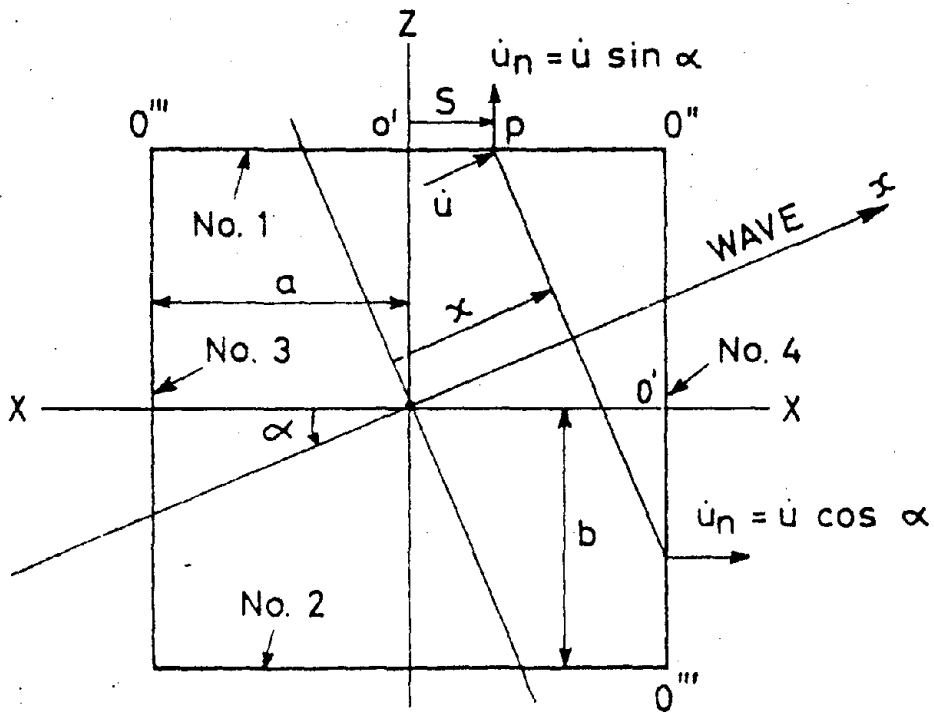
Figure 15. Plan View of Hull Locations
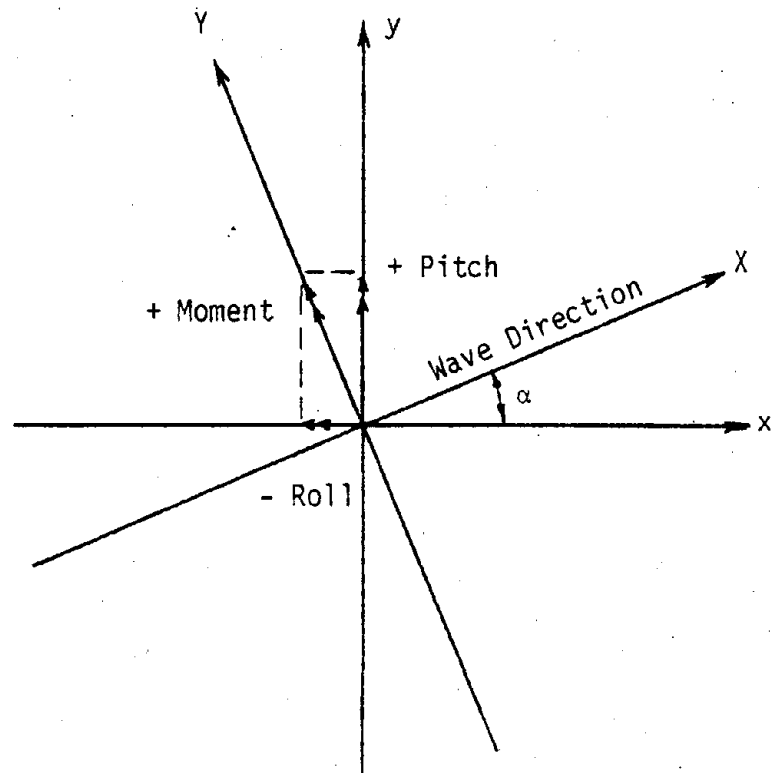
Figure 16. Pitch and Roll Components of Rotation
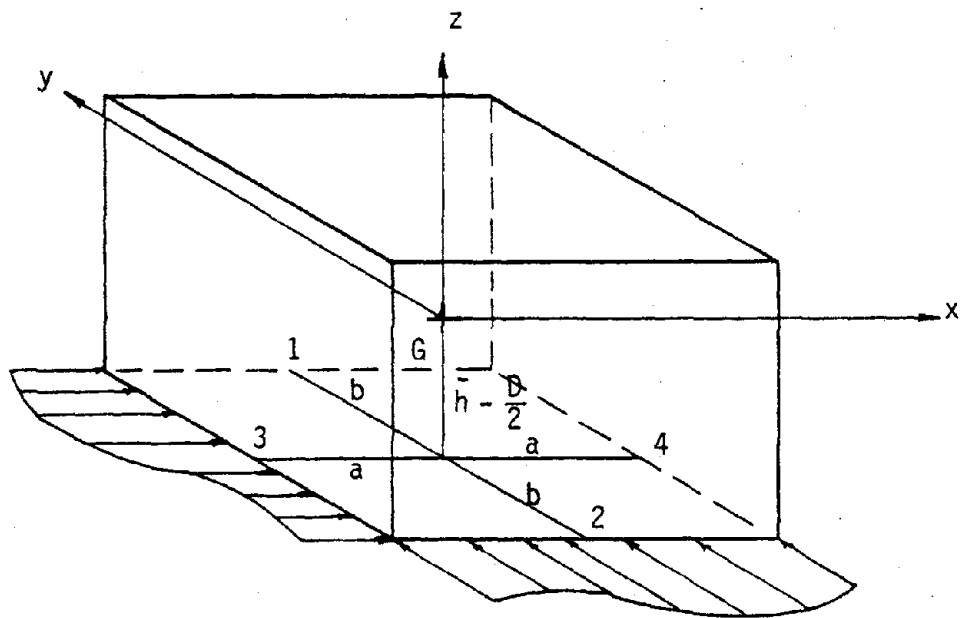
Figure 17. Horizontal Forces on Hulls
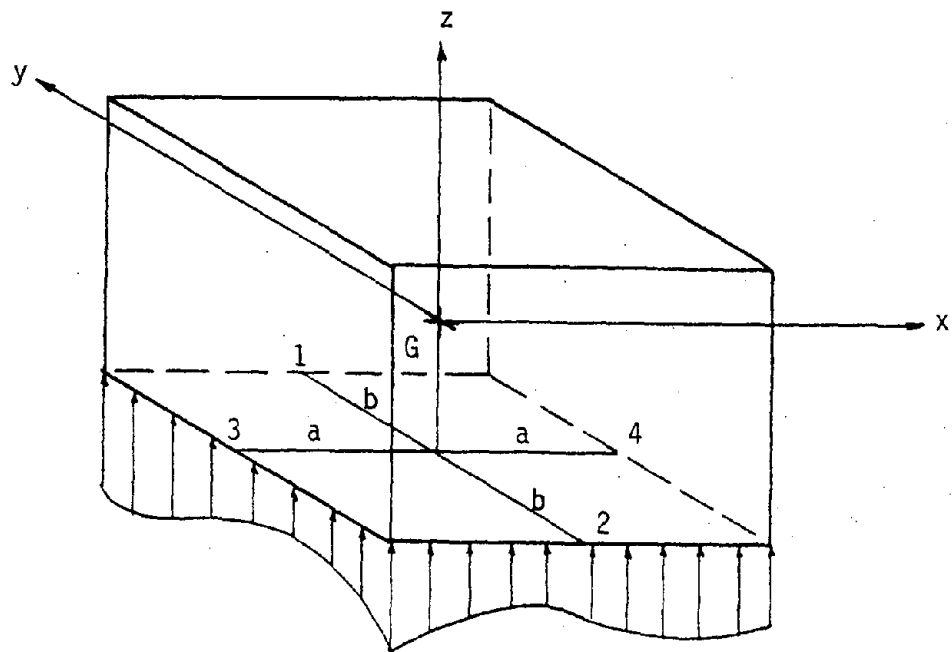
Figure 18. Vertical Forces on Hulls

START

Input: Structure geometry, dimensions, spacings, weight, masses and add masses, mass moments of inertia and added mass moments of inertia; draft height; water depth; cable length and initial tension, cable stiffness; buoyancy; wave period and wave height; coefficients of drag and inertia

Initialize displacement, velocity and acceleration vectors:
$\{x_{i,1}\} = \{\dot{x}_{i,1}\} = \{\ddot{x}_{i,1}\} = \{0\}$

$j = 1$

Assume acceleration vector for next time step
$\{x_{i,2}\} = 0$

$j = j + 1$

Calculate displacement and velocity vectors for next step according to Equations 33 and 34

Calculate forces and moments

Calculate stiffness force vector

Calcuate new values of accelerations according to Equation 35

Assumed $\ddot{x}_{i,j}$
=
Calculated $\ddot{x}_{i,j}$

$>\varepsilon$

Compare calculated and assumed accelerations

$\leq\varepsilon$

No

Check if $t = t_{final}$

Yes

Output: $x, \dot{x}, \ddot{x}$, and cable tension

Calculate maximum values

Plot Results

STOP

Figure 19. Flow Chart of Computer Program
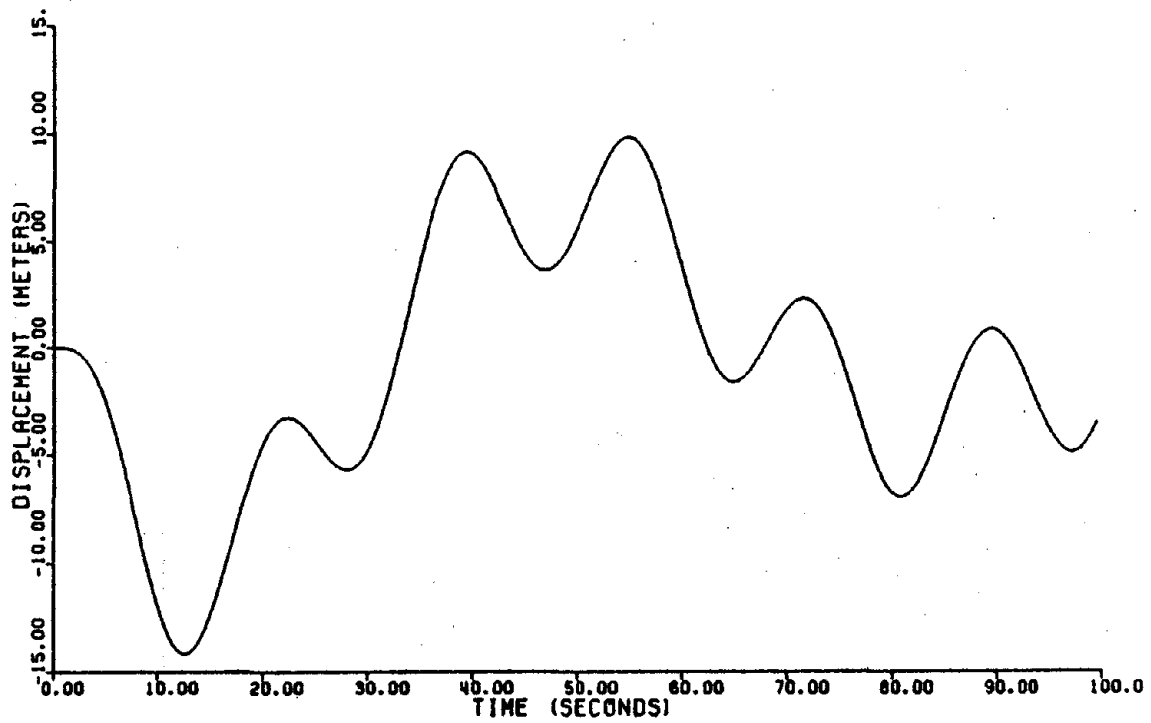
Figure 20. Time History Plot of Surge Displacement (including
Inertia and Drag Forces)
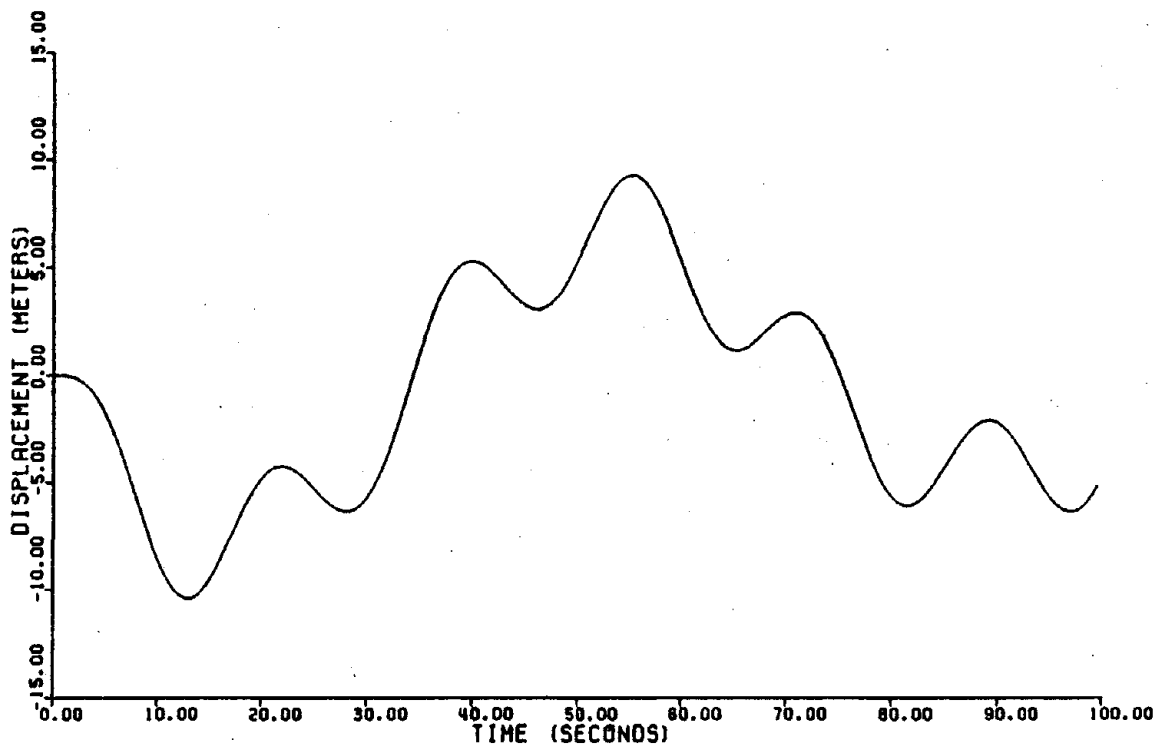
Figure 21. Time History Plot of Sway Displacement (including
Inertia and Drag Forces)
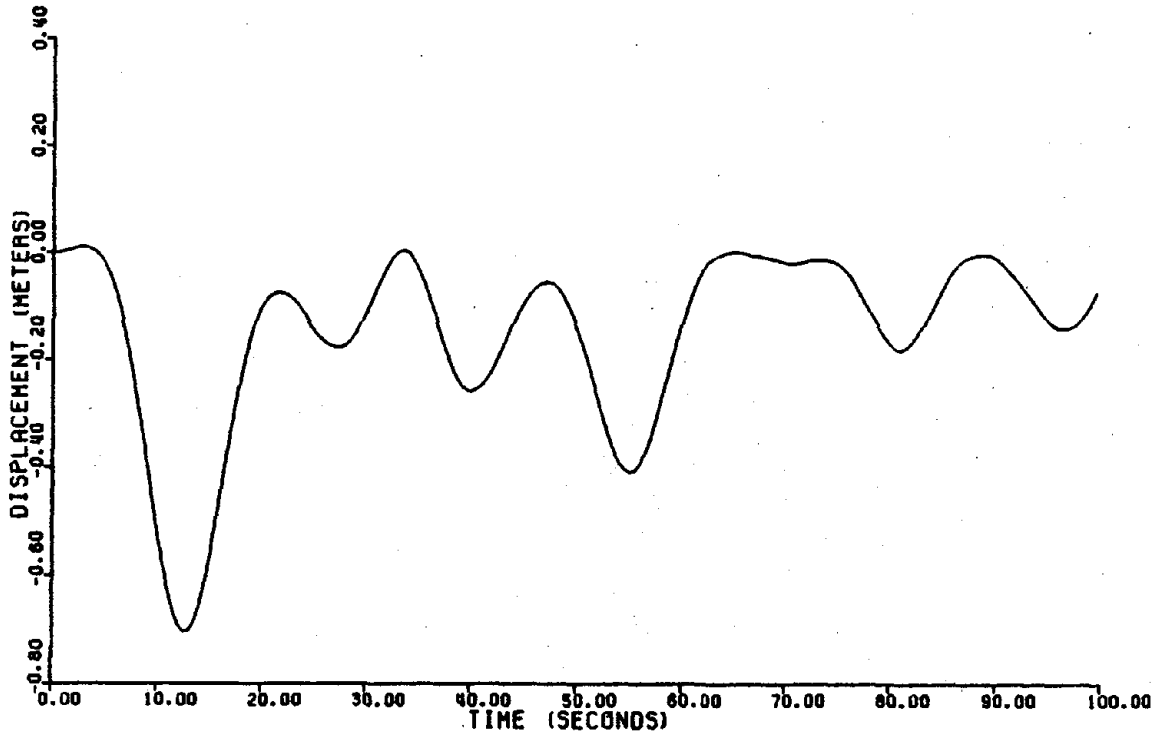
Figure 22. Time History Plot of Heave Displacement (including Inertia and Drag Forces)
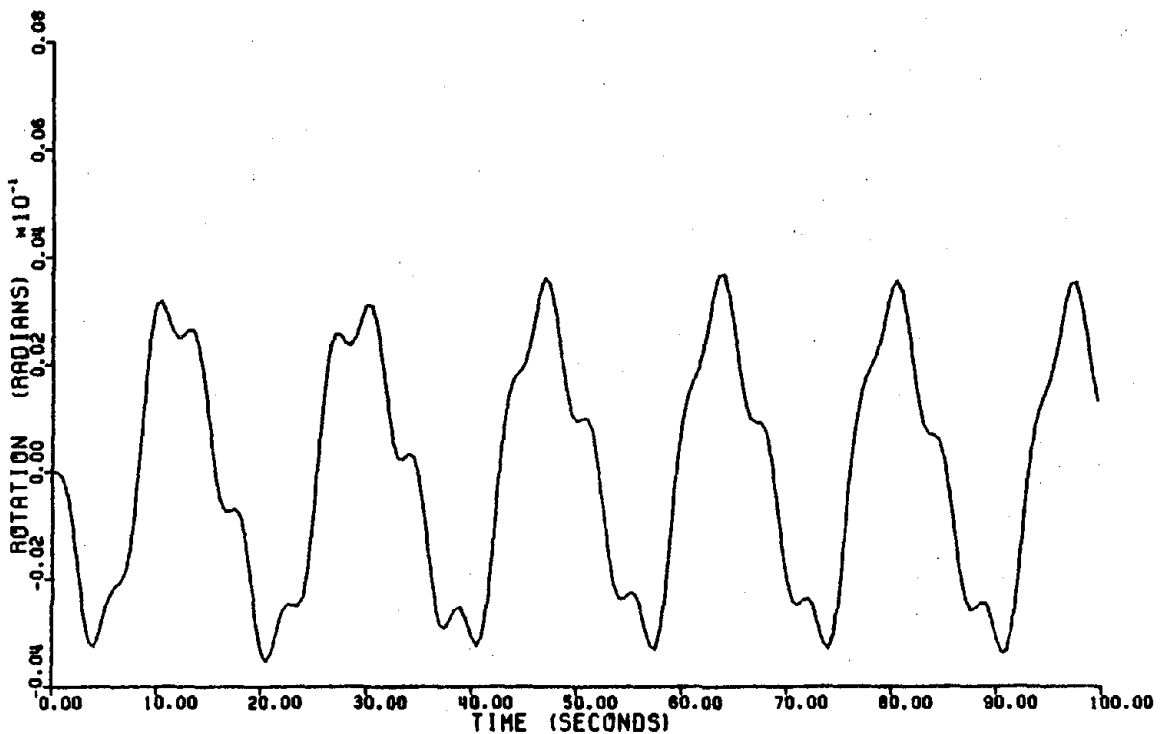

Figure 23. Time History Plot of Pitch Displacement (including Inertia and Drag Forces)
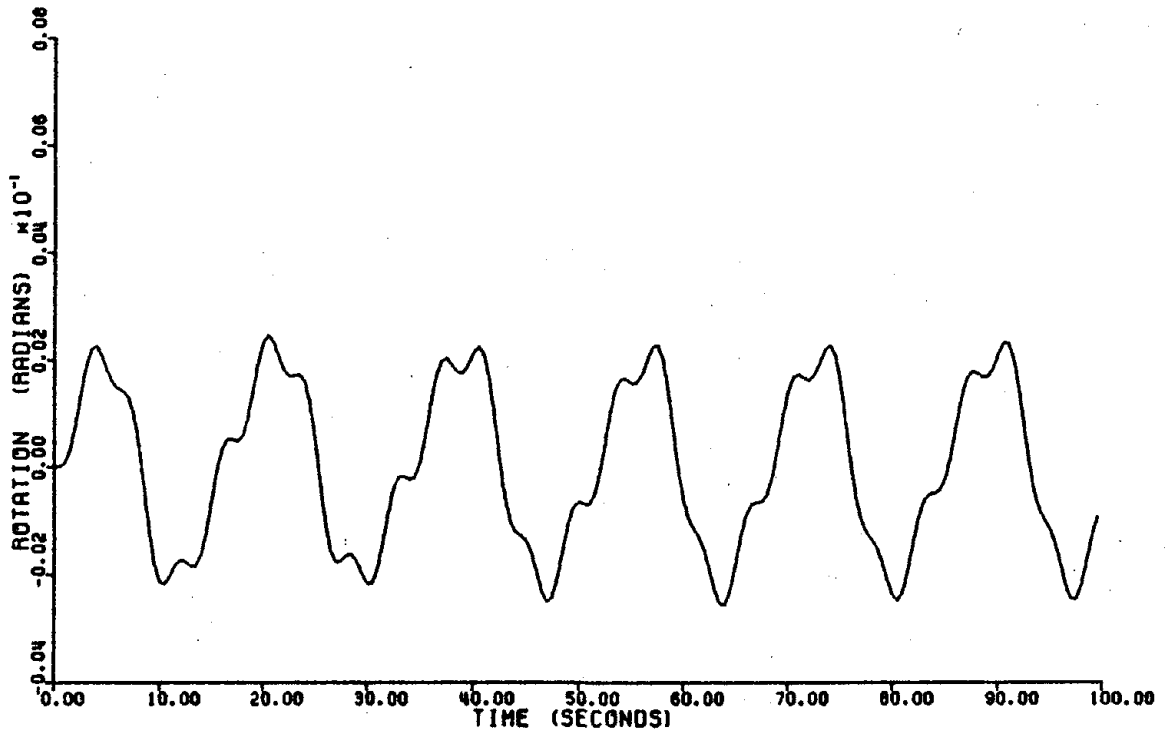
Figure 24. Time History Plot of Roll Displacement (including Inertia and Drag Forces)
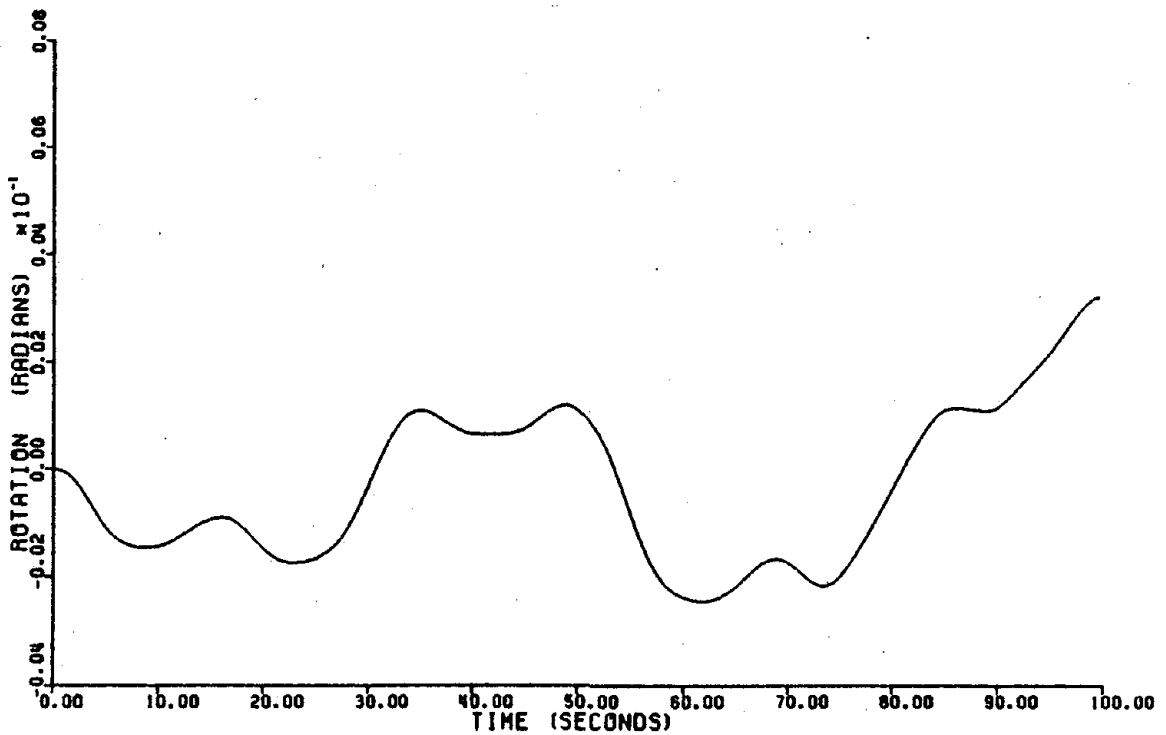
Figure 25. Time History Plot of Yaw Displacement (including Inertia and Drag Forces)
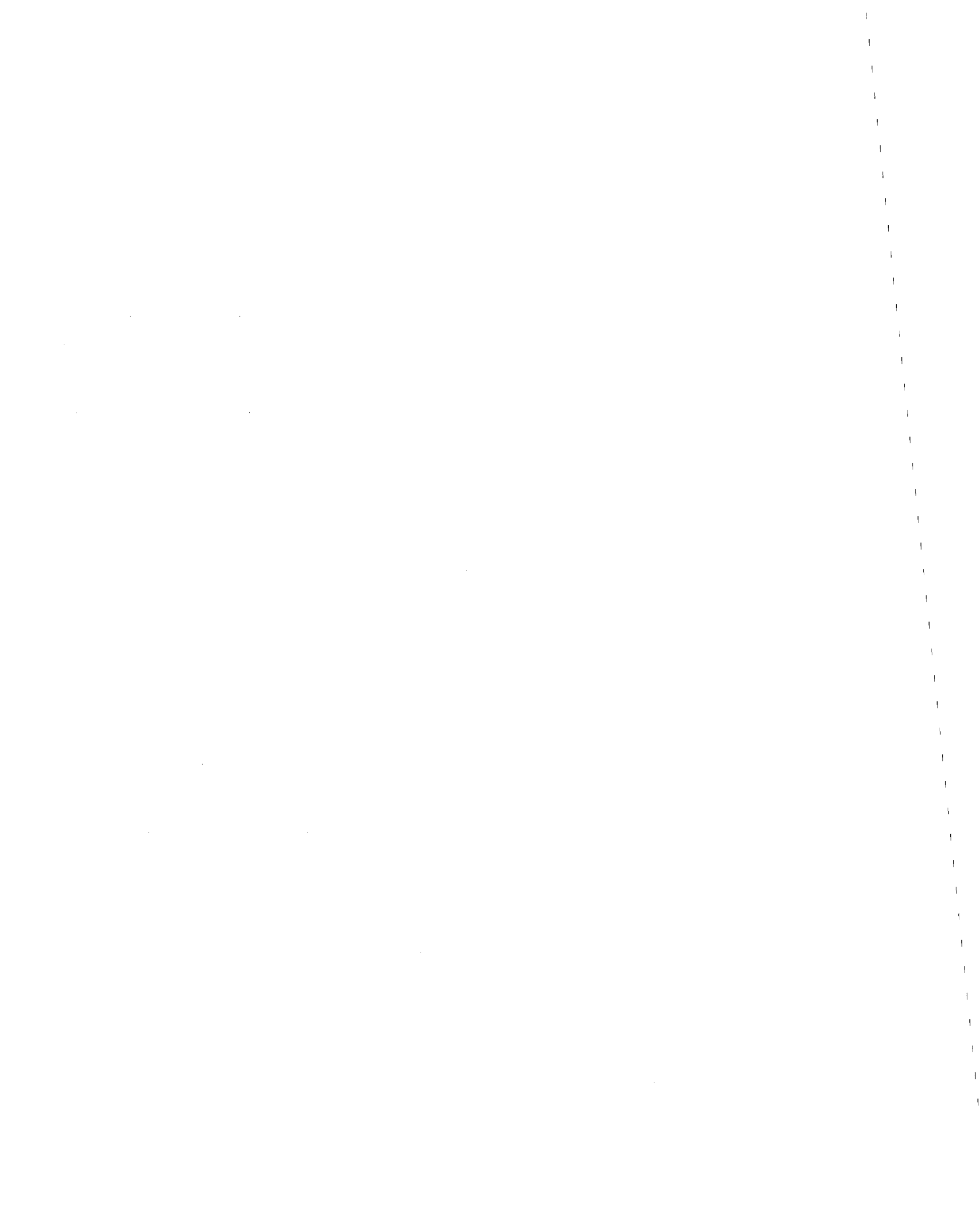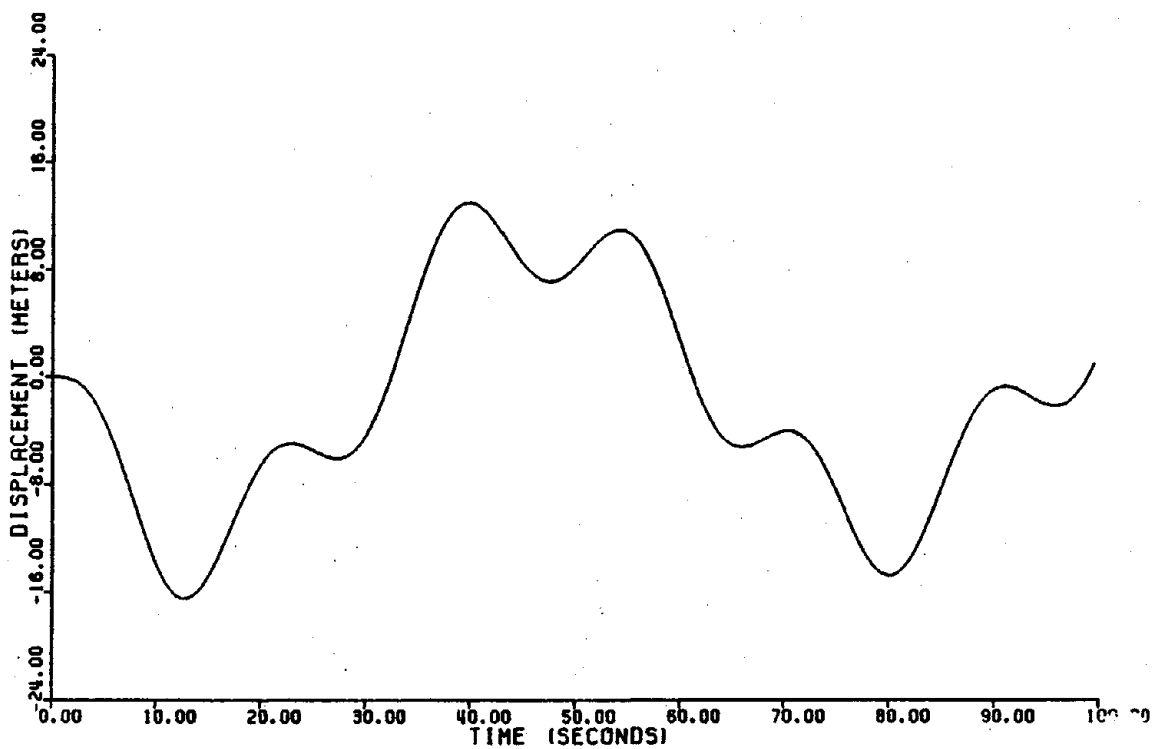
Figure 26. Time History Plot of Surge Displacement (including only Inertia Forces)
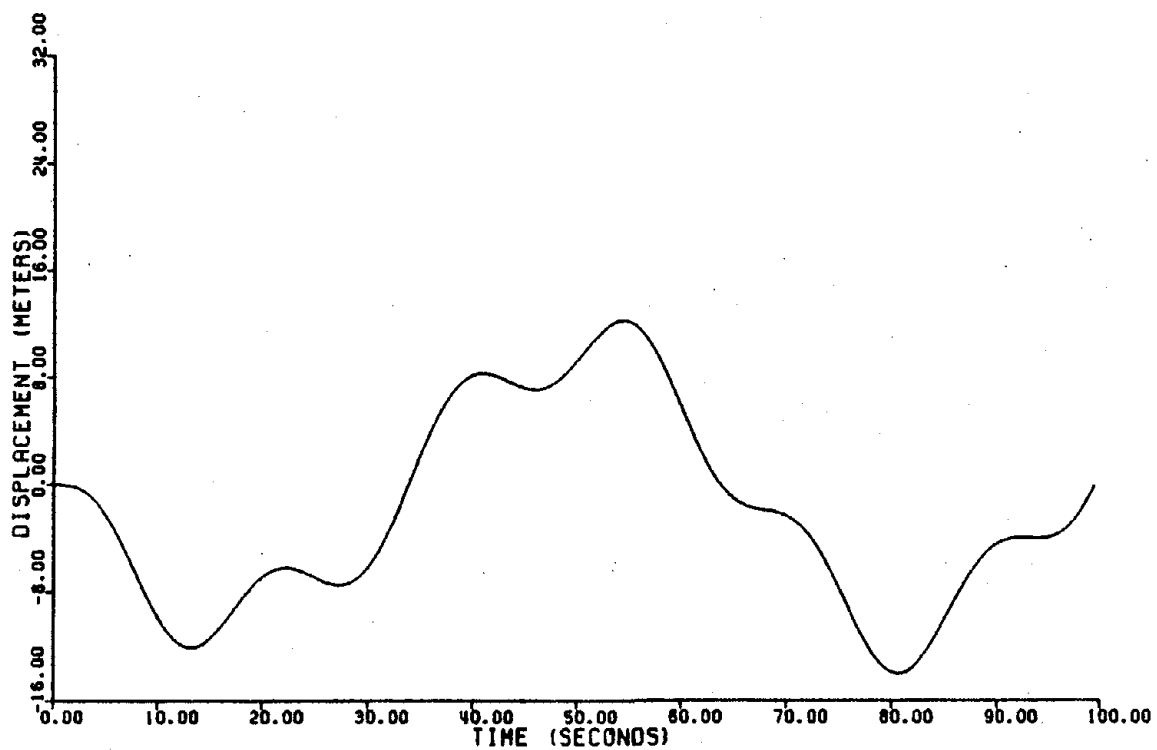
Figure 27. Time History Plot of Sway Displacement (including only Inertia Forces)
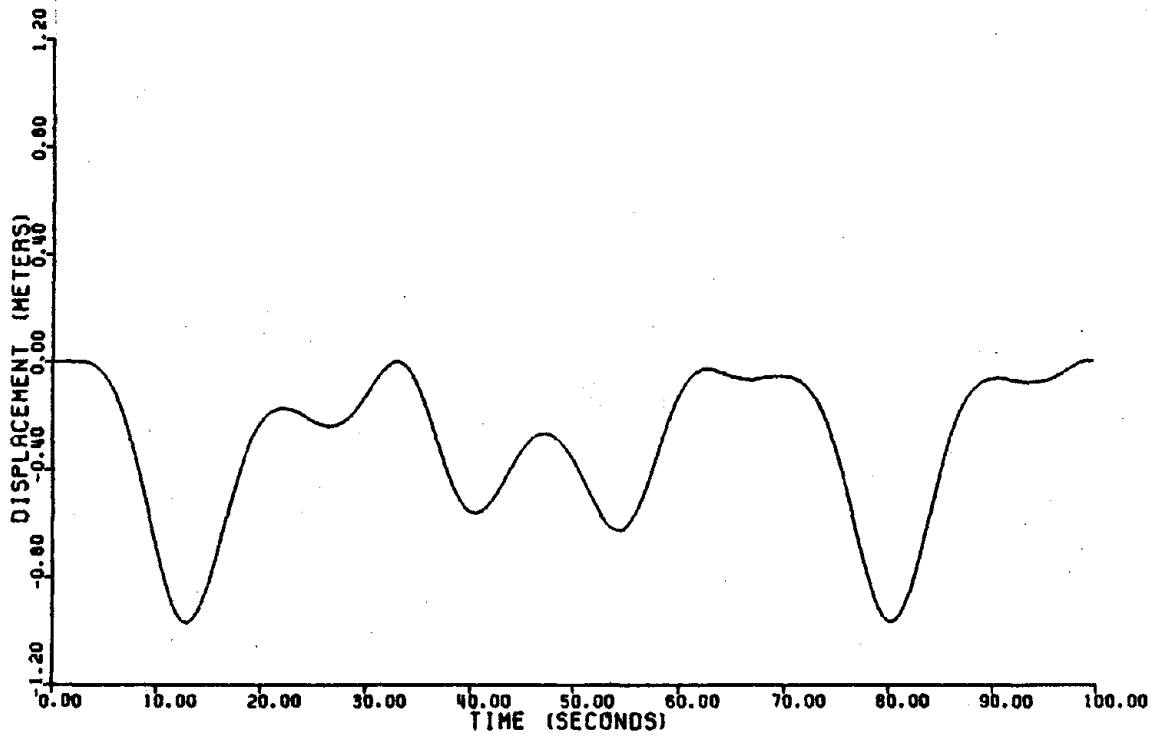
Figure 28. Time History Plot of Heave Displacement (including only Inertia Forces)
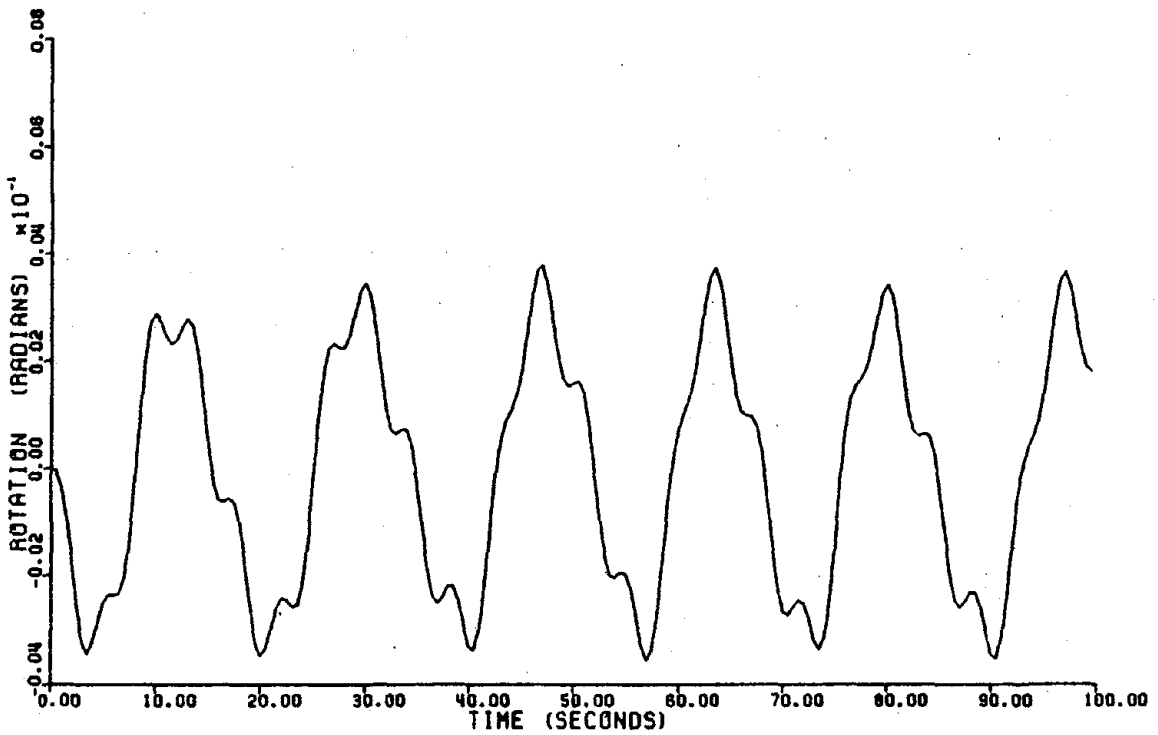
Figure 29. Time History Plot of Pitch Displacement (including only Inertia Forces)
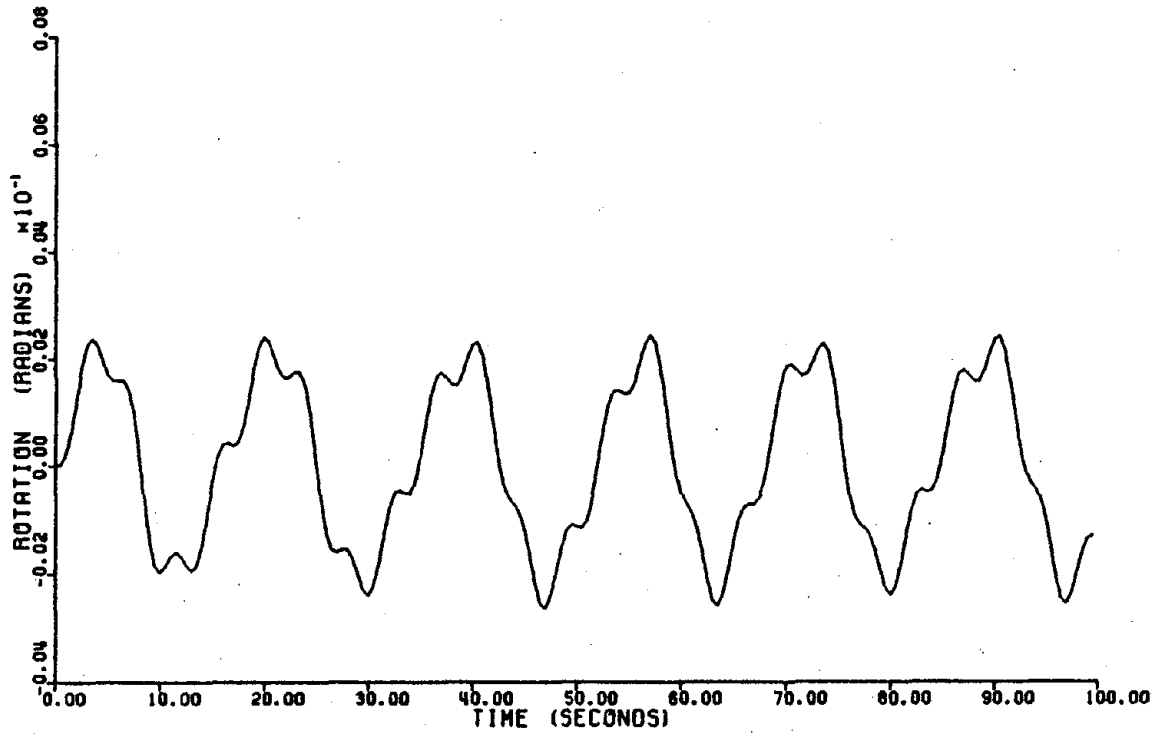
Figure 30. Time History Plot of Roll Displacement (including only Inertia Forces)
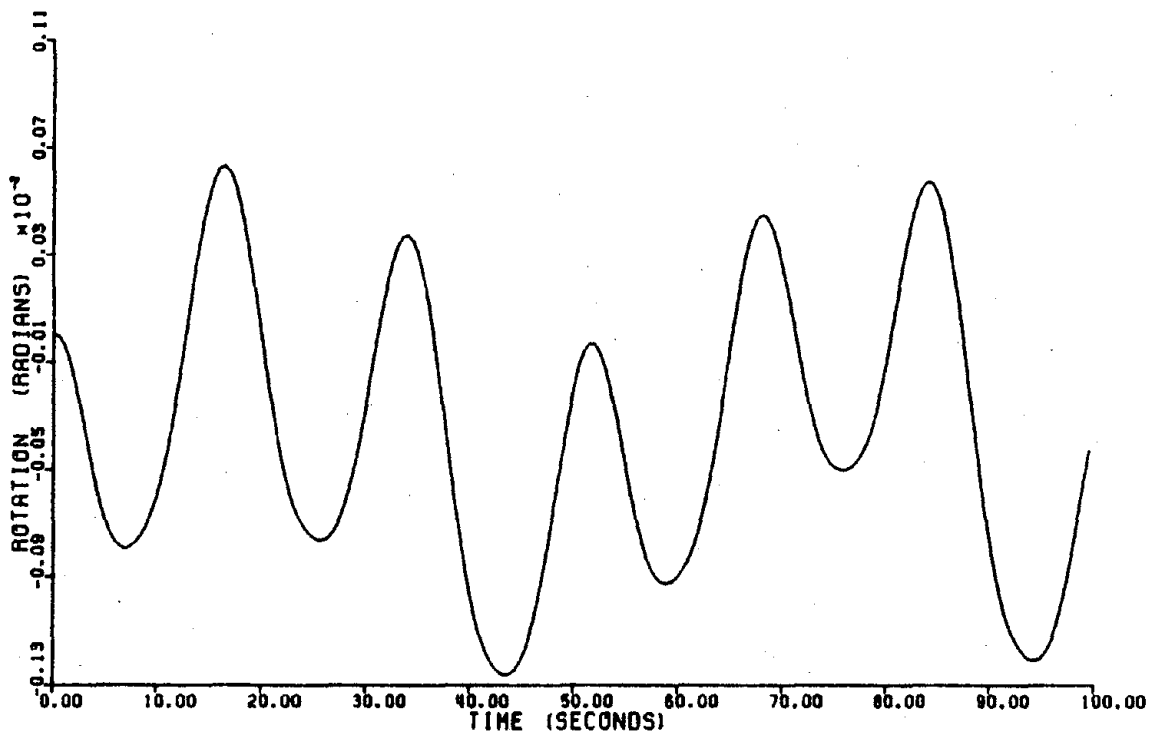
Figure 31. Time History Plot of Yaw Displacement (including only Inertia Forces)
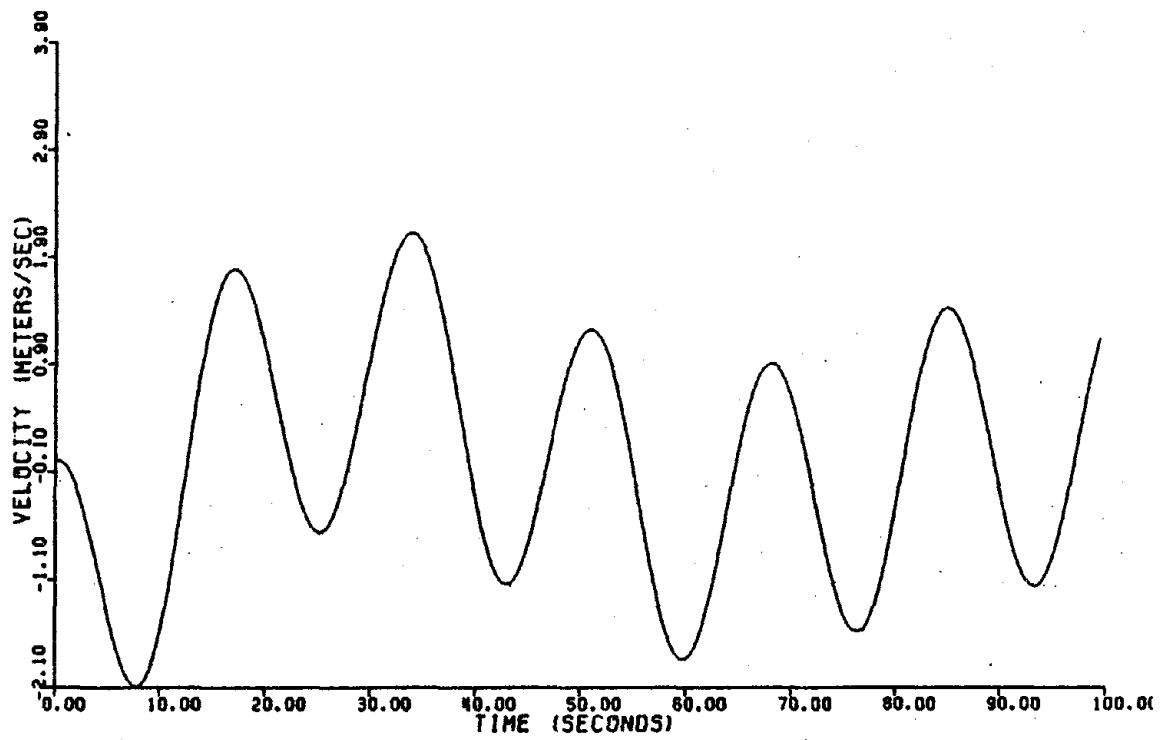
Figure 32. Time History Plot of Surge Velocity (including
Inertia and Drag Forces)
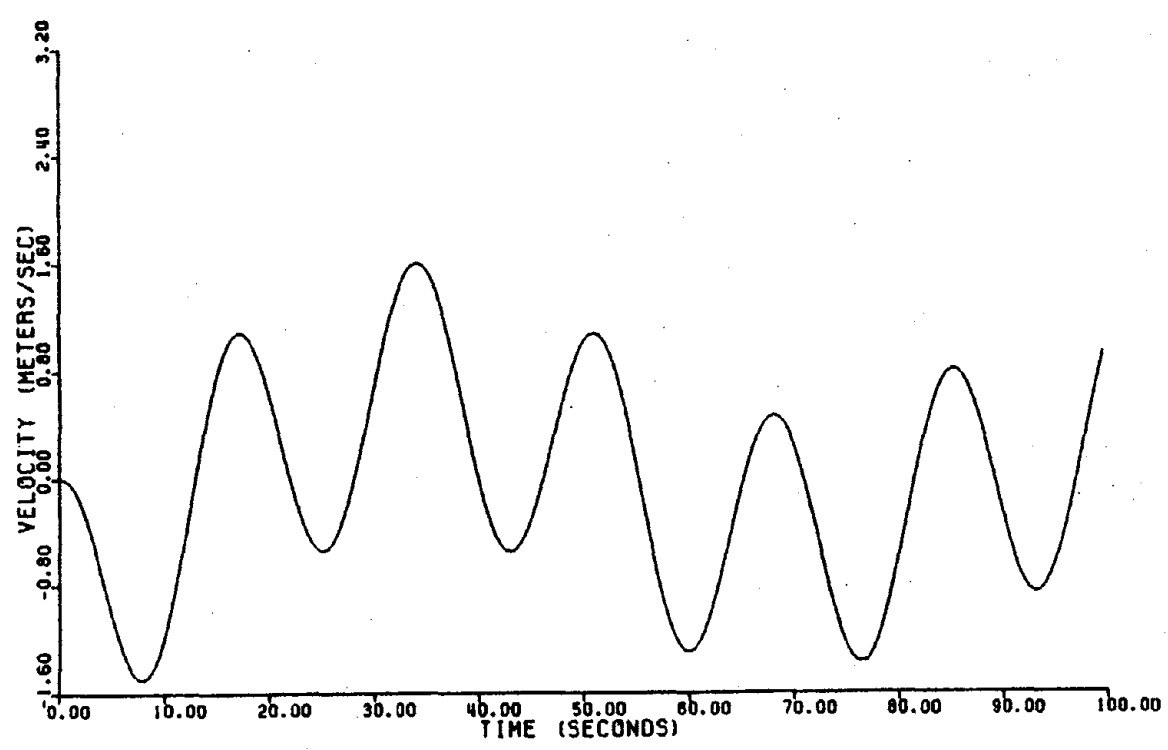
Figure 33. Time History Plot of Sway Velocity (including
Inertia and Drag Forces)
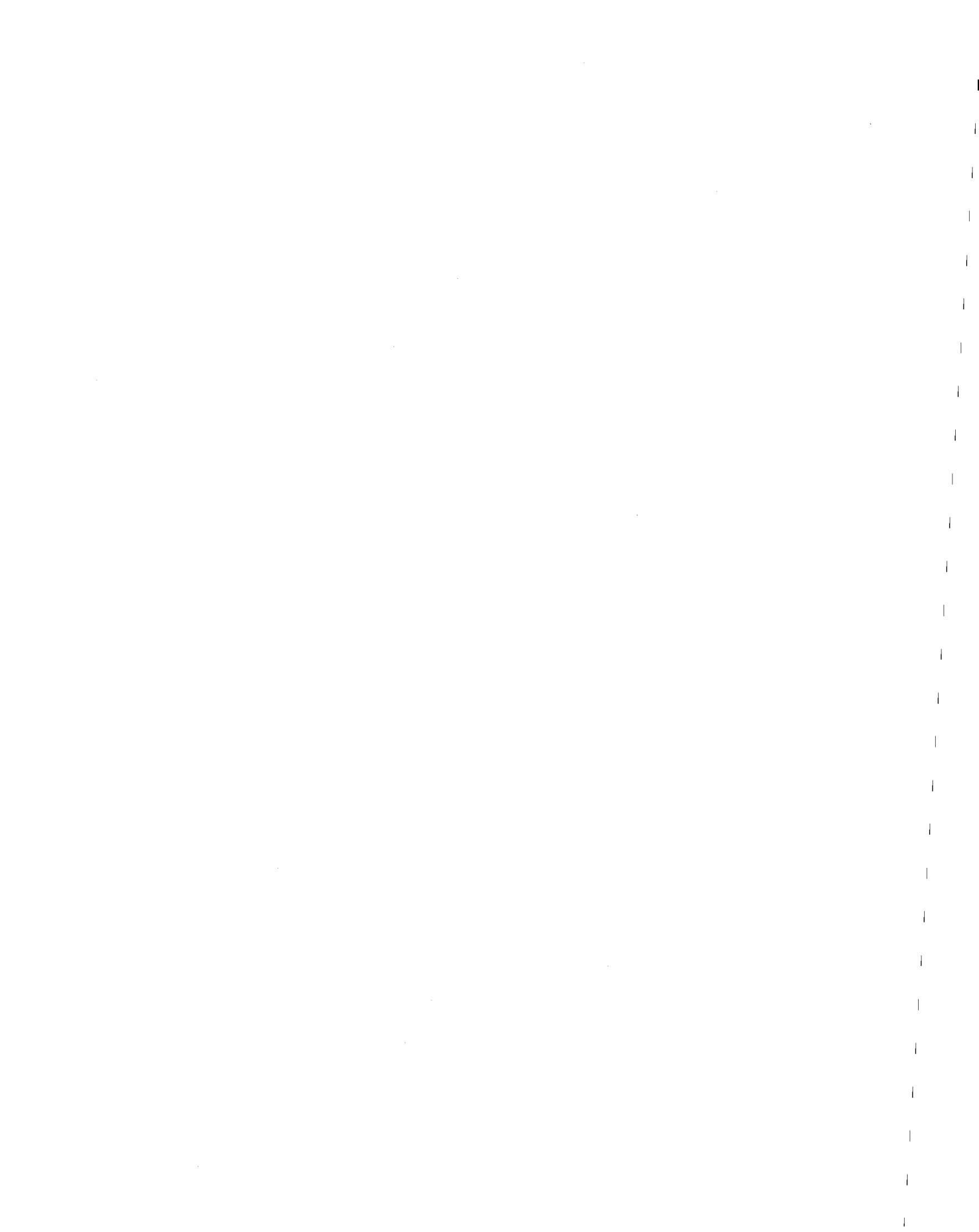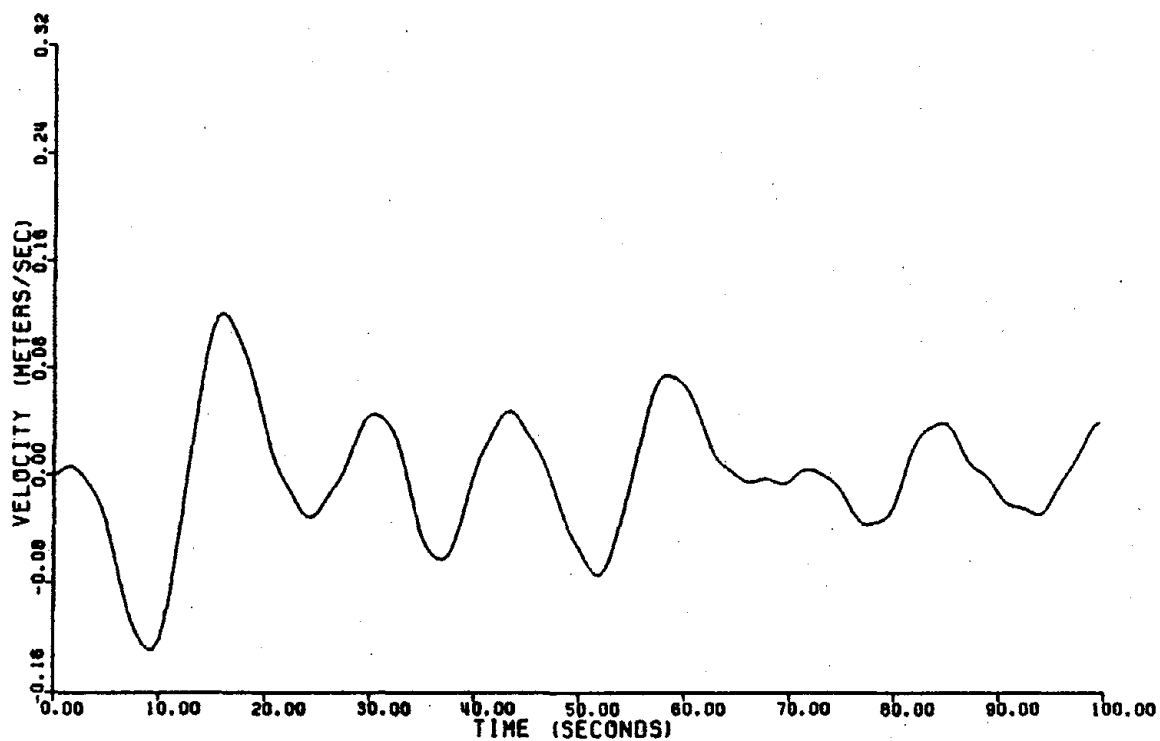
Figure 34. Time History Plot of Heave Velocity (including
Inertia and Drag Forces)
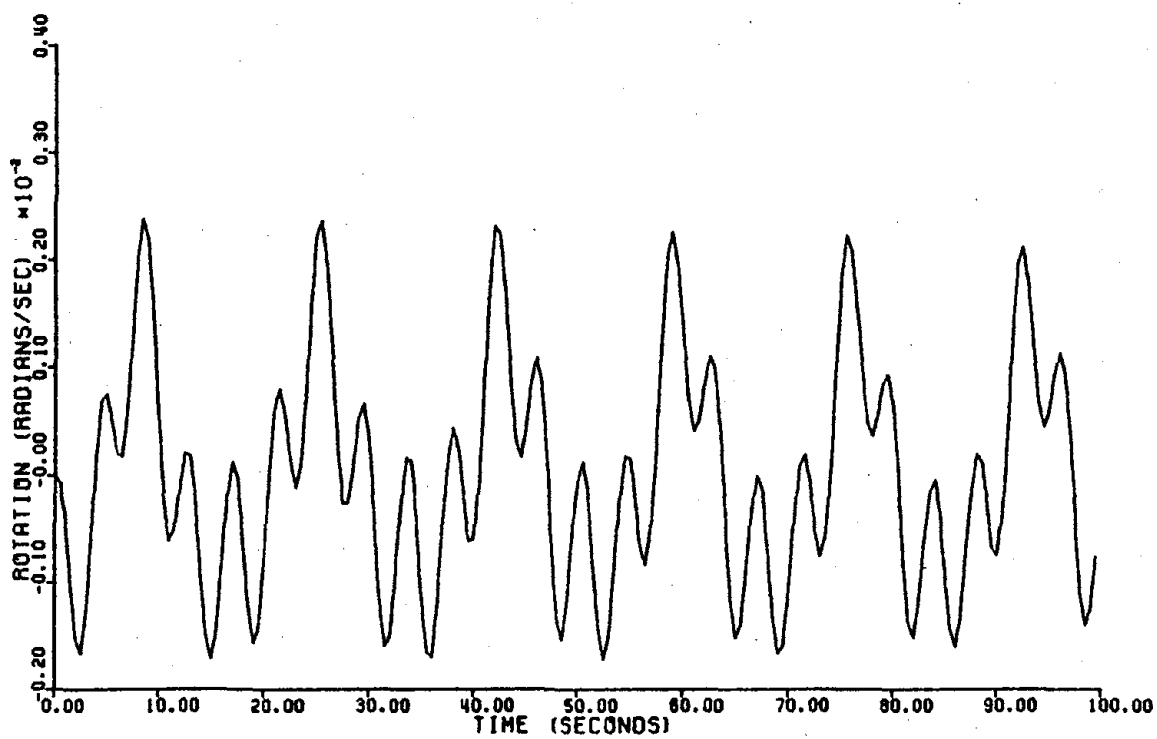
Figure 35. Time History Plot of Pitch Velocity (including
Inertia and Drag Forces)
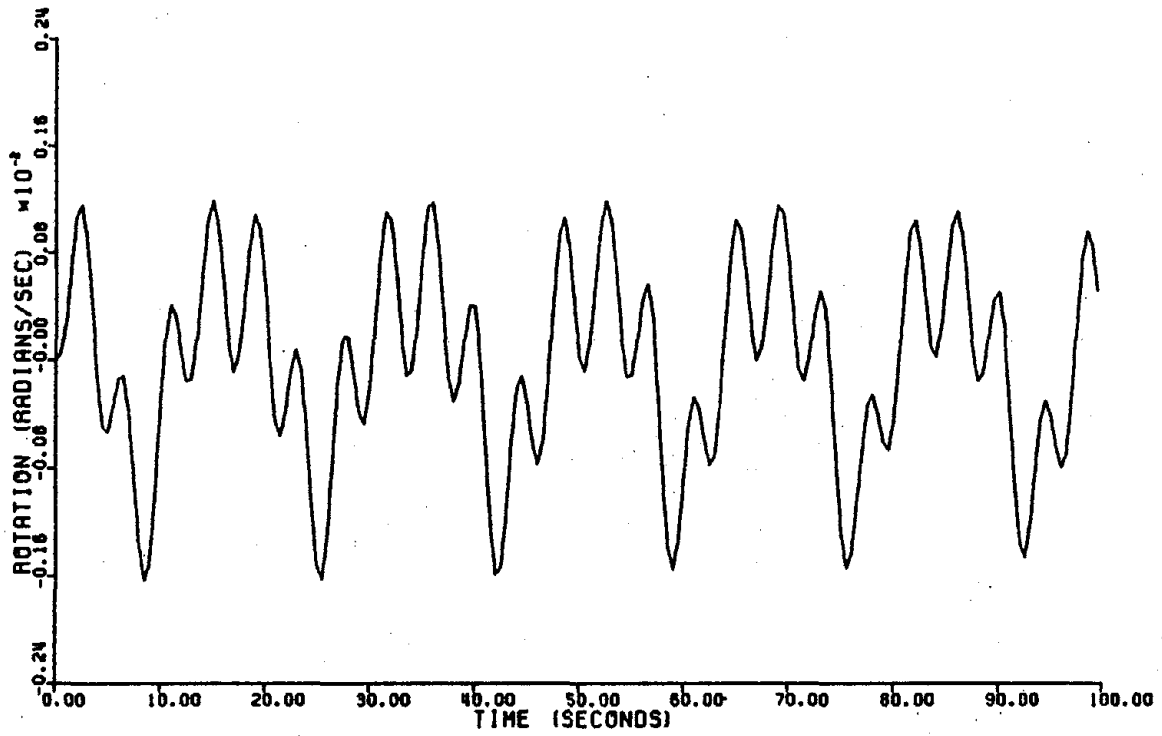
Figure 36. Time History Plot of Roll Velocity (including Inertia and Drag Forces)
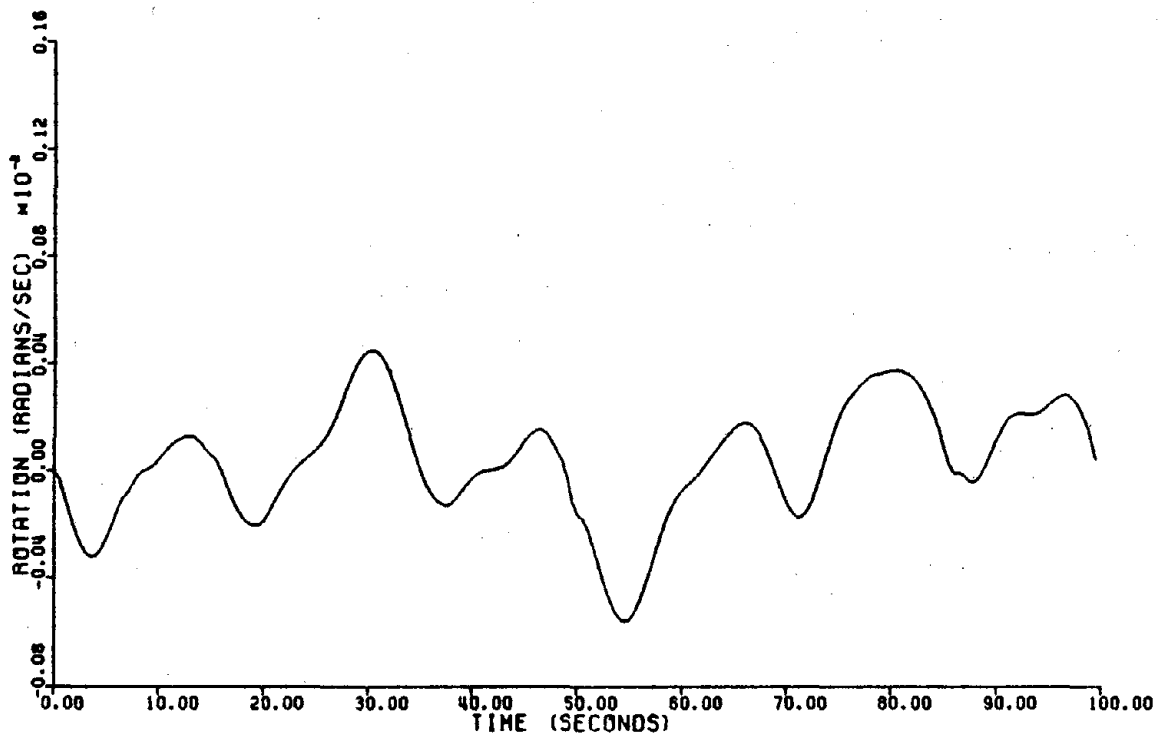
Figure 37. Time History Plot of Yaw Velocity (including Inertia and Drag Forces)
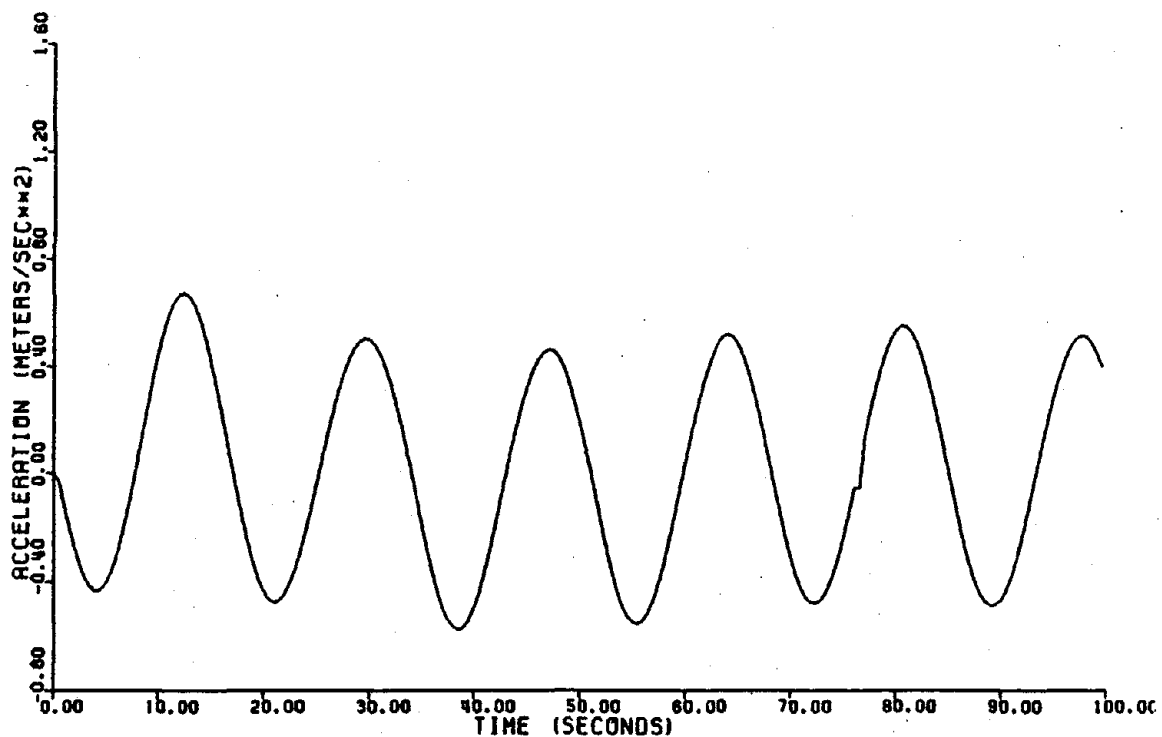
Figure 38. Time History Plot of Surge Acceleration (including Inertia and Drag Forces)
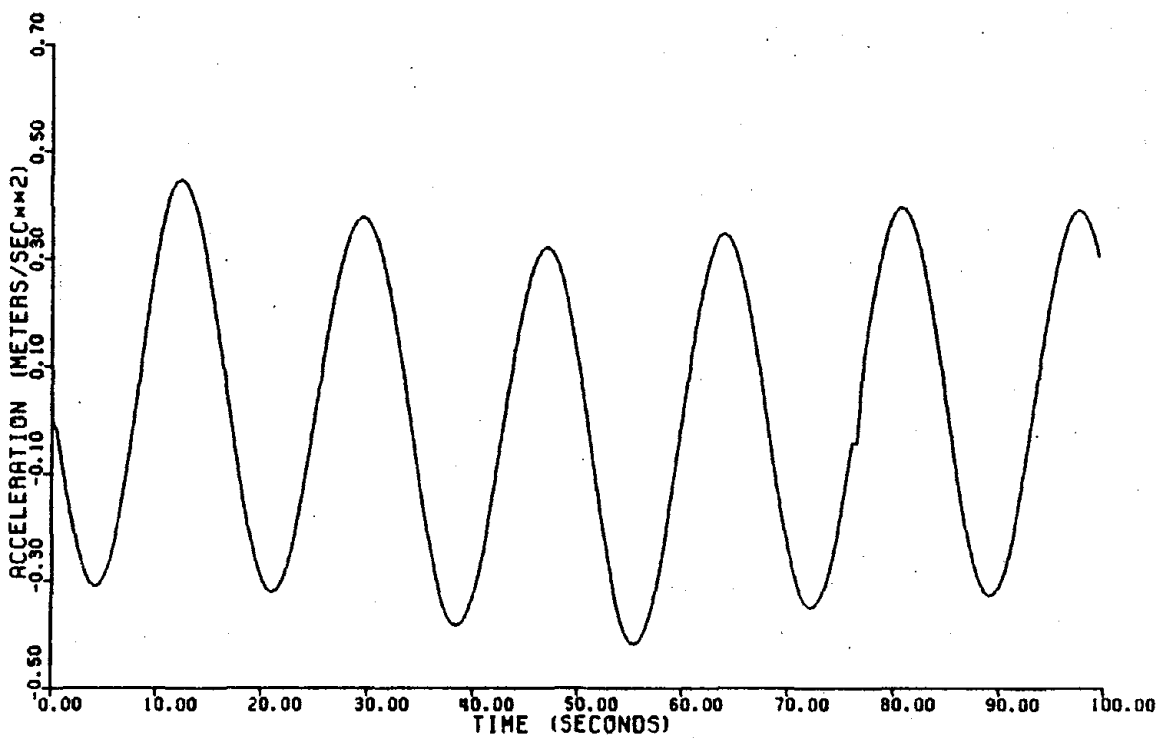
Figure 39. Time History Plot of Sway Acceleration (including Inertia and Drag Forces)
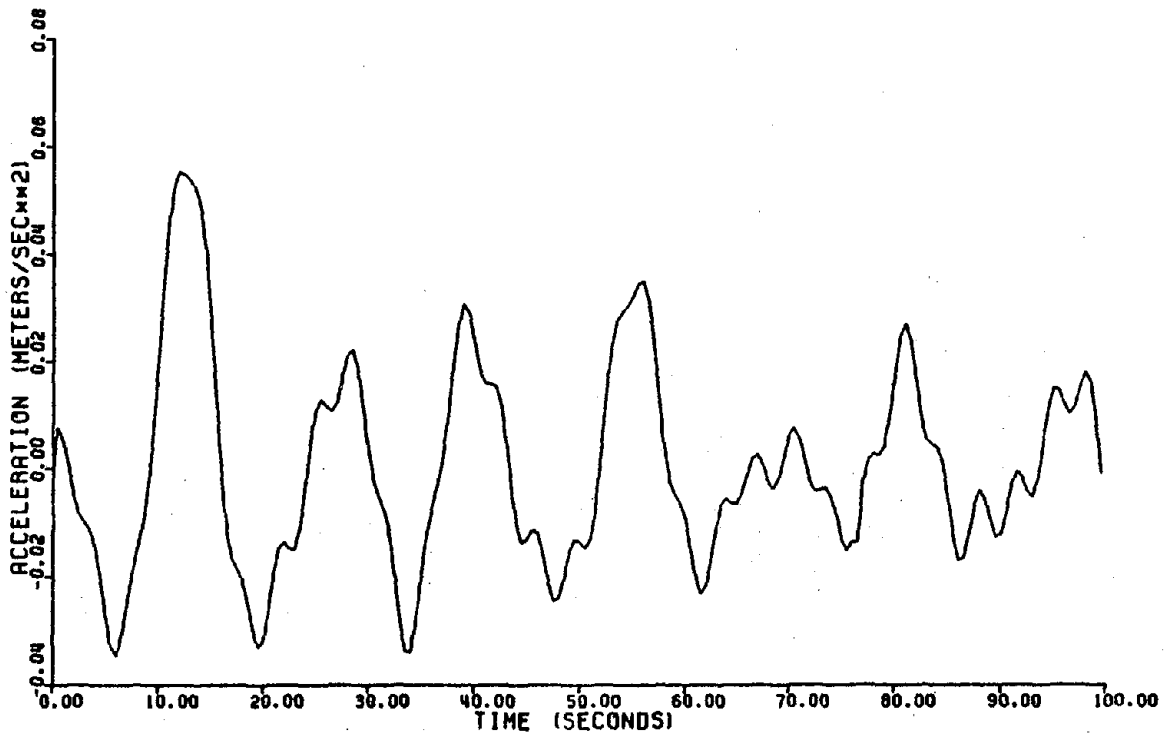
Figure 40. Time History Plot of Heave Acceleration (including Inertia and Drag Forces)
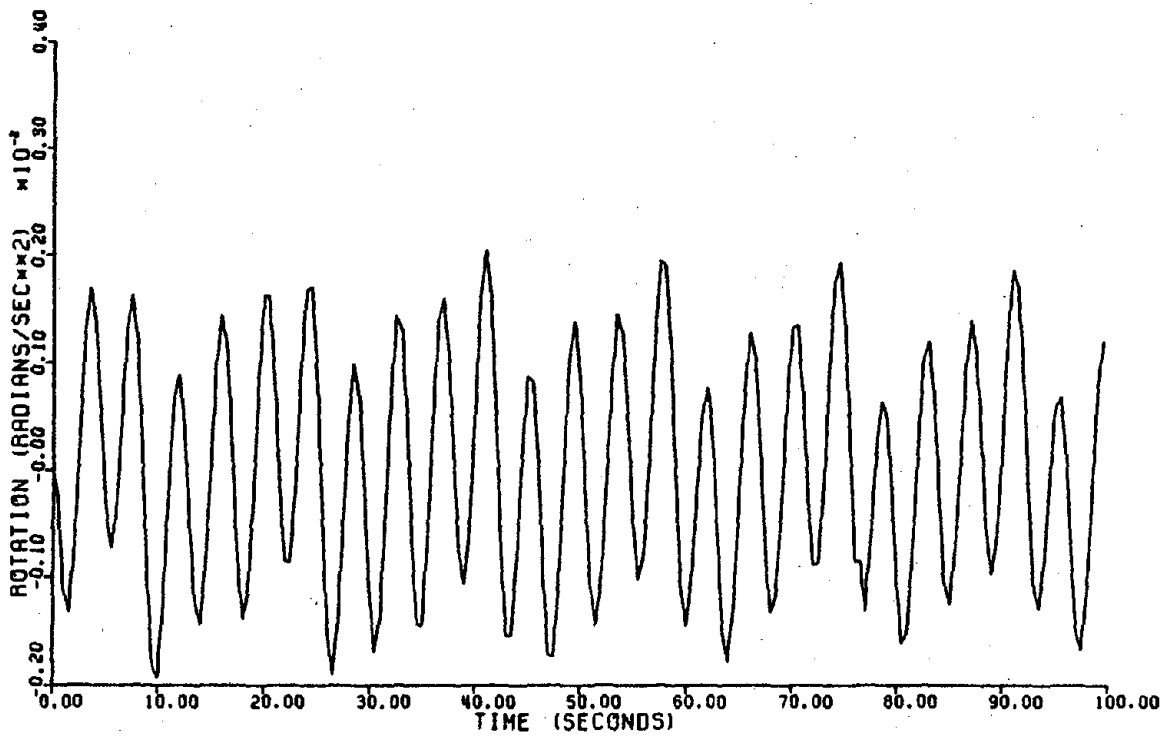

Figure 41. Time History Plot of Pitch Acceleration (including Inertia and Drag Forces)
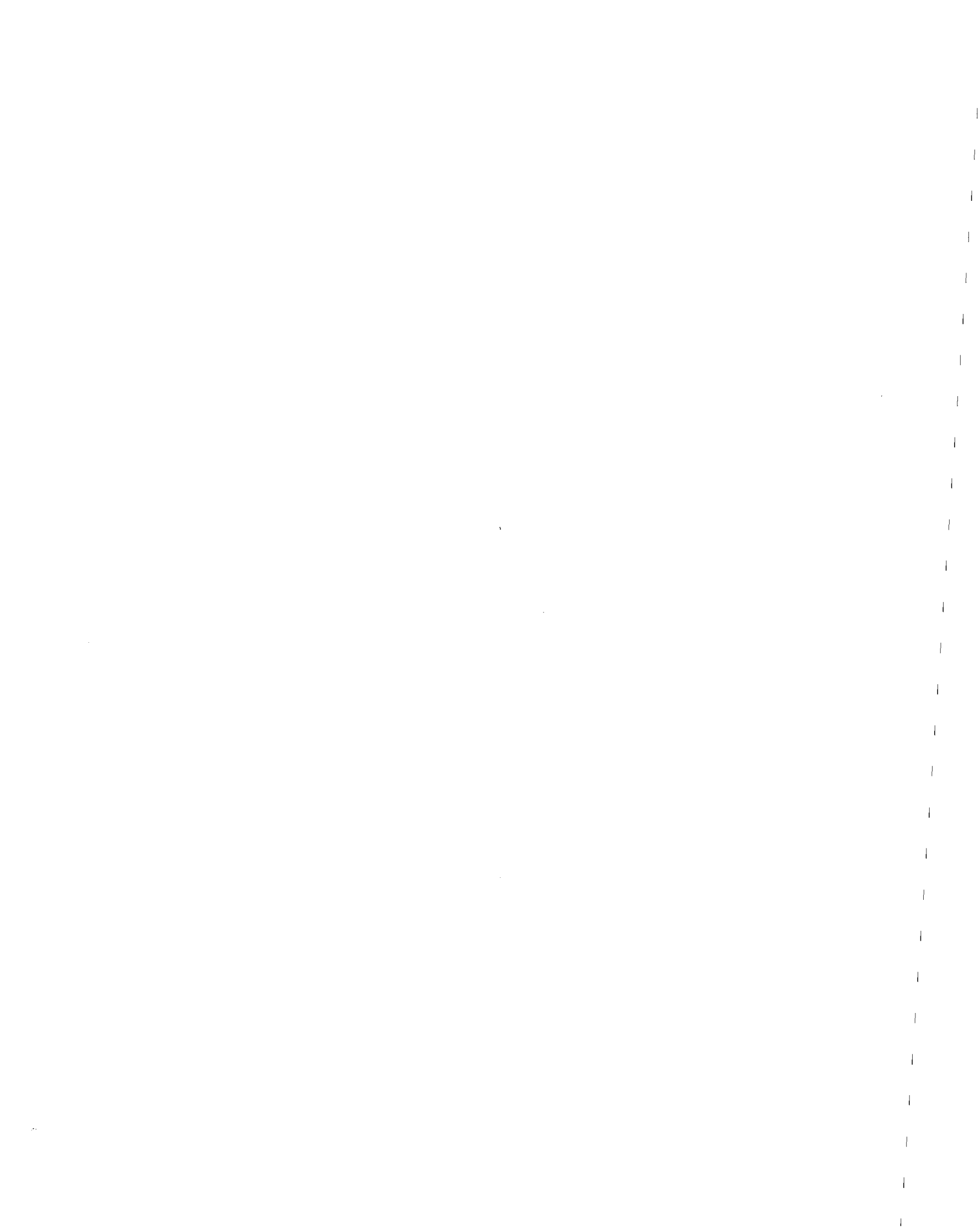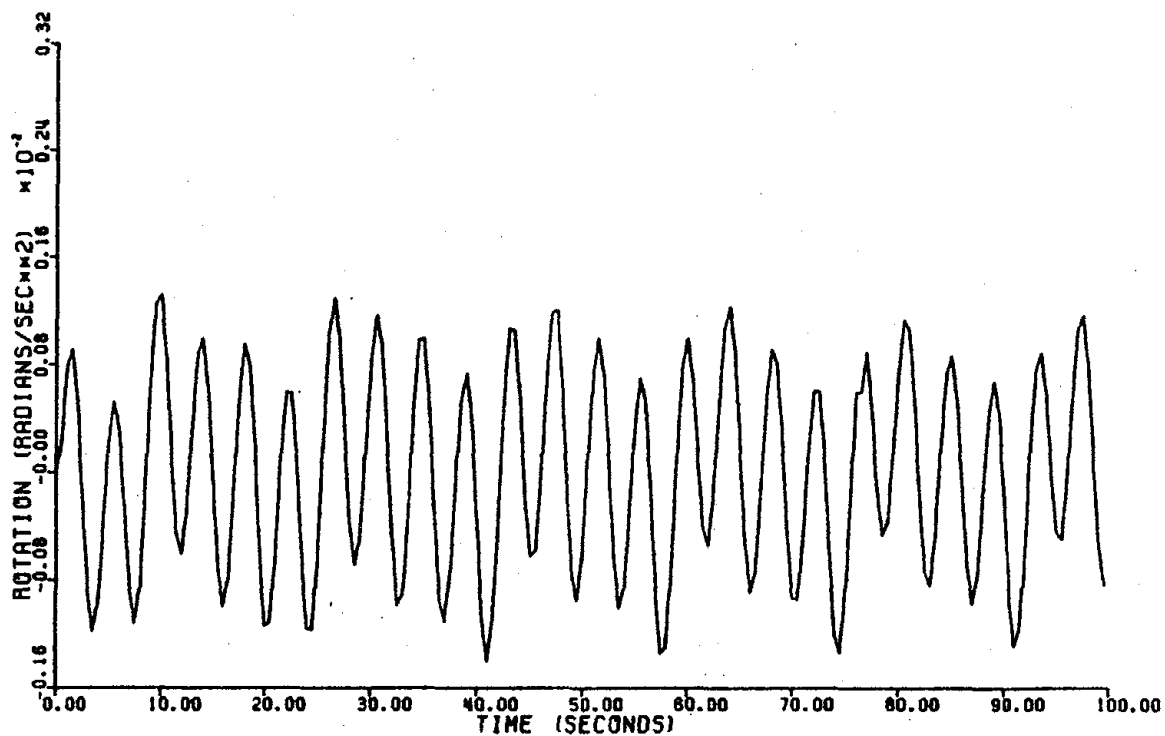
Figure 42. Time History Plot of Roll Acceleration (including Inertia and Drag Forces)
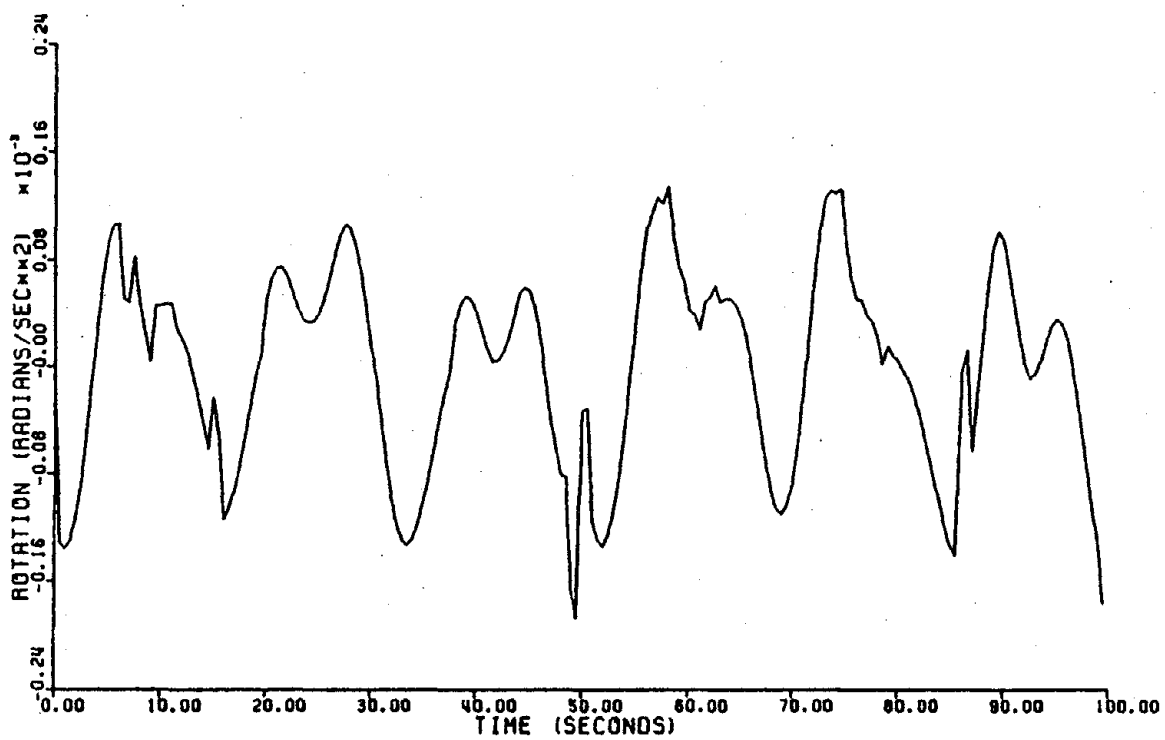
Figure 43. Time History Plot of Yaw Acceleration (including Inertia and Drag Forces)
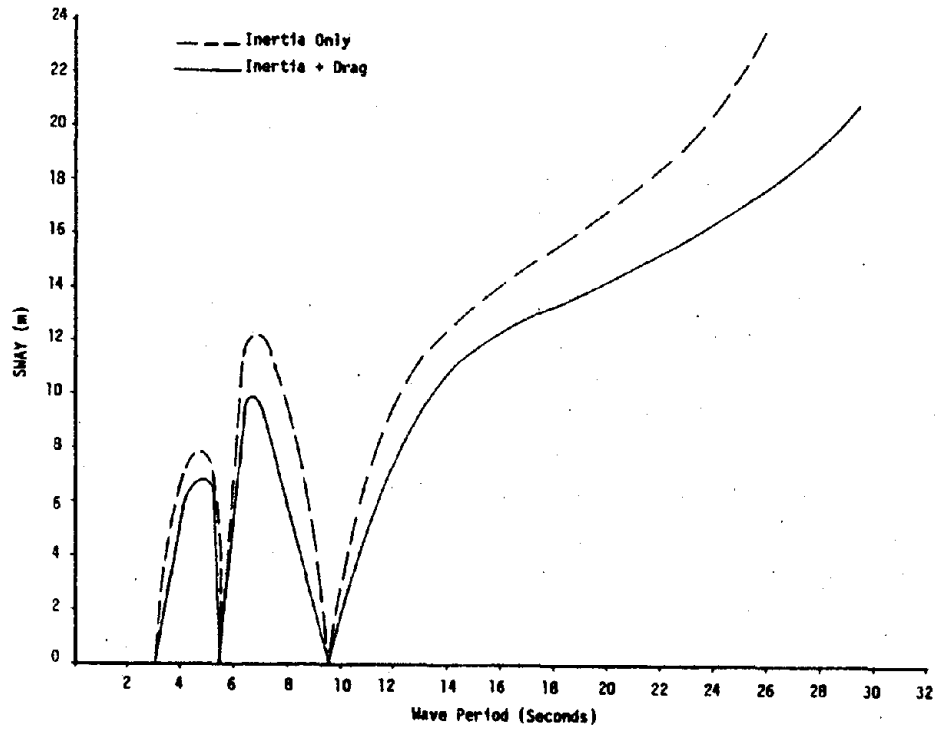
Figure 44. Response Spectrum for Surge Displacement
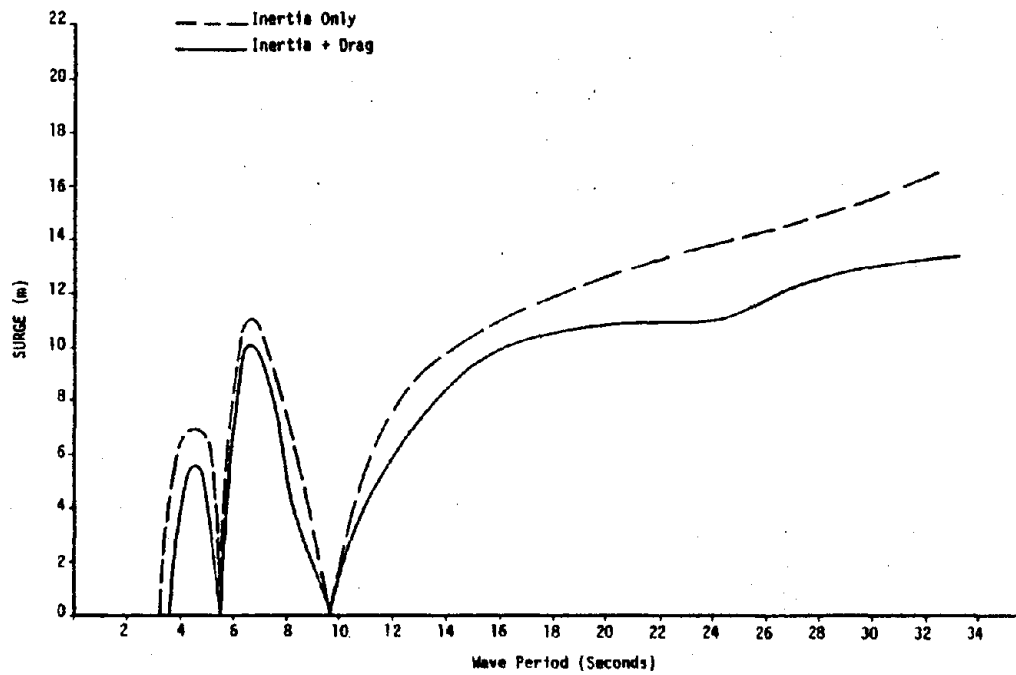
Figure 45. Response Spectrum for Sway Displacement
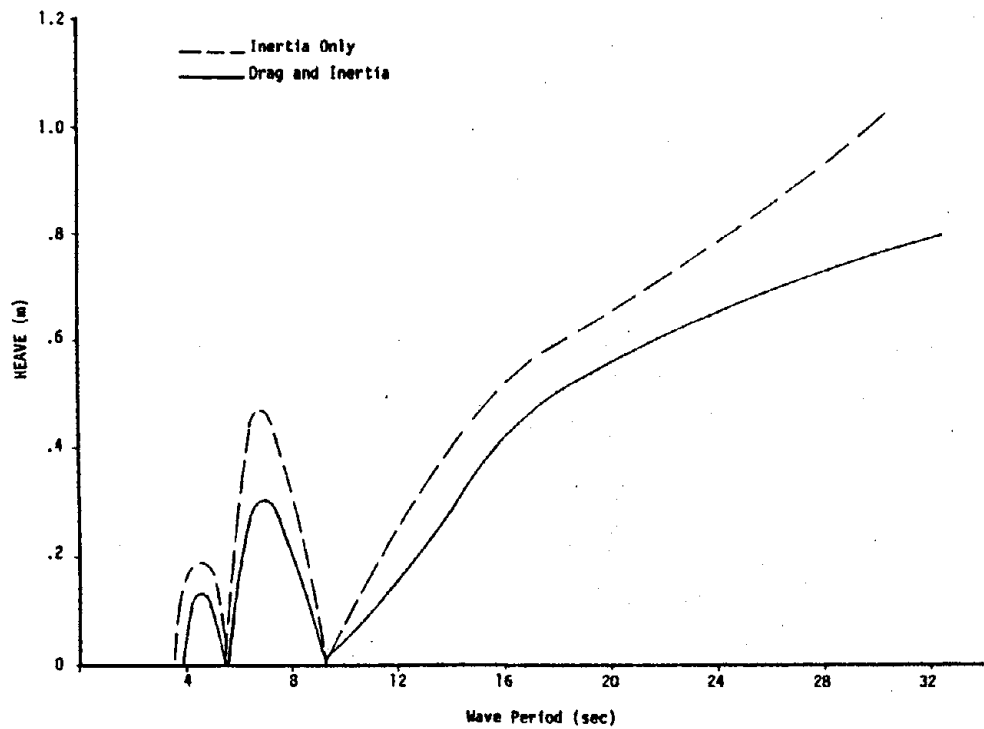
Figure 46. Response Spectrum for Heave Displacement for $\alpha = 0^0$
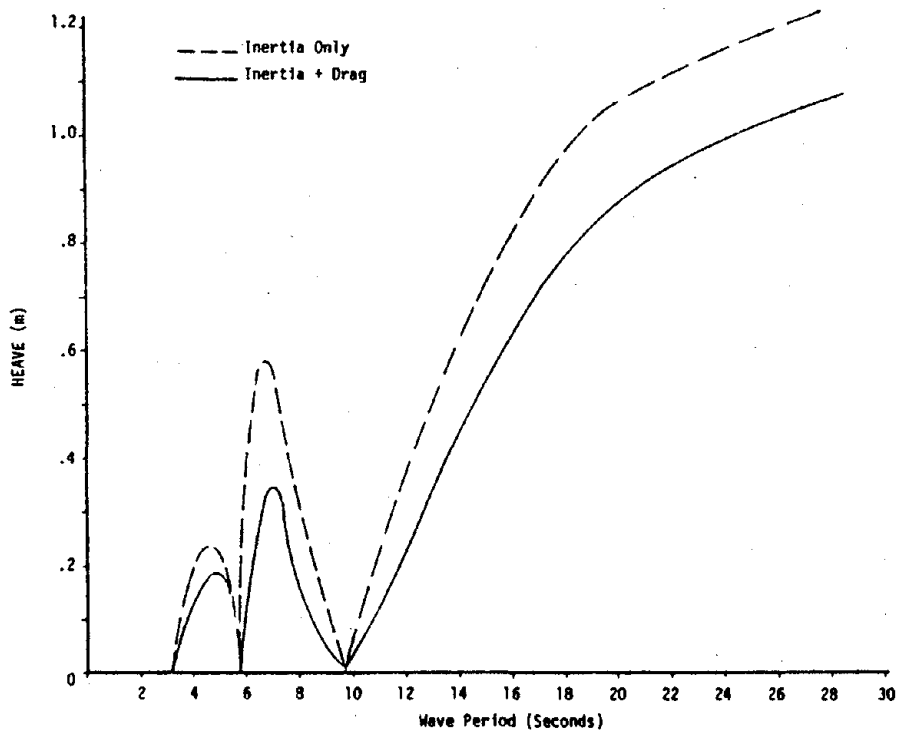
Figure 47. Response Spectrum for Heave Displacement for $\alpha = 90^0$
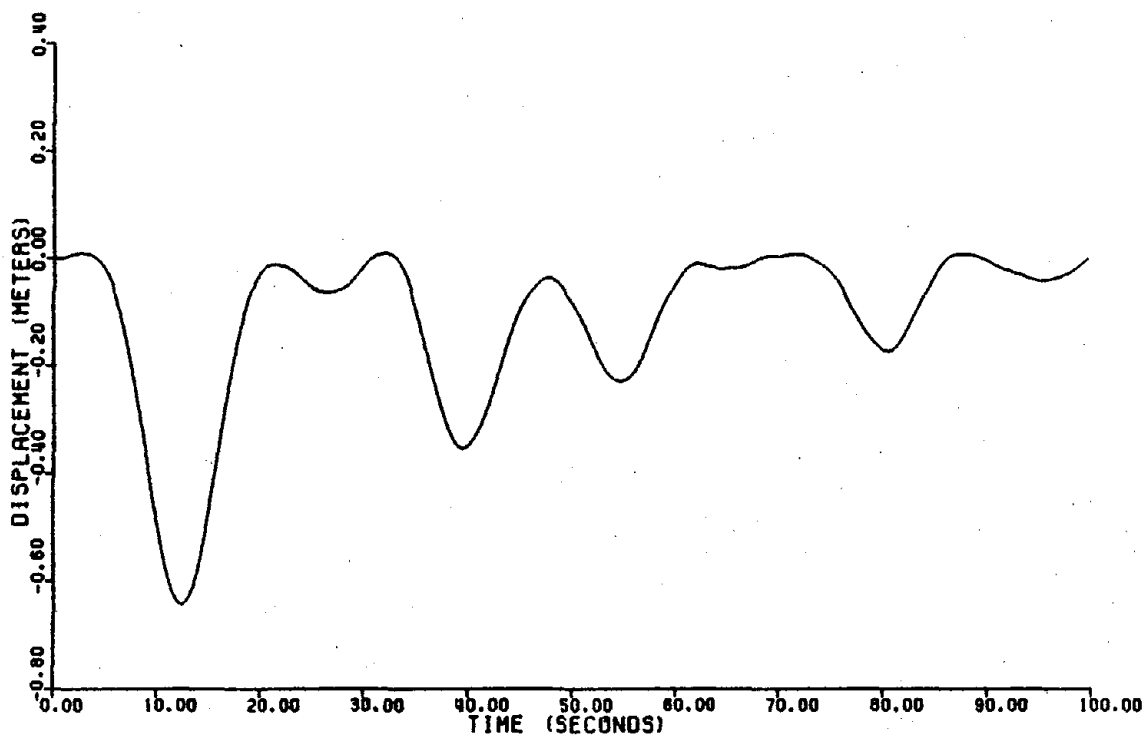
Figure 48. Time History of Coupled Heave Response
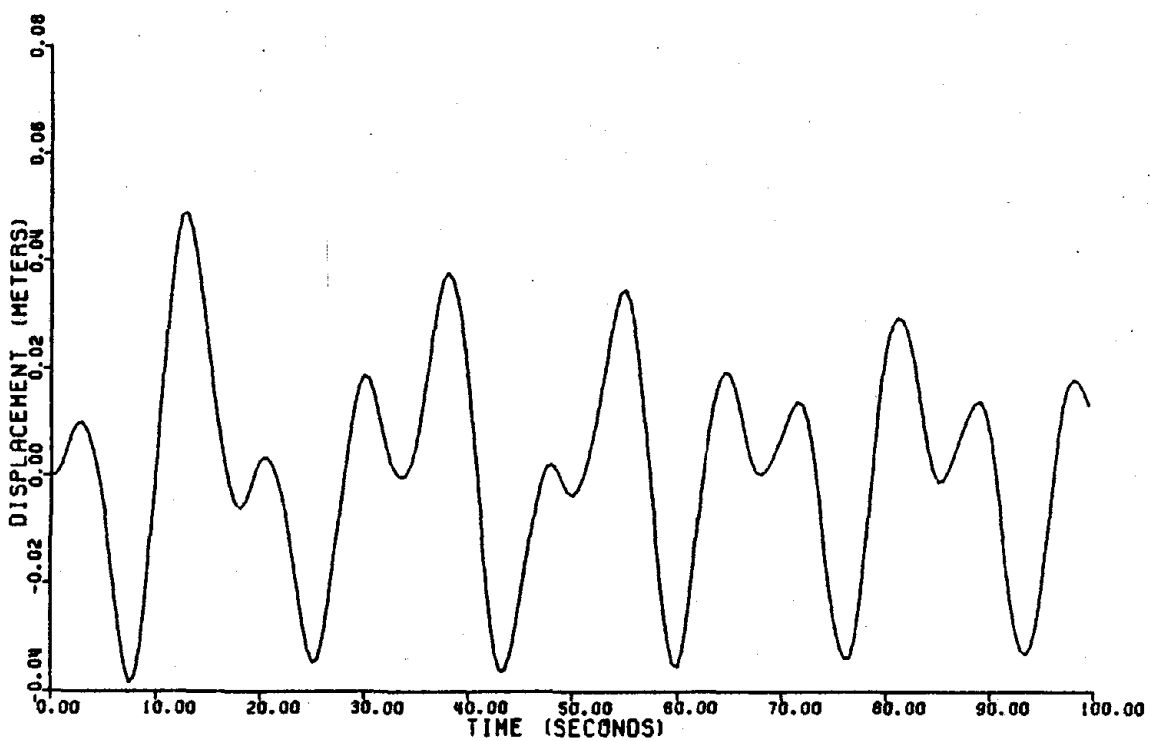
Figure 49. Time History of Uncoupled Heave Response
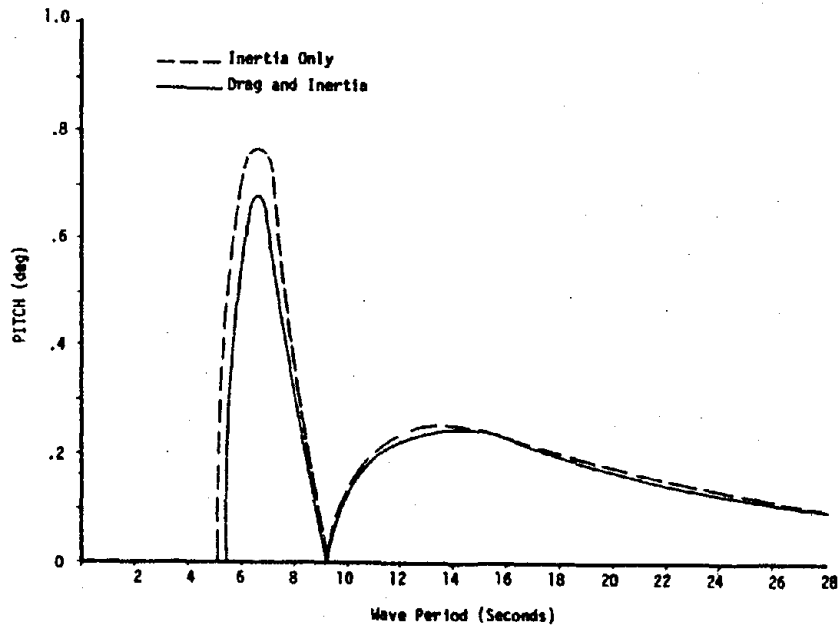
Figure 50. Response Spectrum of Pitch Rotation
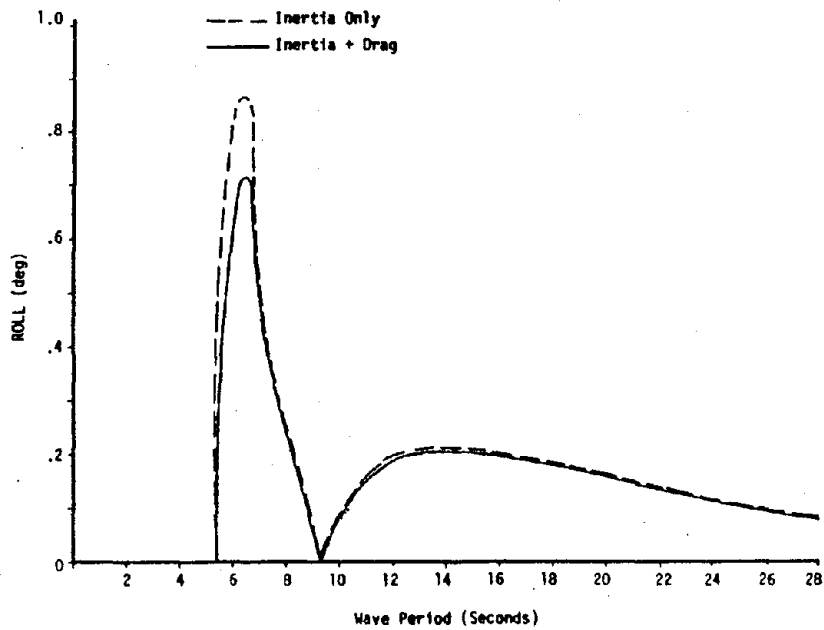
Figure 51. Response Spectrum of Roll Rotation
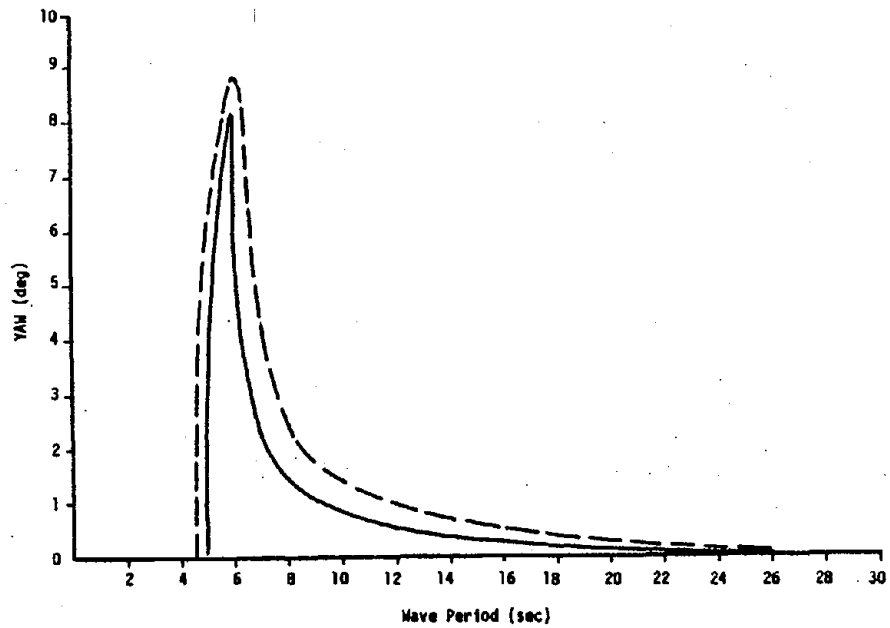
Figure 52. Response Spectrum of Yaw Rotation
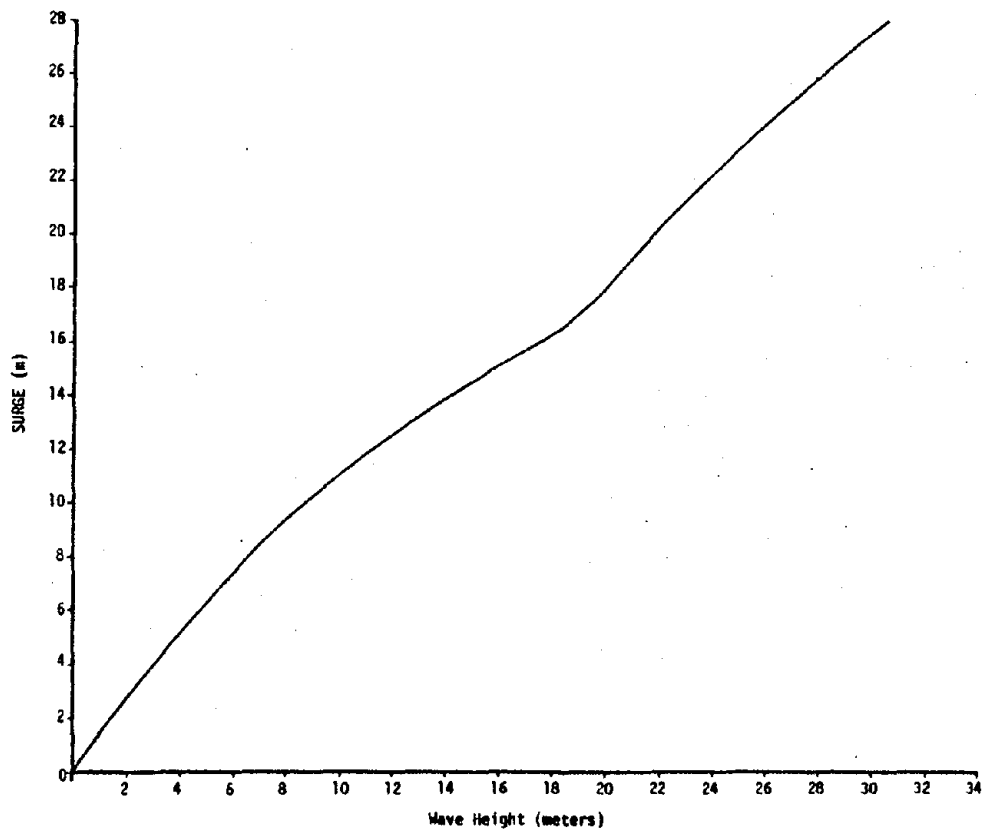
Figure 53. Variation of Surge Response Amplitude with Wave Height
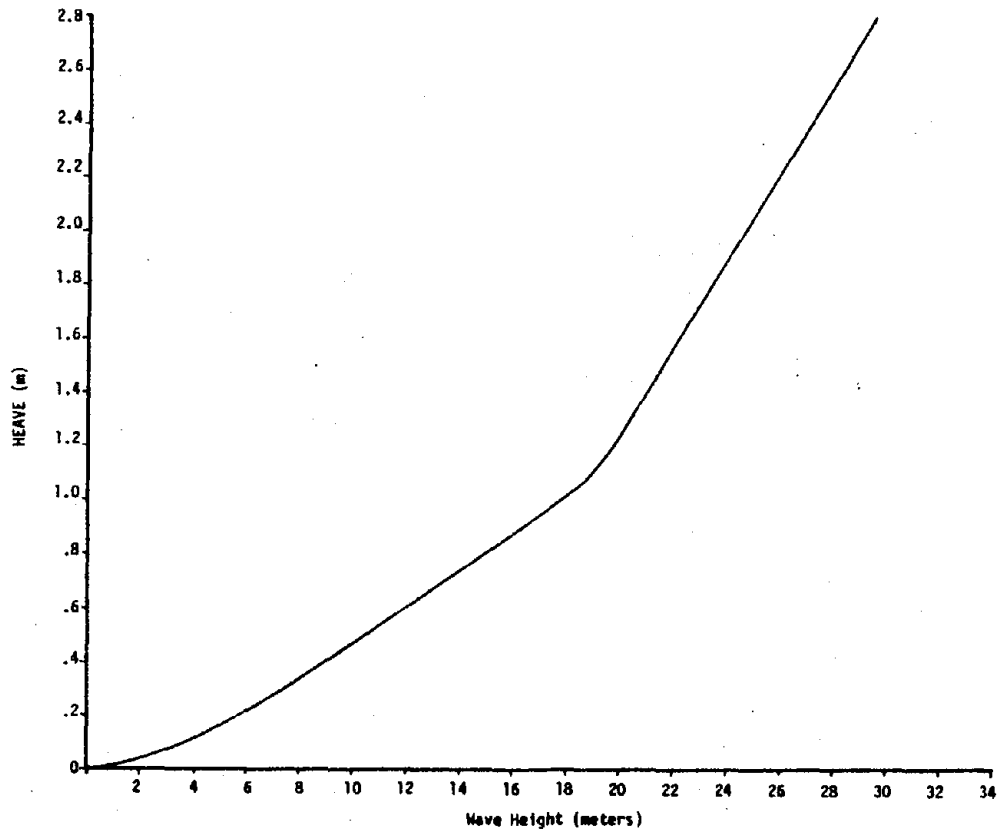
Figure 54. Variation of Heave Response Amplitude with Wave Height
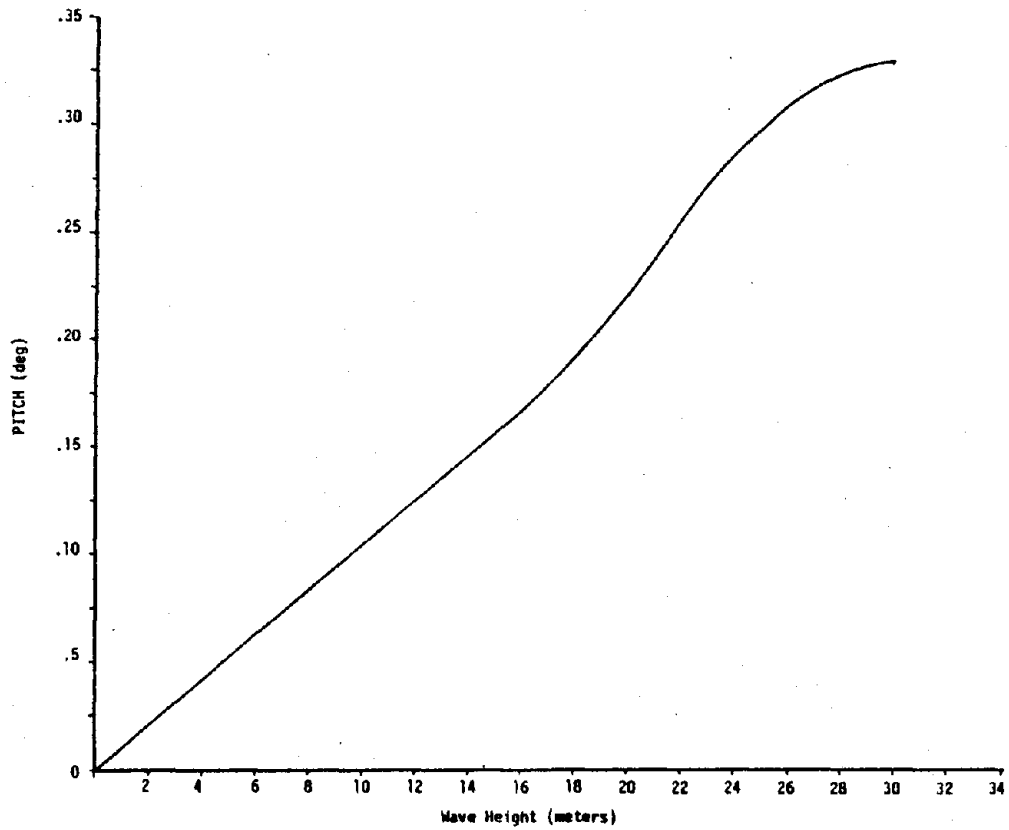
Figure 55. Variation of Pitch Response Amplitude with Wave Height
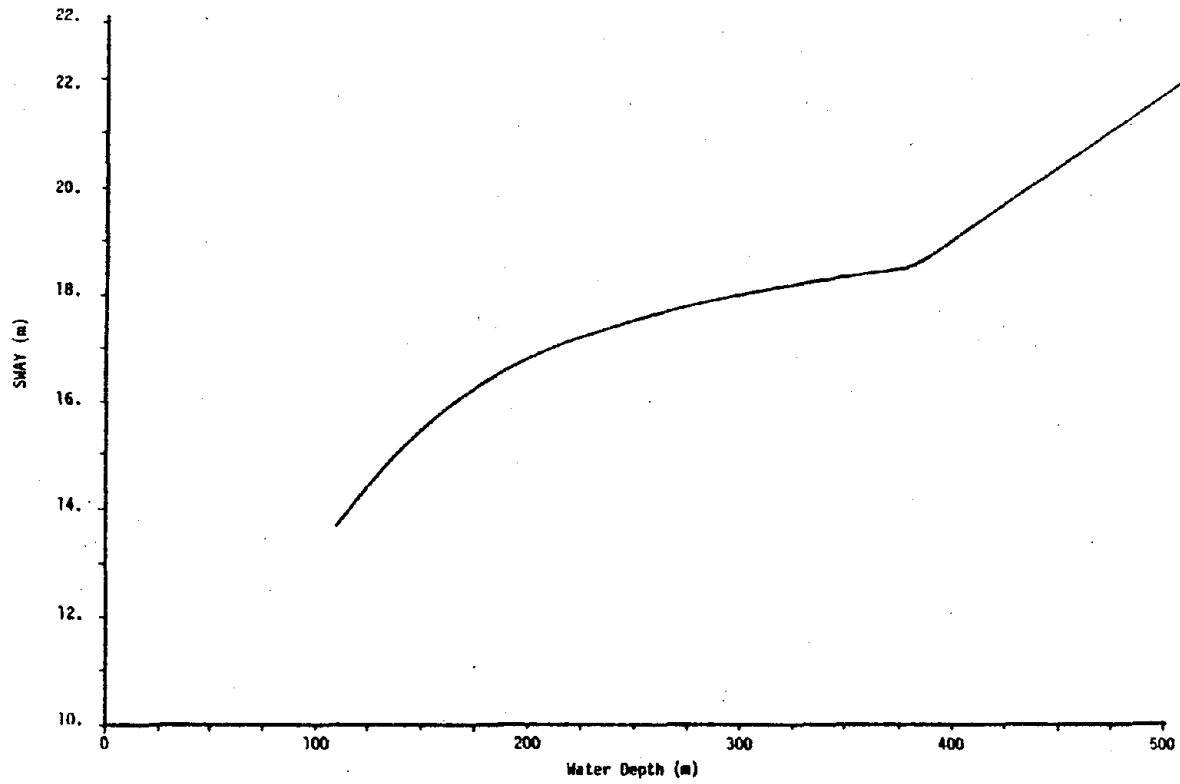
Figure 56. Variation of Sway Response Amplitude with Water Depth
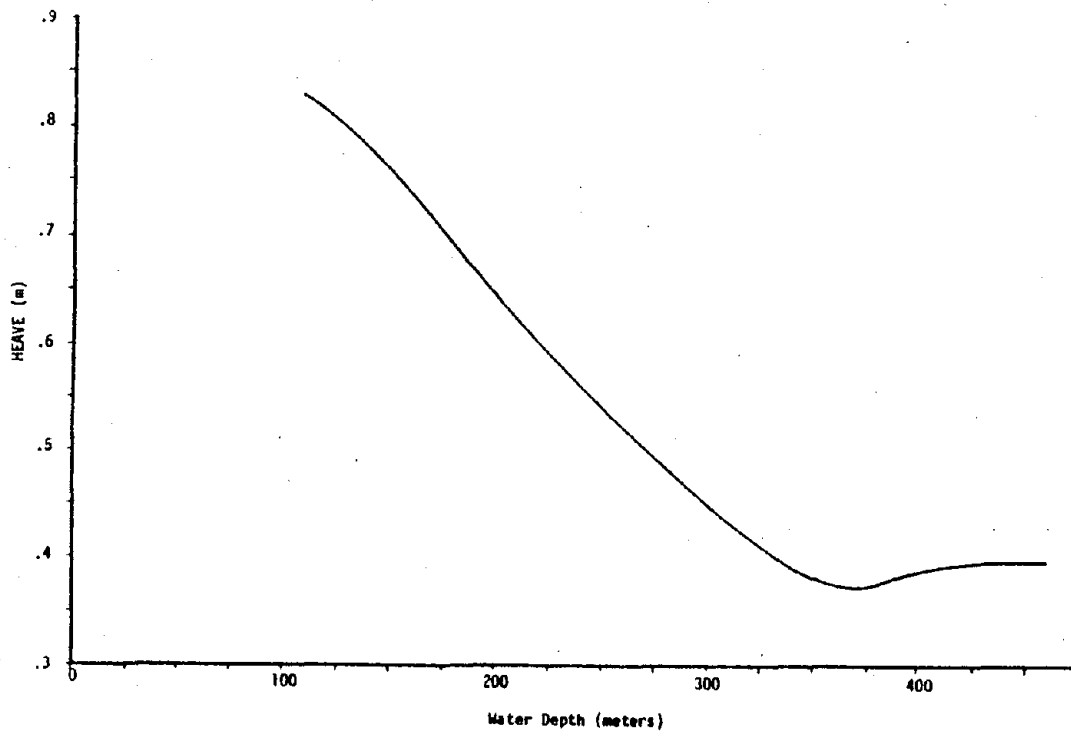
Figure 57. Variation of Heave Response Amplitude with Water Depth
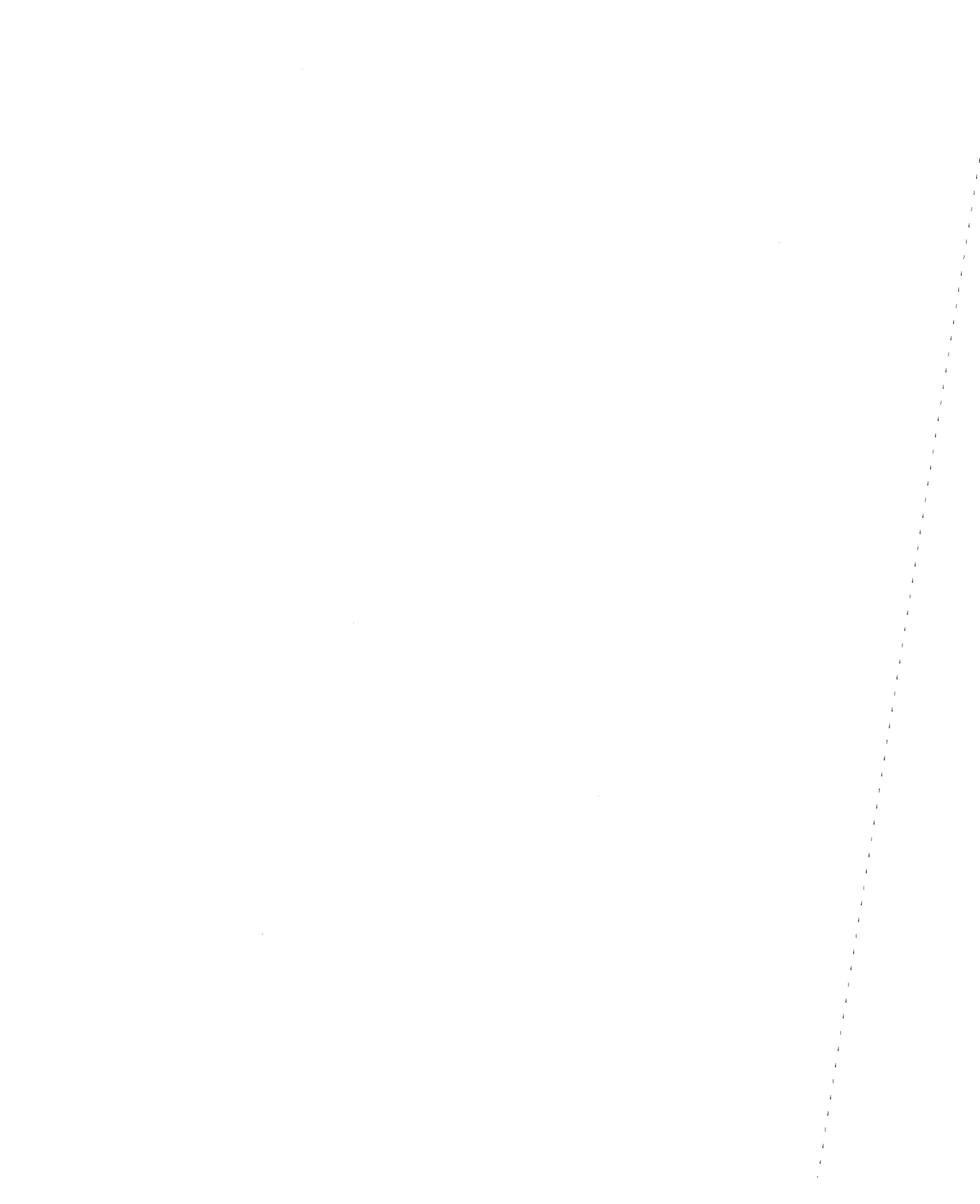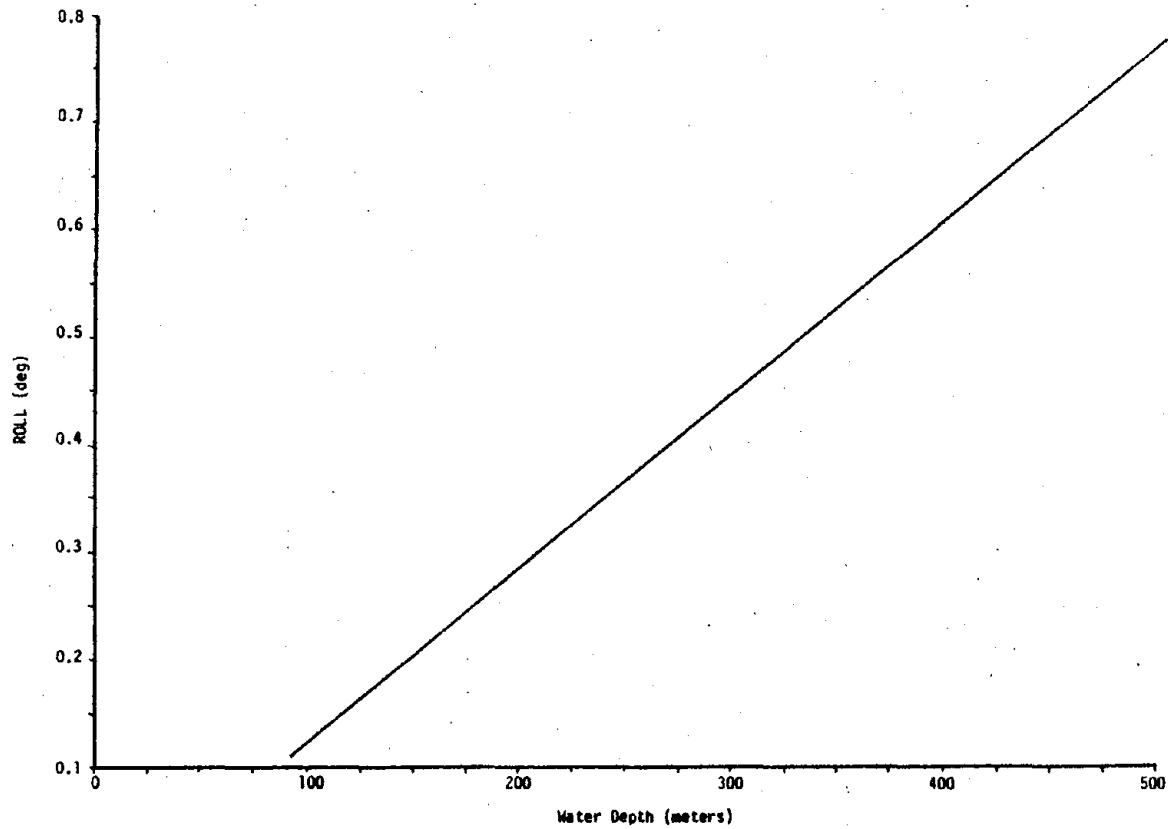
Figure 58. Variation of Roll Response Amplitude with Water Depth
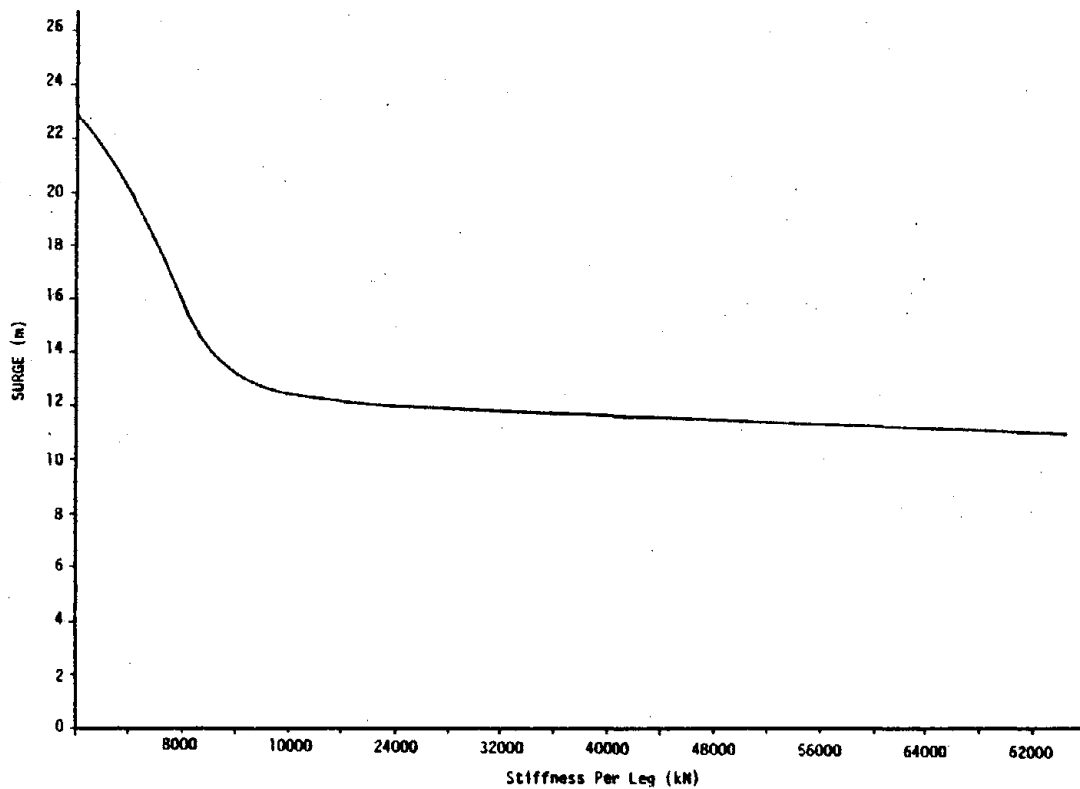
Figure 59. Variation of Surge Response Amplitude with Cable Stiffness
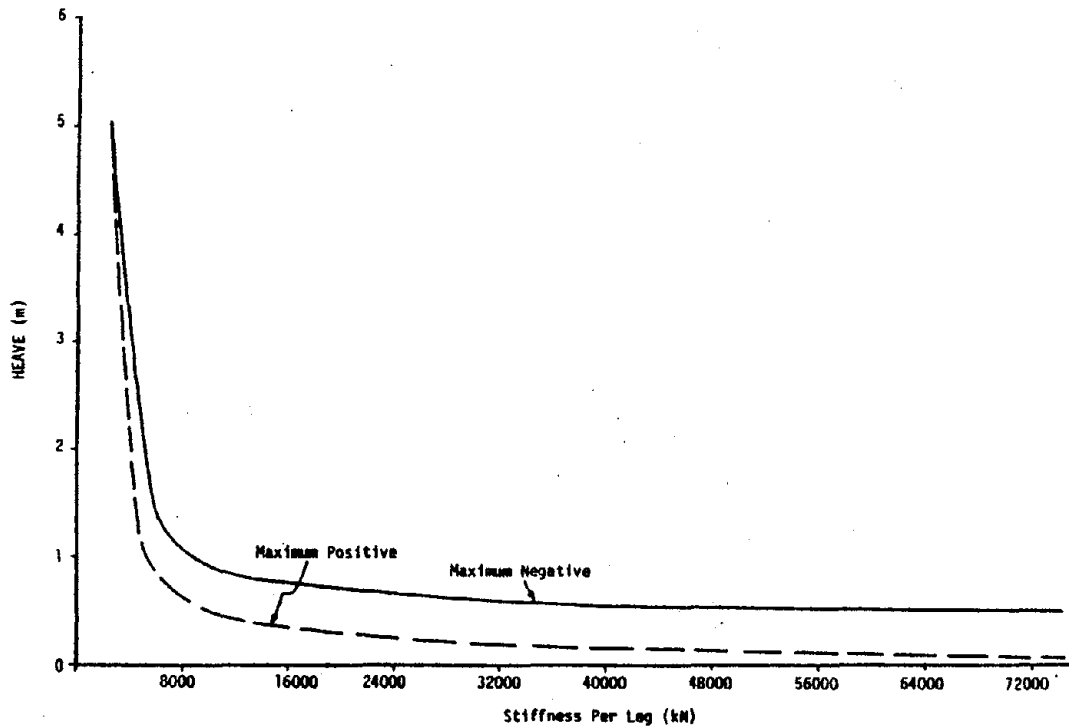
Figure 60. Variation of Heave Response Amplitude with Cable
Stiffness
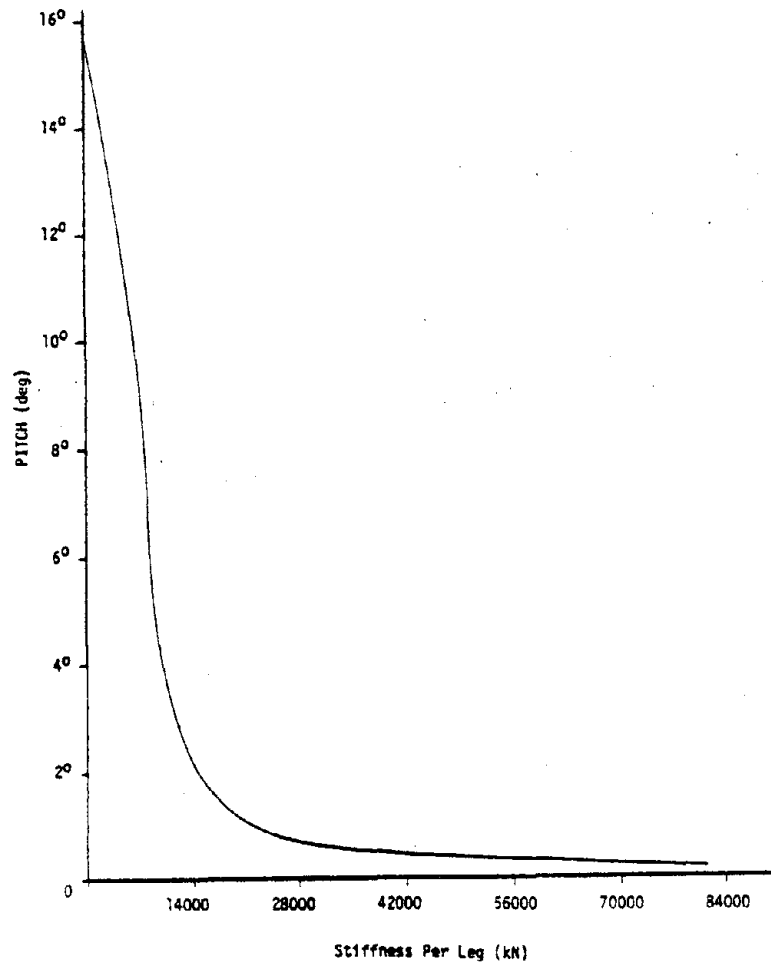
Figure 61. Variation of Pitch Response Amplitude with Cable
Stiffness
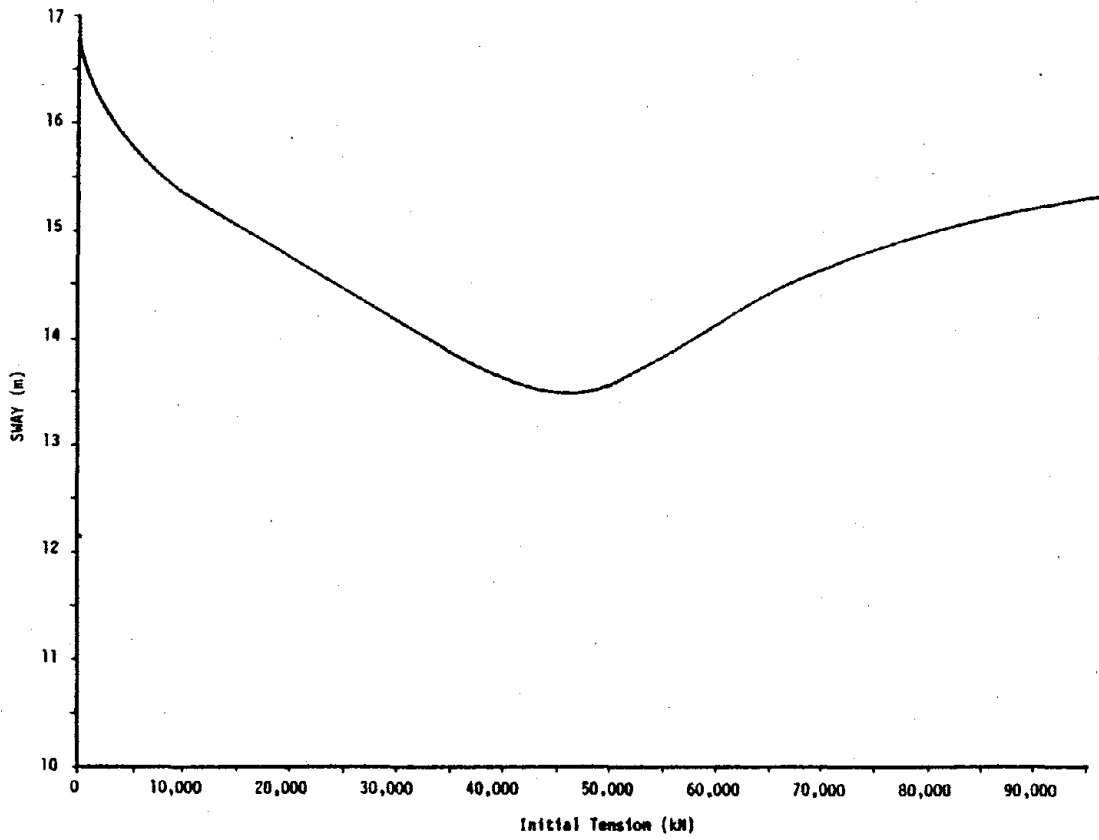
Figure 62. Variation of Sway Response Amplitude with Initial Tension
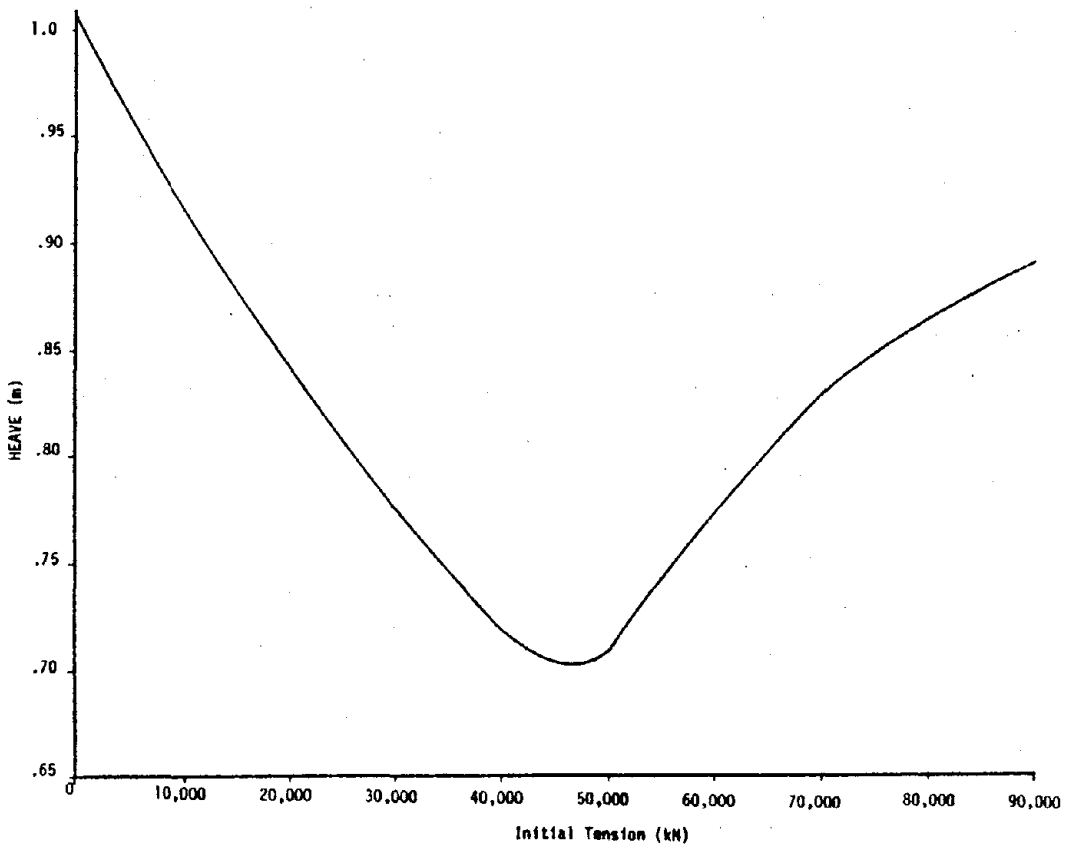
Figure 63. Variation of Heave Response Amplitude with Initial Tension
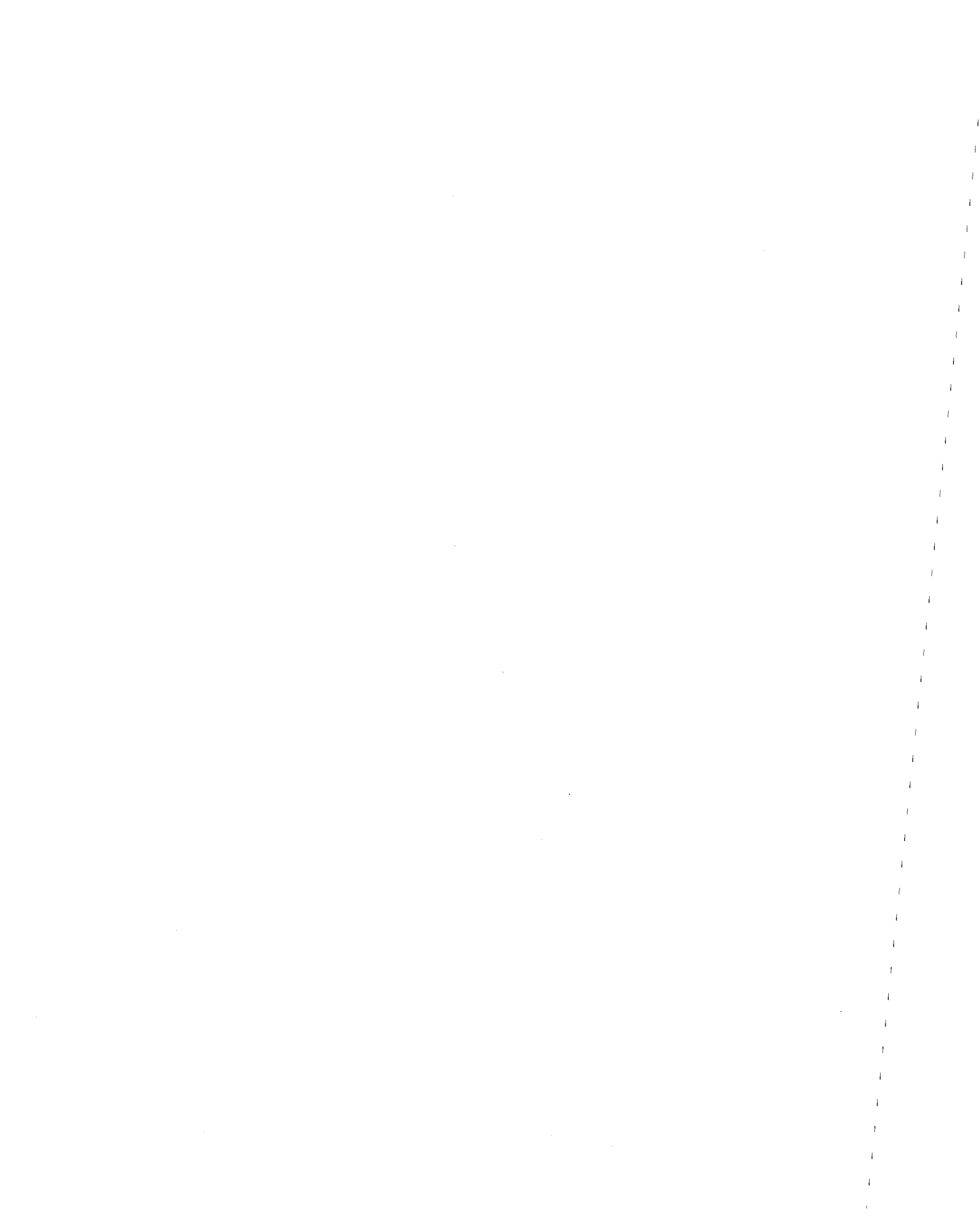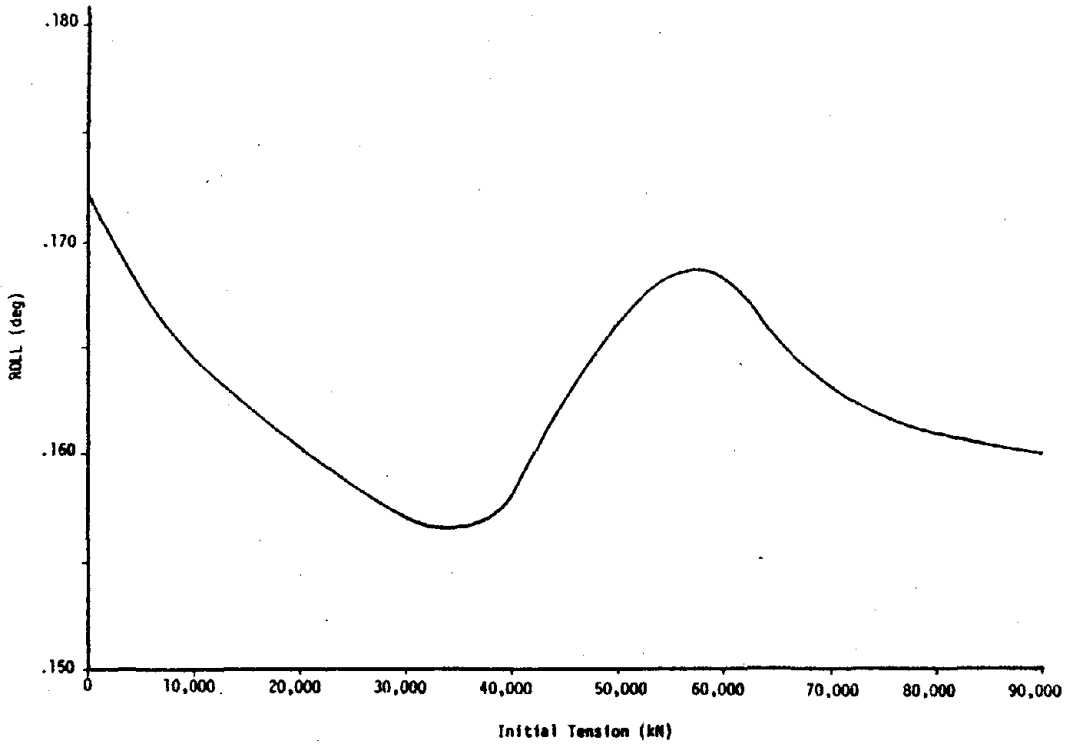
Figure 64. Variation of Roll Response Amplitude with Initial
Tension
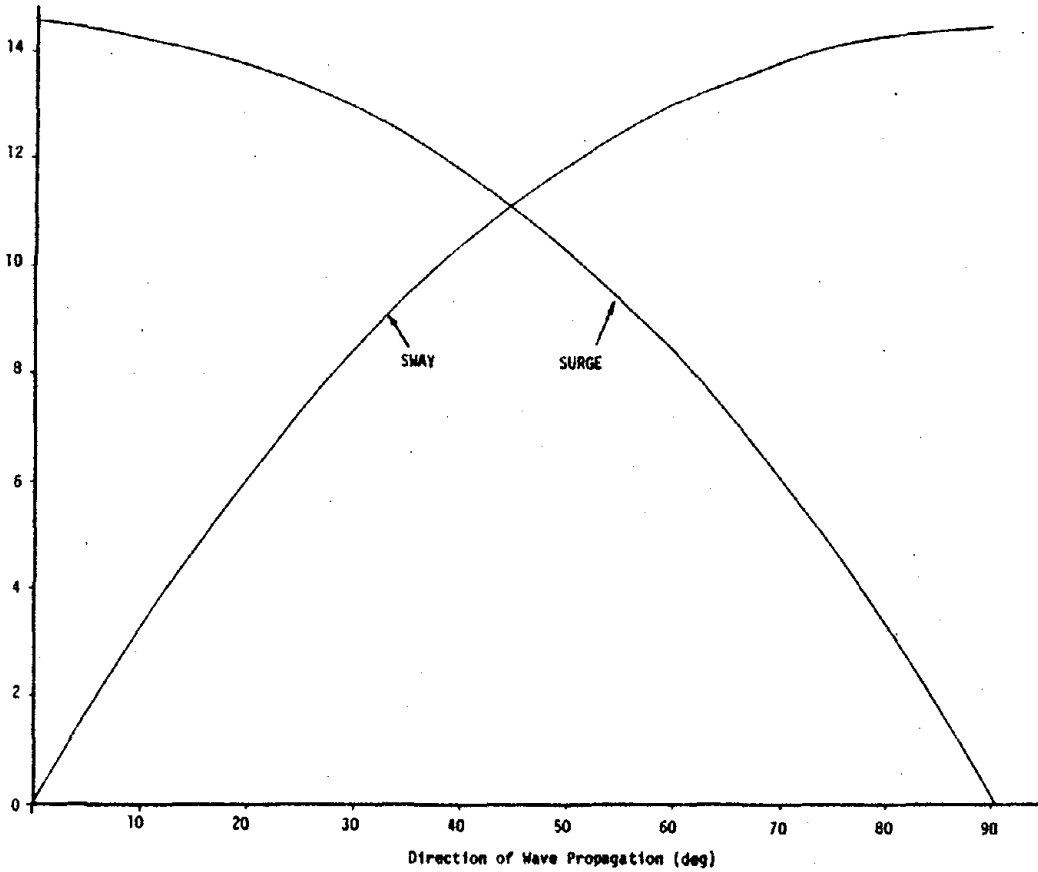
Figure 65. Variation of Surge or Sway with the Direction of
Wave Propagation
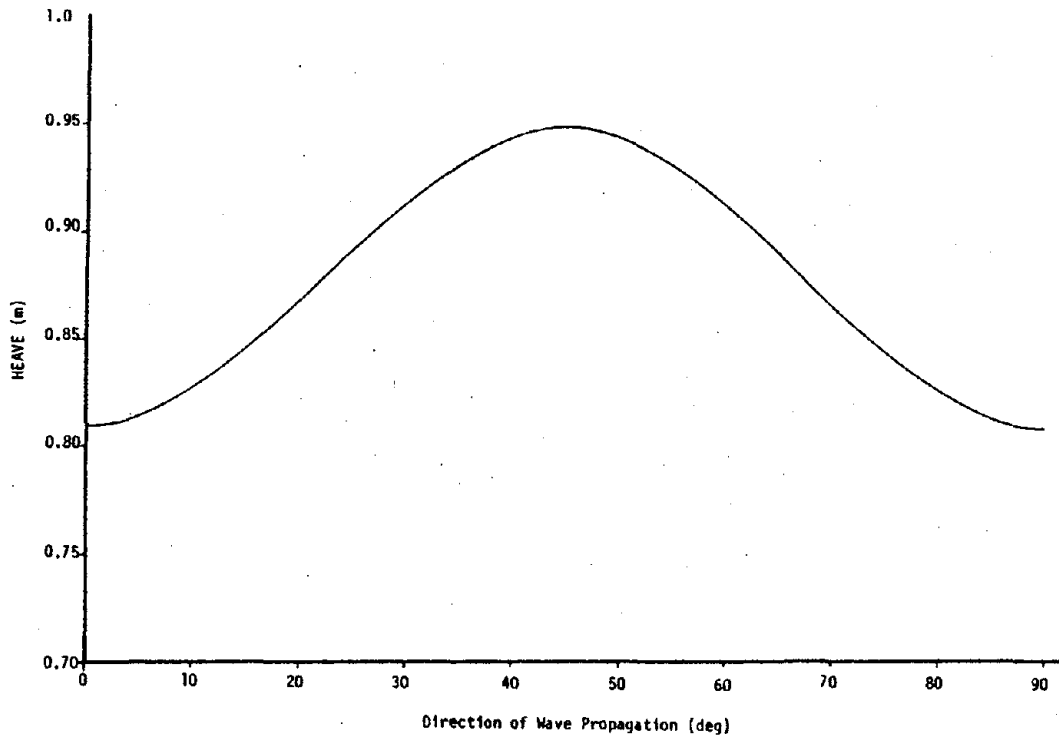
Figure 66. Variation of Heave with the Direction of Wave
Propagation
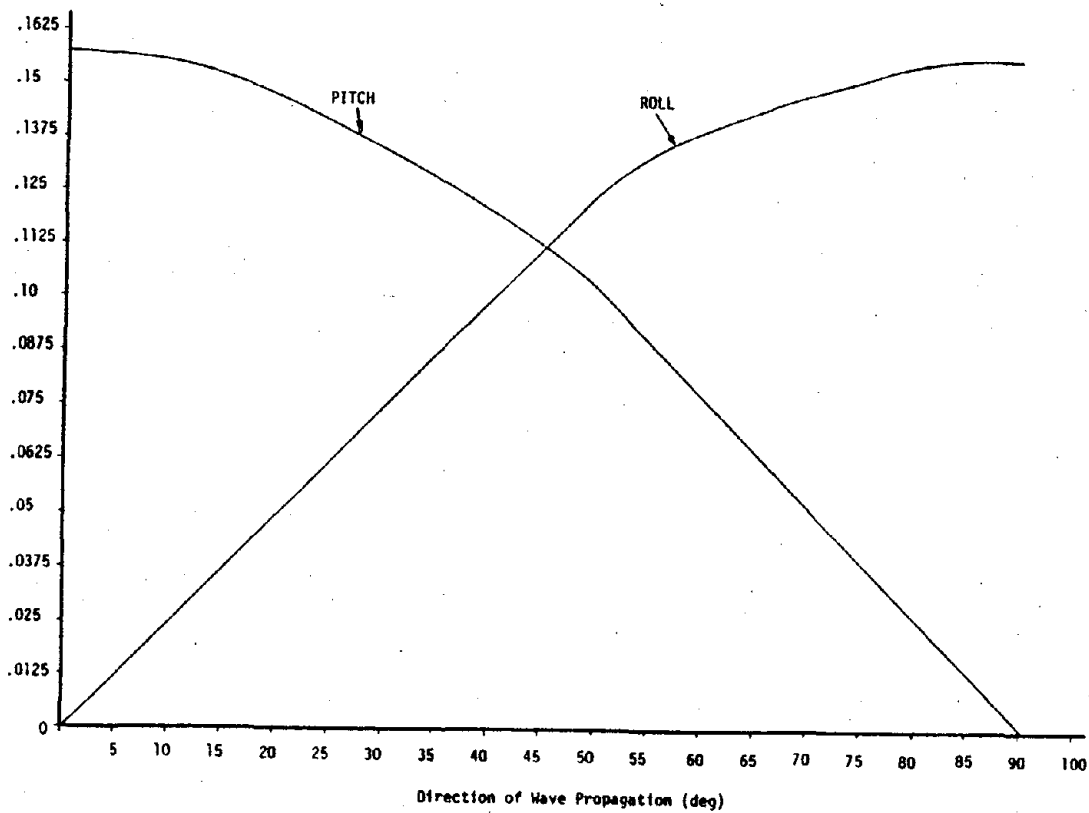
Figure 67. Variation of Pitch and Roll with the Direction of
Wave Propagation
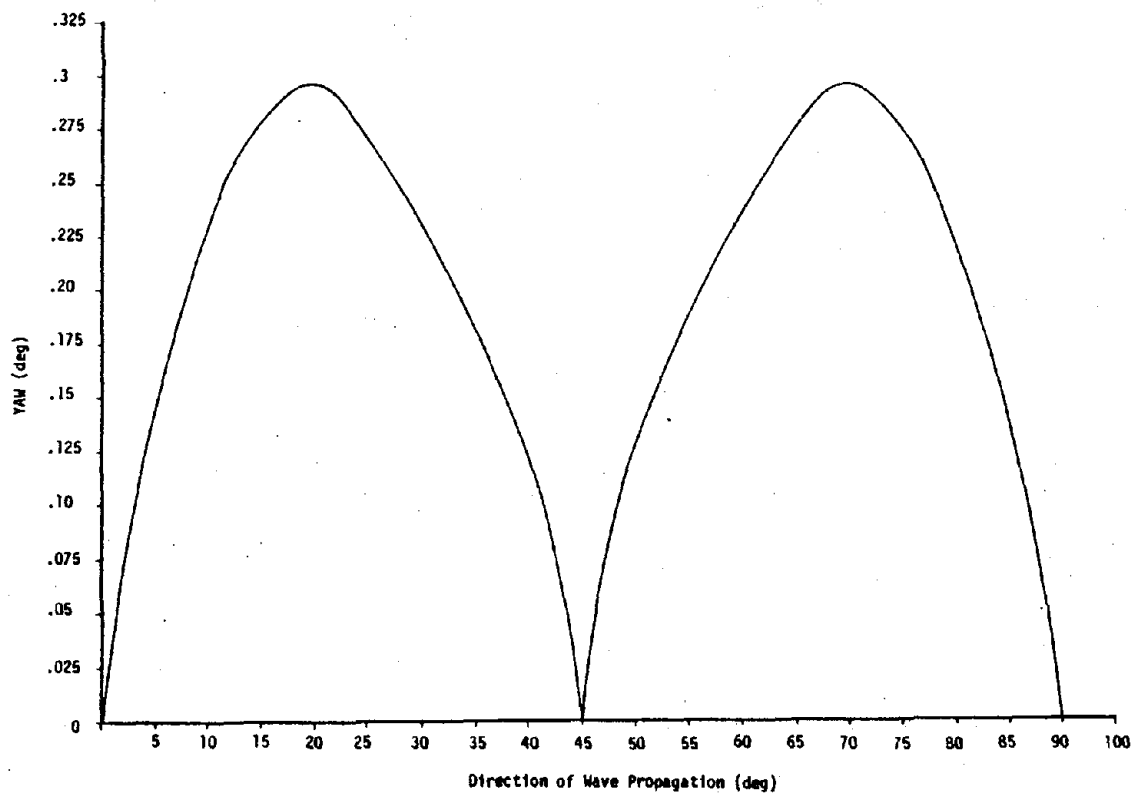
Figure 68. Variation of Yaw with the Direction of Wave Propagation
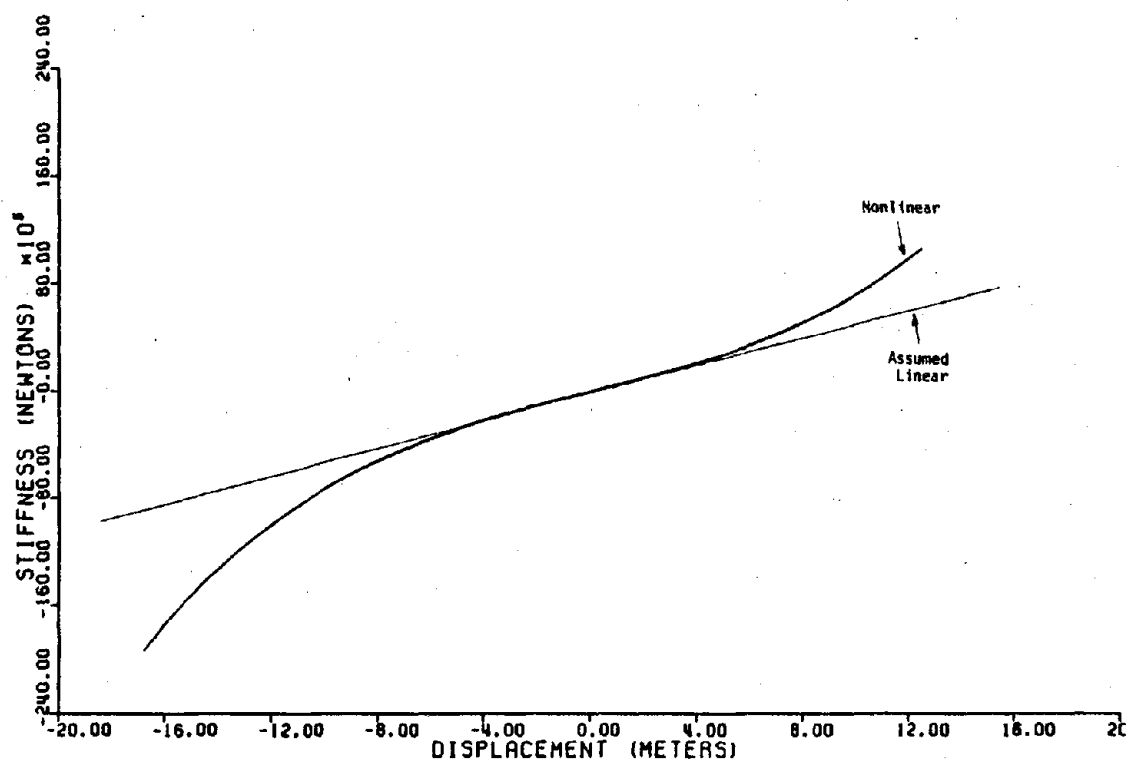
Figure 69. Plot of Cable Restoring Force for Surge Displacement
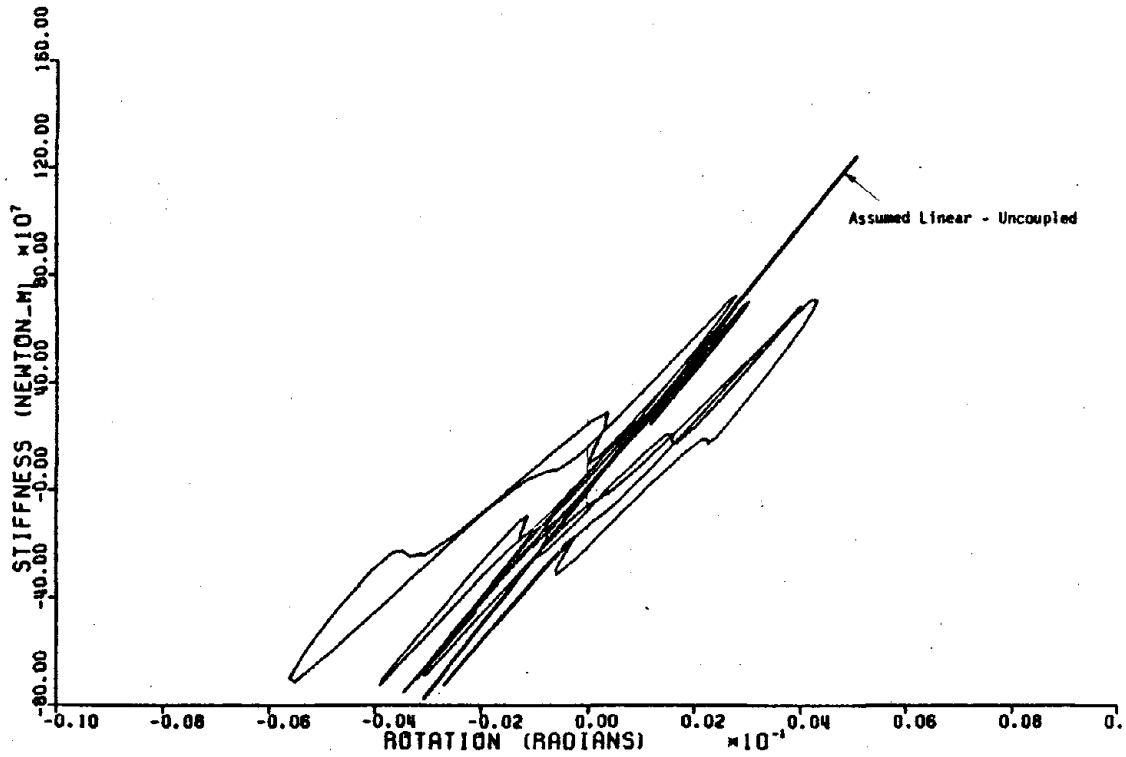
Figure 70. Plot of Cable Restoring Force for Pitch Displacement
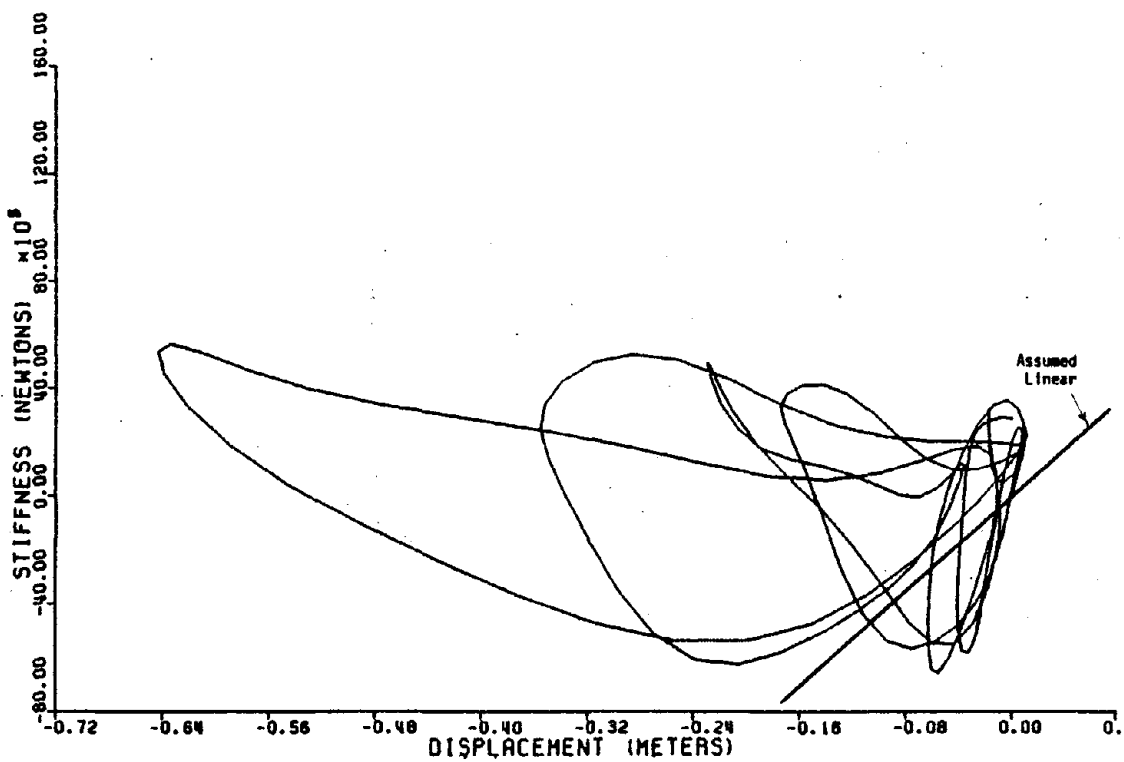
Figure 71. Plot of Cable Restoring Force for Heave Displacement
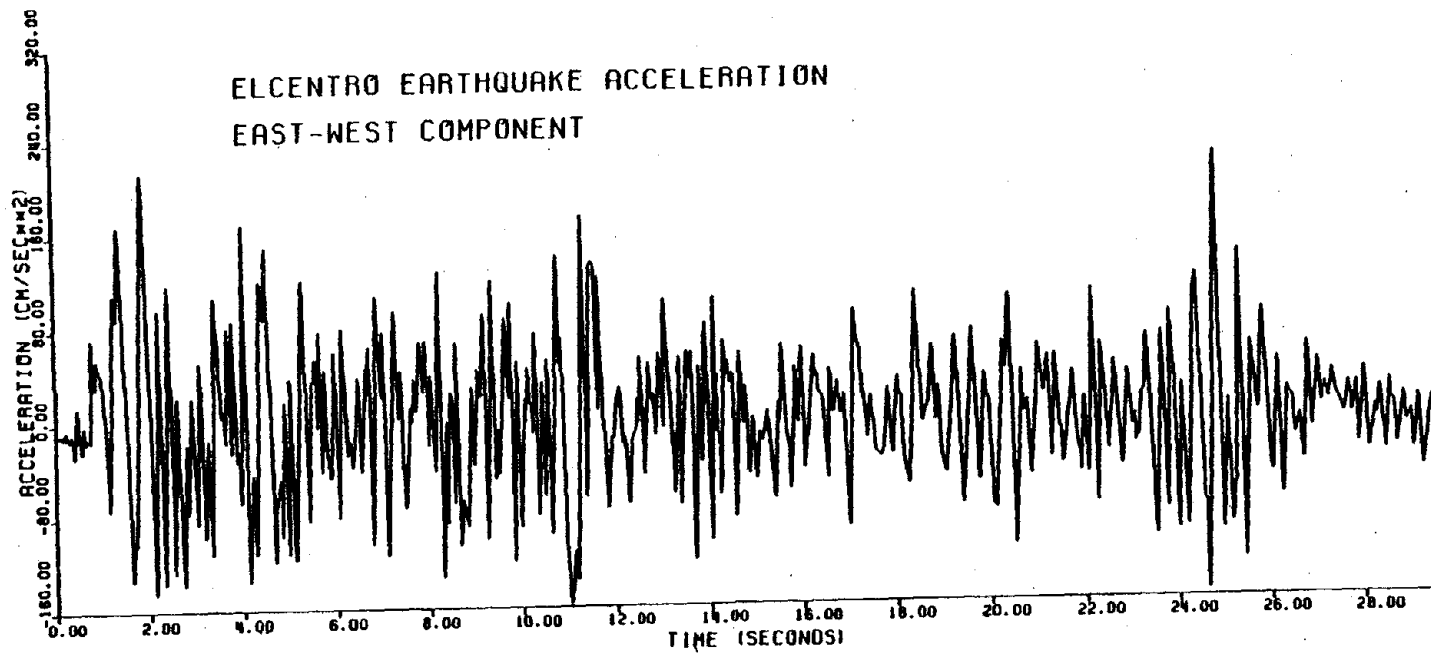
Figure 72. Acceleration Time History for the East-West Component
of El Centro, 1940
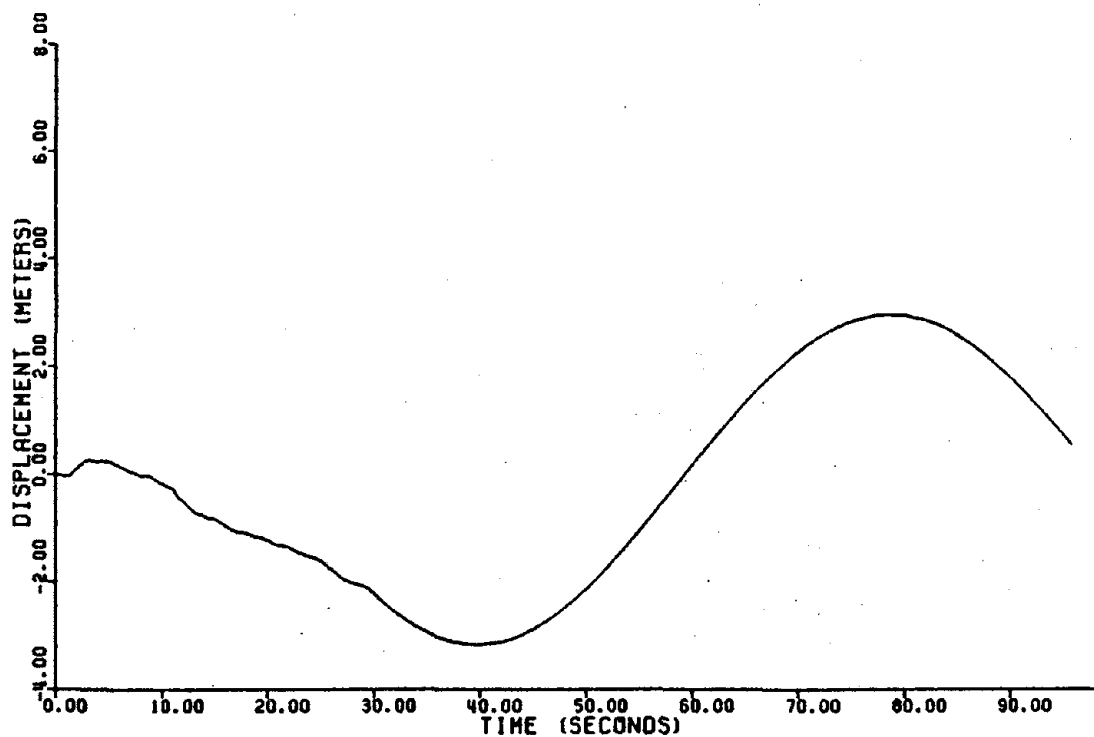
Figure 73. Time History of Surge Response for El Centro Earthquake
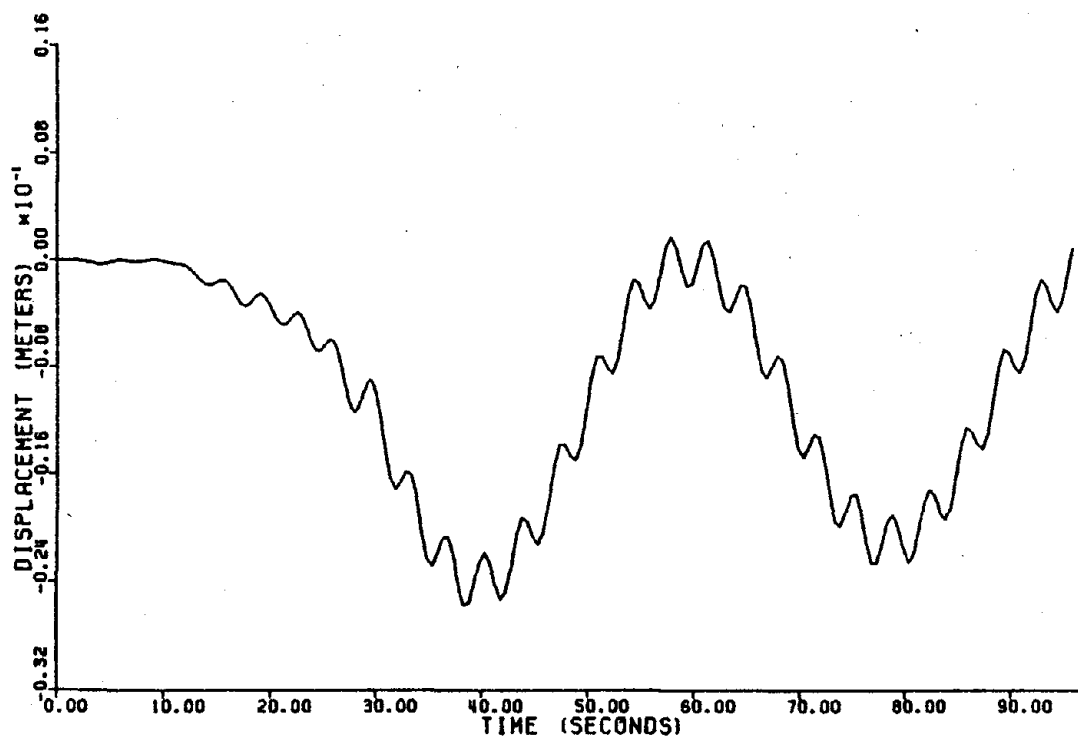
Figure 74. Time History of Heave Response for El Centro Earthquake
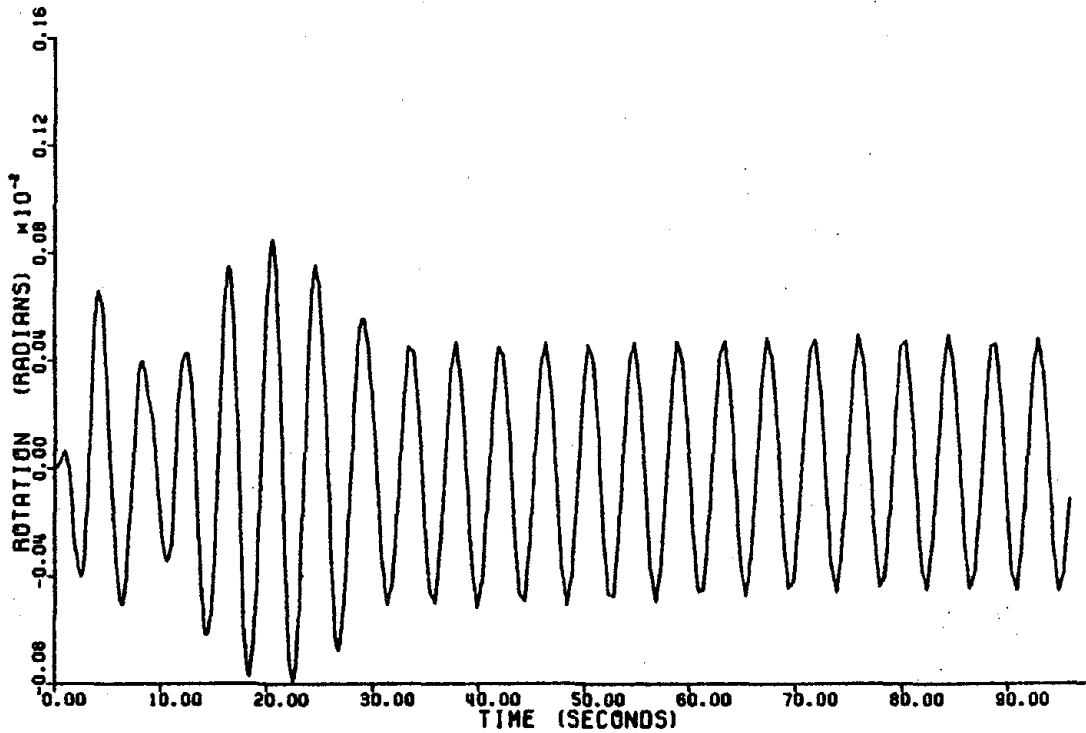
Figure 75. Time History of Pitch Response for El Centro Earthquake
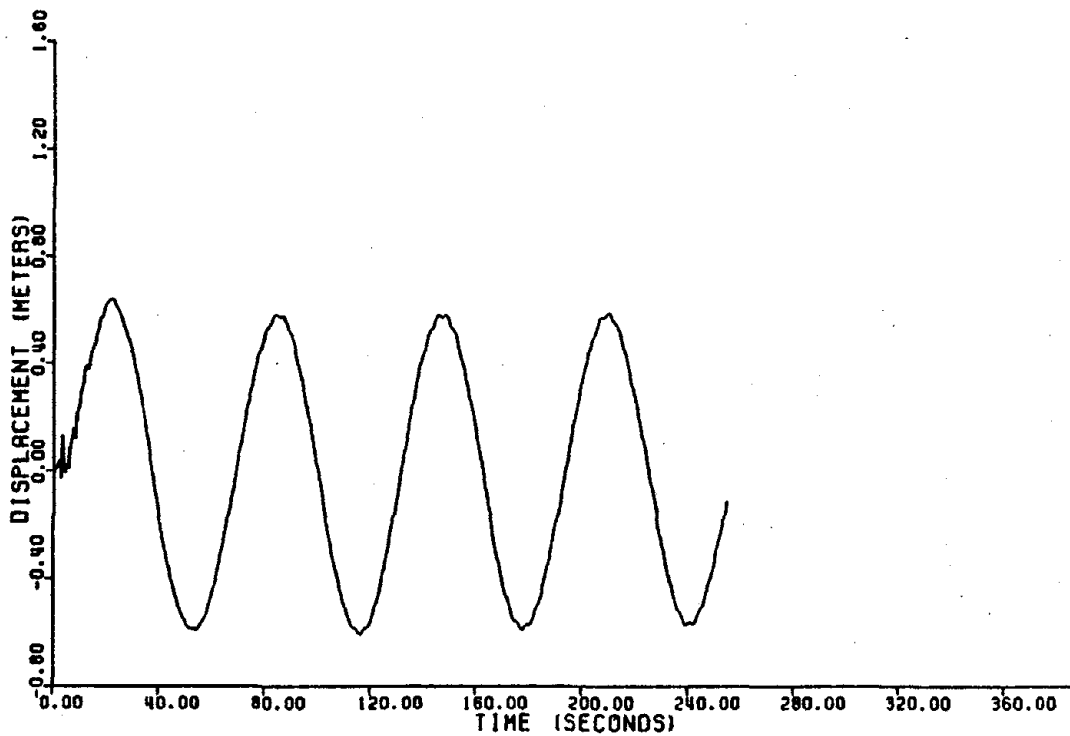
Figure 76. Time History of Surge Response to the S16E Component of
Pacoima Dam Record of San Fernando Earthquake, 1971
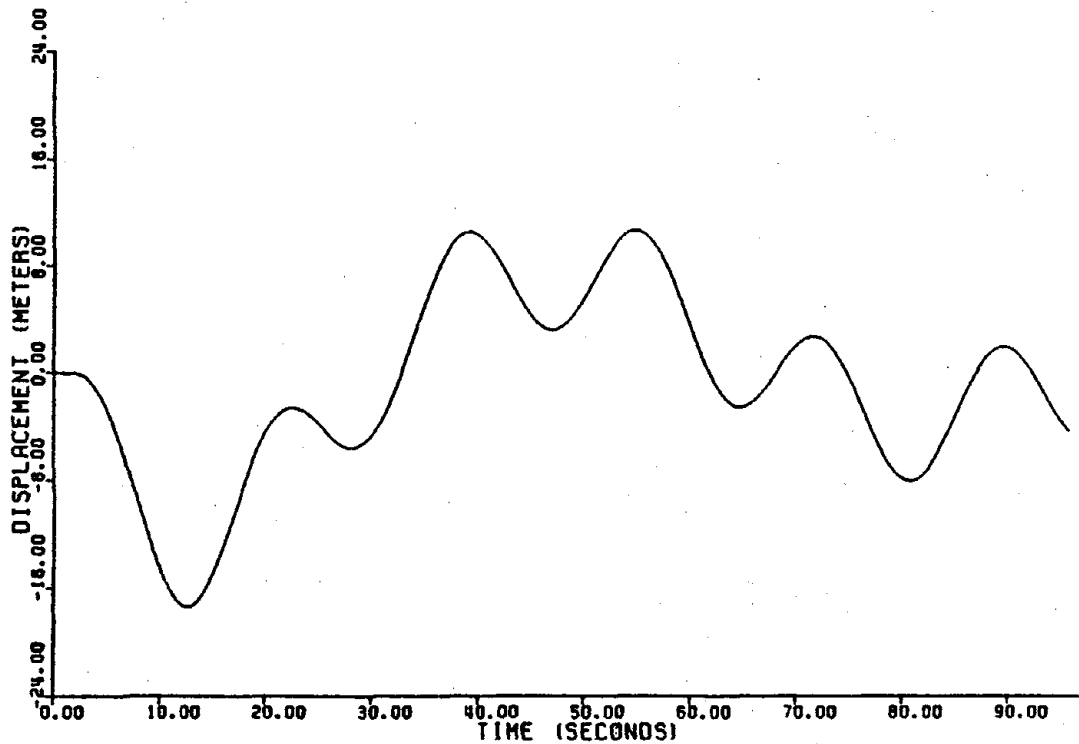
Figure 77. Time History of Surge Response to Combined El Centro
Earthquake and 17 Second Wave
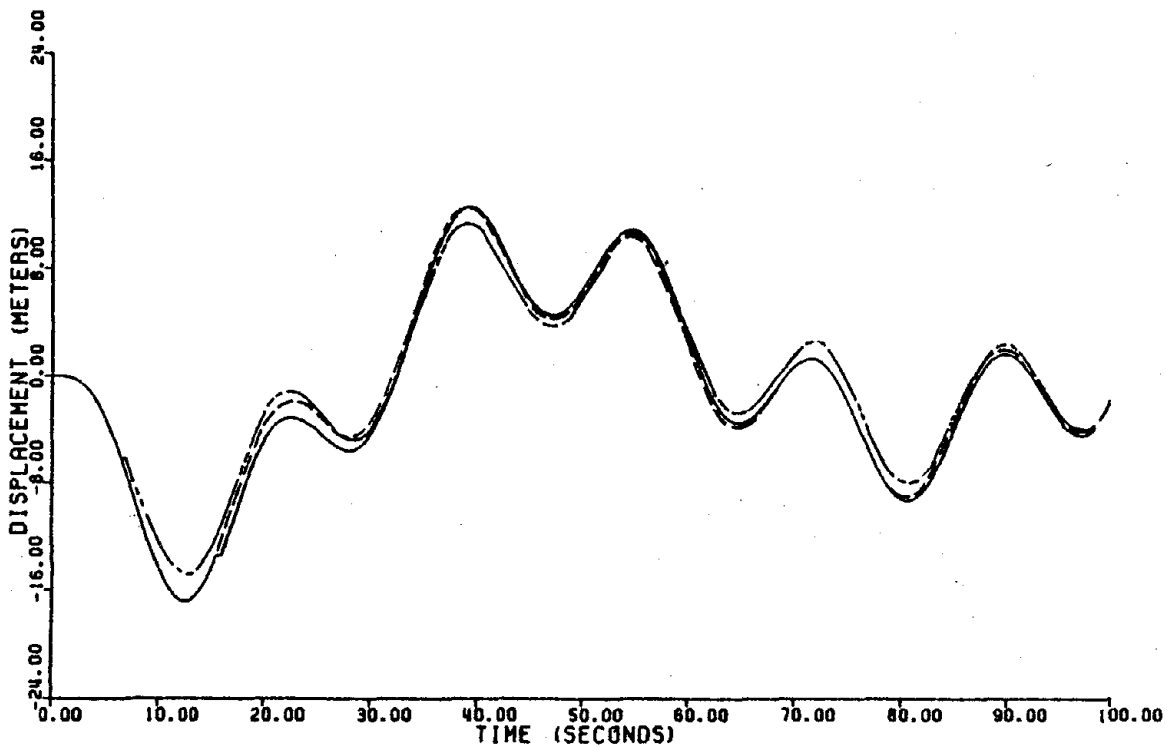
Figure 78. Time History of Surge Response to Combined 17 Second
Wave and El Centro Earthquake Loading with Earthquake
Introduced at Different Times
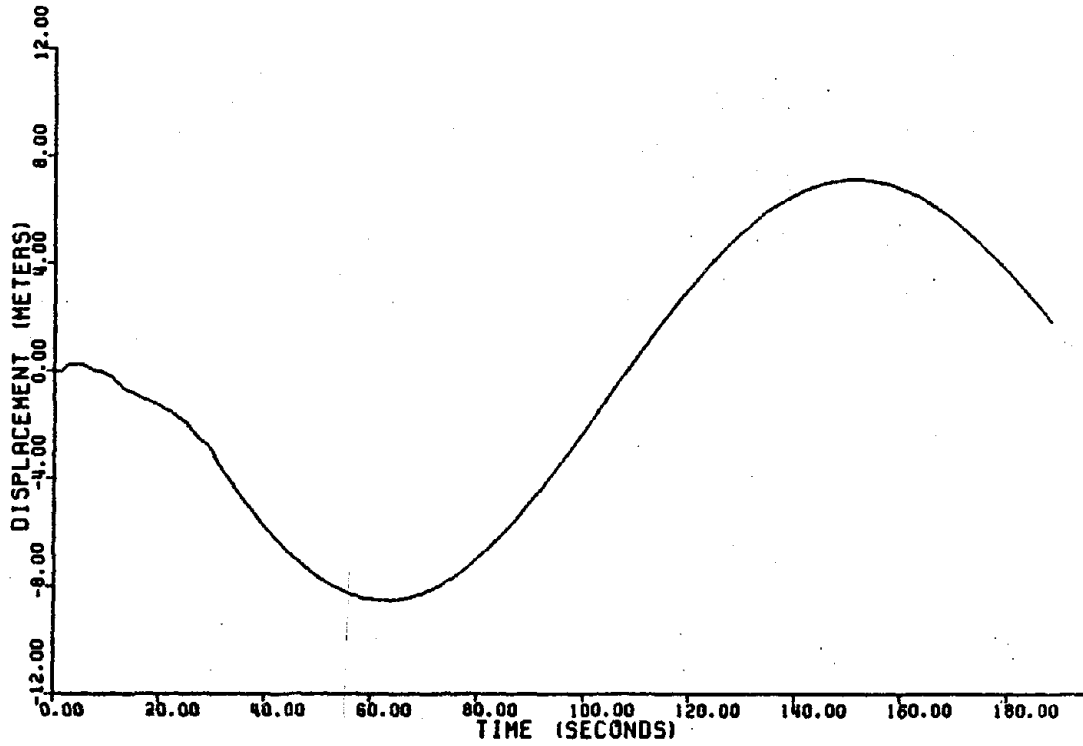
Figure 79. Time History of Surge Response to El Centro in 1000 m
Water Depth
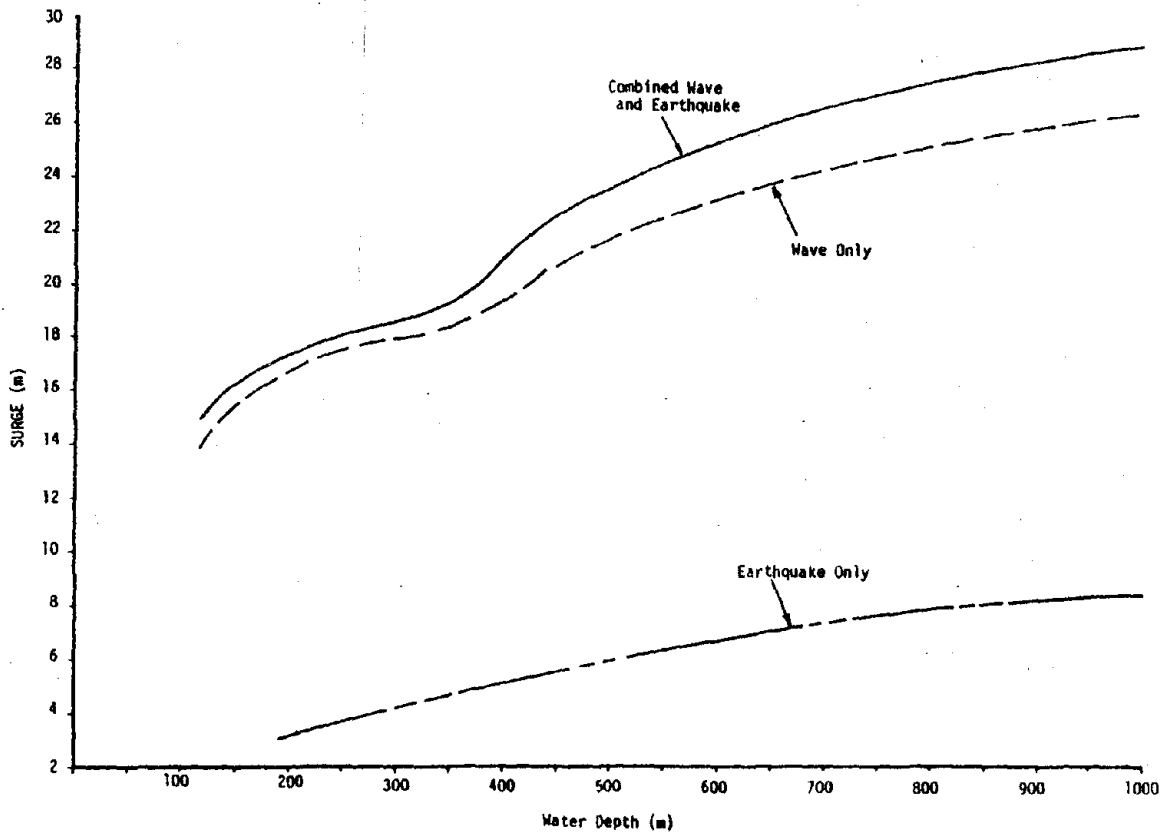
Figure 80. Variation of Surge Response with Water Depth for
17 Second Wave, El Centro Earthquake, and Combined
Loading
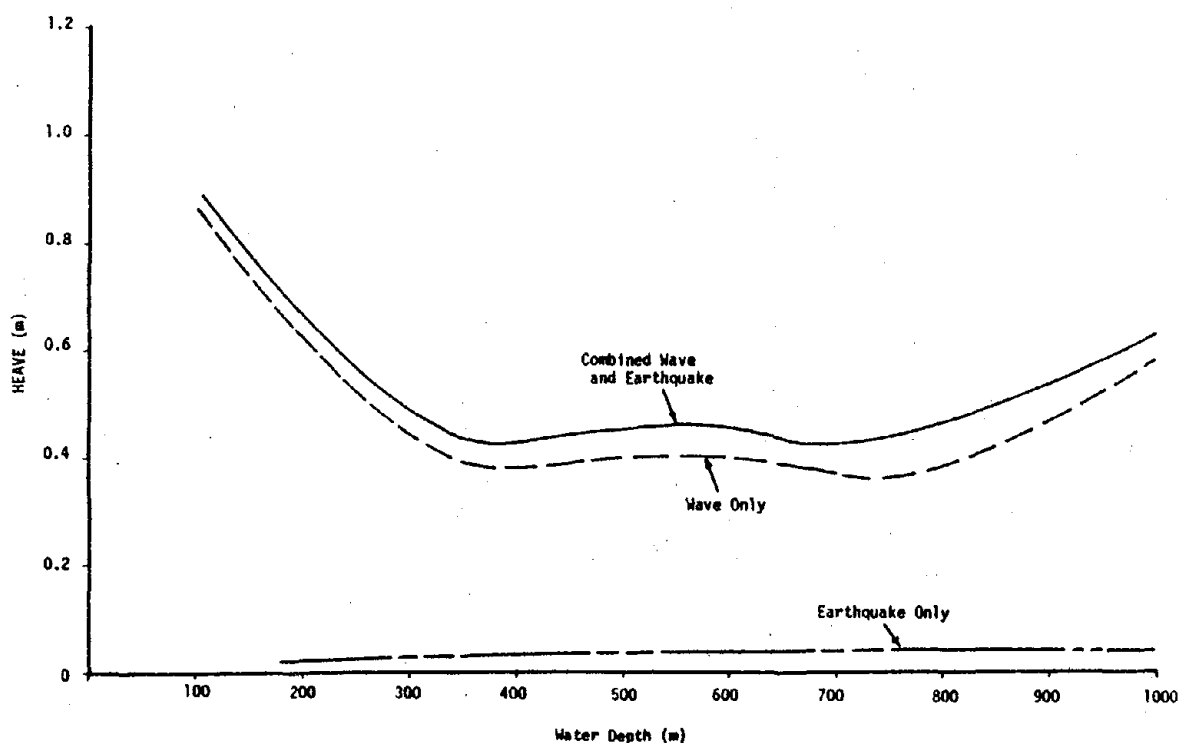
Figure 81. Variation of Heave Response with Water Depth for 17 Second Wave, El Centro Earthquake, and Combined Loading
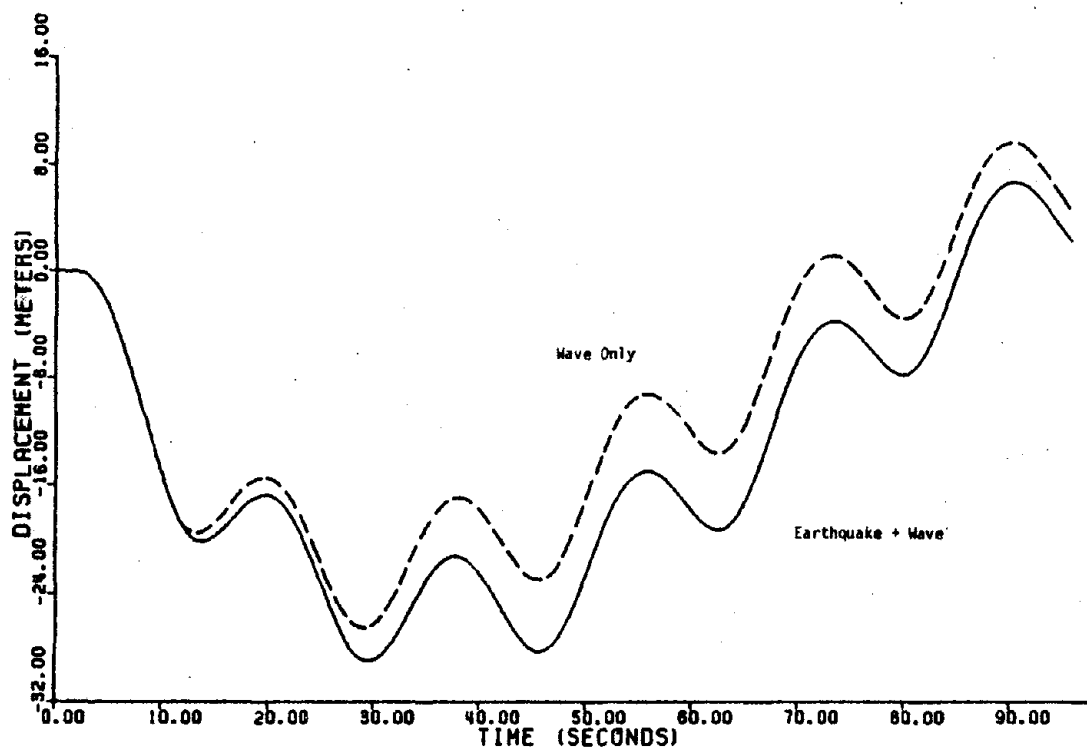
Figure 82. Comparison of Surge Response to 17 Second Wave with that from Combined Loading in 1000 m Water Depth
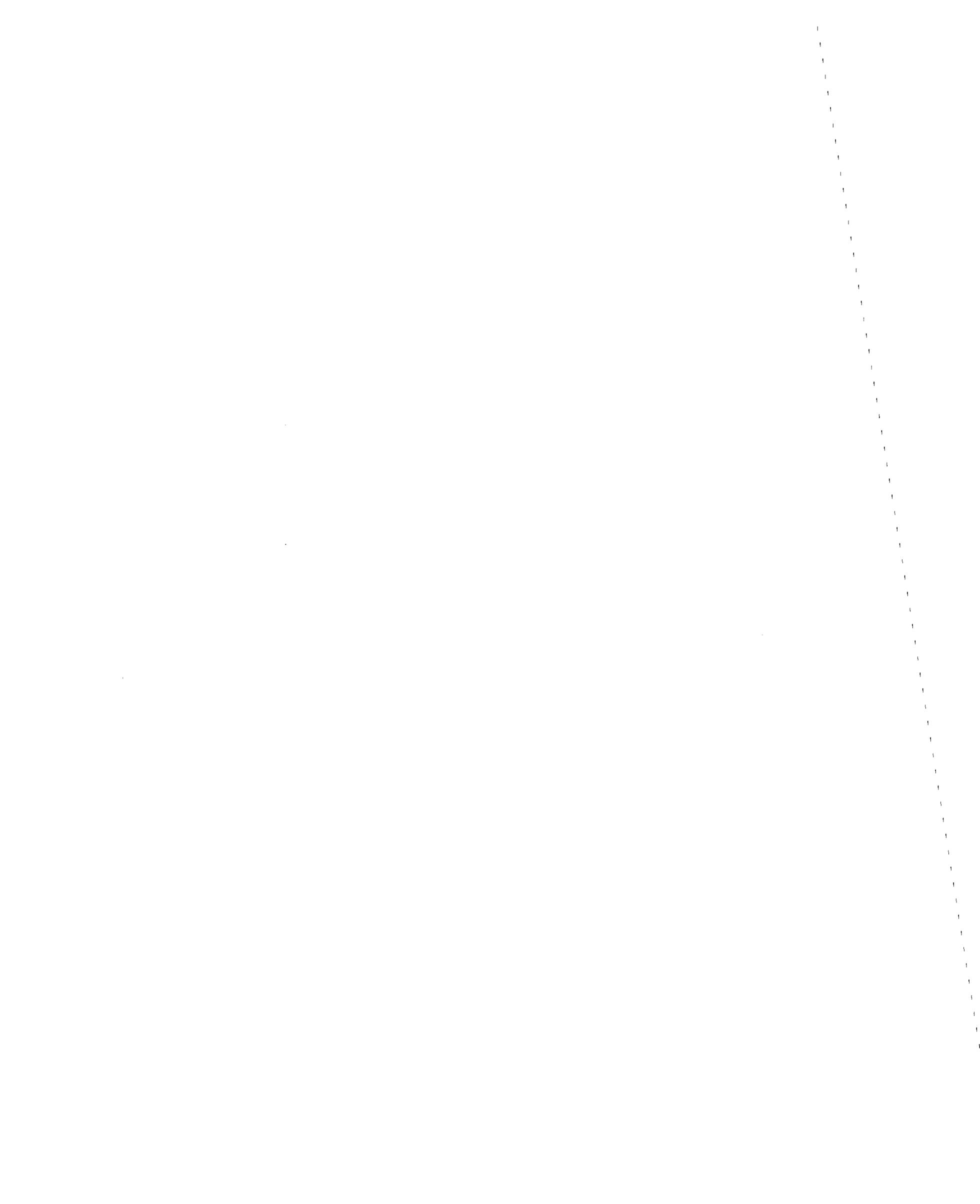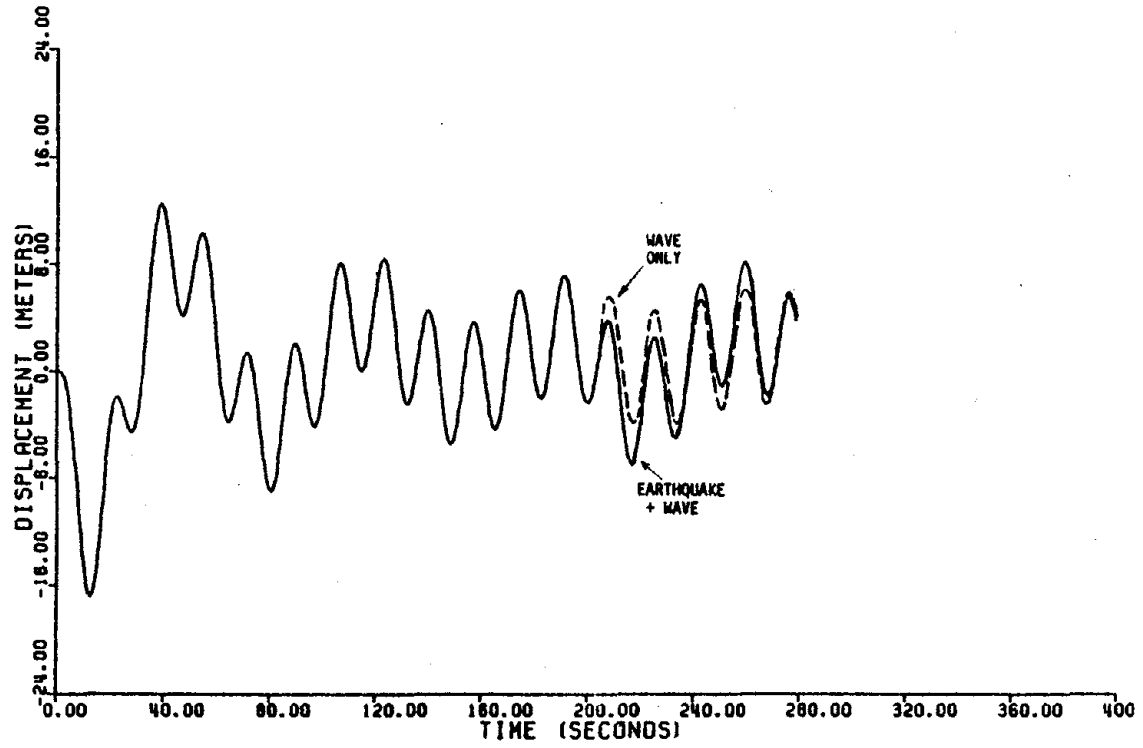
Figure 83. Time History of Surge Response to 17 Second Wave and Combined Loadings with El Centro Earthquake Introduced at t = 200 Seconds

V. APPENDIX I: DERIVATION OF WAVE FORCES

1. Horizontal Forces

a) Inertia Force on Columns

The integration of the inertia force acting on element dz of column i (Equation 24) yields:

$$F_{I_i} = \rho \frac{\pi D_i^2}{4} \int_0^{h_i} [C_m \dot{u}_i - (C_m - 1)\{\ddot{x} - (z - \bar{z})\ddot{\alpha} + 1/2\, X_i\, \dot{\alpha}^2\}]dz \qquad (V-1)$$

Substituting from Equation (17) and rearranging terms gives:

$$F_{I_i} = \rho \frac{\pi D_i^2}{4}\{[C_m \frac{2\pi^2 H}{T^2} \sin[k(\bar{X} - ct)] \int_0^{h_i} e^{-kz}\, dz]$$

$$- [(C_m - 1) \int_0^{h_i} [\ddot{x} - (z - \bar{z})\ddot{\alpha} + \tfrac{1}{2}X_i \dot{\alpha}^2]\, dz]\} \qquad \ldots\ldots (V-2)$$

which can be simplified by integrating and lumping coefficients as follows:

$$F_{I_i} = a_1 D_i^2 (1 - e^{-kh_i}) \sin[k(\bar{X} - ct)] - a_2 D_i^2 (\ddot{x} + \bar{z}\,\ddot{\alpha} + X_i \dot{\alpha}^2 - \frac{h_i \ddot{\alpha}}{2})h_i \qquad (V-3)$$

where

$$a_1 = \frac{\rho \pi^3 C_m H}{2kT^2}, \qquad\qquad a_2 = \frac{\rho \pi (C_m - 1)}{4},$$

and

$$\bar{X} = x + X_i.$$

Where X is the instantaneous position of the center of gravity of the structure taken in the direction of the wave, and X_i is the x-coordinate of each of the eight columns in the direction of the wave and calculated as follows:

$$X_5 = b \sin \alpha - a \cos \alpha$$

$$X_6 = a \cos \alpha + b \sin \alpha$$

$$X_7 = -X_6$$

$$X_8 = -X_5$$

$$X_9 = b \sin \alpha$$

$$X_{10} = -X_9$$

$$X_{11} = -a \cos \alpha$$

$$X_{12} = -X_{11}$$

with a and b equal to one-half the distance between the corner columns in the x and y directions, respectively, and   is the angle of wave direction measured from the x-axis (see Figure 15).

b) Drag Force on Columns

Equation (19) can be rewritten as

$$\delta F_d = (\mp) \frac{\rho C_d D}{2} (u_{rel})^2 \, dz \tag{V-4}$$

where the $(\mp)$ sign depends on the sign of the relative fluid velocity, u_{rel}.

Substituting u_{rel} (Equation 21) into Equation (V-4), and integrating over the length of each cylinder gives:

$$F_{d_i} = (\mp) \frac{\rho C_d D_i}{2} \int_0^{h_i} \{\frac{\pi H}{T} e^{-kz} \cos [k(\overline{X} - ct)] - [\dot{x} - (z-\overline{z}) \dot{\alpha} + \frac{X_i \dot{\alpha}^2}{2}]\}^2 \, dz$$

Resolving the square and separating the z-terms gives:

$$F_{d_i} = (\mp)\frac{\rho C_d D_i}{2} \left\{ \left[\frac{\pi^2 H^2}{T^2} \cos^2 [k(\overline{X} - ct)] \int_0^{h_i} e^{-2kz} dz \right] - \right.$$

$$2 \int_0^{h_i} \frac{\pi H}{T} \cos [k(\overline{X} - ct)]_i (\dot{x} + \overline{z} \dot{\alpha} + \frac{X_i \dot{\alpha}^2}{2}) - z\dot{\alpha}] [e^{-kz}] dz$$

$$+ \int_0^{h_i} [\frac{(\dot{x} + \overline{z}\dot{\alpha} + X_i\dot{\alpha}^2)^2}{2} - 2(\dot{x} + \overline{z} \dot{\alpha} + \frac{X_i\alpha^2)z\dot{\alpha}}{2} + z^2\dot{\alpha}^2] dz \}$$

and

$$F_{d_i} = (\mp)\frac{\rho C_d D_i}{2} \left\{ \left[\frac{\pi^2 H^2}{T^2} \cos^2 [k(\overline{X} - ct)] \frac{1}{2k} (1 - e^{-2kh_i}) \right] \right.$$

$$-2[\frac{\pi H}{T} \cos [k(\overline{X} - ct)] (\dot{x} + z\dot{\alpha} + \frac{X_i\dot{\alpha}^2}{2}) (1 - e^{-kh_i}) (\frac{1}{k}) - \frac{\dot{\alpha}\pi H}{kT} (\frac{1}{k} - \frac{e^{-kh_i}}{k})$$

$$\cos [k(\overline{X} - ct)]] + [\frac{(\dot{x} + \overline{z} \dot{\alpha} + \frac{X_i\dot{\alpha}^2}{2})^2 h_i - (\dot{x} + \overline{z} \dot{\alpha} + \frac{X_i\dot{\alpha}^2}{2})h_i^2\dot{\alpha} + \frac{\dot{\alpha}^2h_i^3}{3}] \}}{}$$

By lumping parameters and rearranging terms one obtains:

$$F_{d_i} = (\mp) \{ b_1 D_i \cos^2[k(\overline{X} - ct)] (1-e^{-2kh_i}) - b_{2_i} b_3 D_i (1-e^{-kh_i})$$

$$\cos [k(\overline{X} - ct)] + D_i b_3\dot{\alpha} \frac{1}{k} (1-e^{-kh_i}) \cos [k(x - ct)] - b_3\dot{\alpha} h_i D_i$$

$$e^{-kh_i} \cos [k(\overline{X} - ct)] + b_{2_i}^2 b_0 D_i h_i - b_{2_i} b_0\dot{\alpha} h_i^2 + \frac{b_0 \dot{\alpha} D_i h_i^3}{3} \}$$

and a collection of terms that contains: $\cos k(X-ct)$ $(1-e^{-kh})D_i$ yields:

$$F_{d_i} = (\mp) \{\cos [k(\overline{X} - ct)] (1-e^{-2kh_i}) D_i [b_1 \cos [k(\overline{X} - ct)] (1 + e^{-kh_i})$$

$$- b_2 b_3 + \frac{b_3\dot{\alpha}}{k} - b_3\dot{\alpha}h_i D_i e^{-kh_i} \cos [k(\overline{X} - ct)] + b_{2_i}^2 b_0 D_i h_i$$

$$- b_{2_i} b_0\dot{\alpha} h_i^2 + \frac{1}{3} b_0\dot{\alpha} D_i h_i^3 \} \tag{V-5}$$

where $\qquad b_o = 1/2 \, \rho \, C_d \qquad\qquad b_1 = \dfrac{\pi^2 H^2}{2kT^2} \, b_o$

$$b_{2_i} = \dfrac{(\dot{x} + \bar{z}\,\dot{\alpha} + X_i\dot{\alpha}^2)}{2} \qquad\qquad b_3 = \dfrac{2\pi H}{kT} \, b_o$$

c) Inertia Forces on Hulls and Cross Bracings

For hull No. 1 in Figure 15 the normal component of the fluid acceleration at point p, distance S from O_1, for the section O_1O_2 is:

$$u_n = \dot{u} \sin \alpha \quad = \dfrac{2\pi^2 H}{T^2} \; e^{-k\bar{h}} \quad \sin \, [k(\bar{x} - ct)] \, \sin \, \alpha$$

and a substitution for X in terms of S yields:

$$\bar{x} = \beta'S + \gamma'$$

where

$$\beta' = \cos \alpha, \text{ and } \gamma' = b \sin \alpha.$$

Since S is a positive quantity, the value of X for O_1O_3 becomes:

$$\bar{x} = -\beta'S + \gamma'$$

For hull No. 1, the inertia force in the y-direction is:

$$F_{1_y} = \int_{-a}^{a'} \dfrac{\rho\pi D^2_1}{4} \; C_m \; (\dfrac{2\pi^2 H}{T^2} \; e^{-kh} \sin \, [k(\bar{x} - ct)]) \, \sin \, \alpha \; d\bar{x}$$

$$= a_y \int_0^{a'} \sin \, [k(-\beta'S+\gamma'-ct)] \; dS + a_y \int_0^{a'} \sin \, [k(\beta'S + \gamma' - ct)]dS$$

where $\qquad a_y = \dfrac{\rho\pi^3 D_1^2 H}{2T^2} \; e^{-k\bar{h}} \, C_m \, \sin \, \alpha$

$$F_{1_y} = \dfrac{1}{k\beta'} \; a_y \; \{\cos \, [-k\beta'S + k \, (\gamma'-ct)] \; |_0^{a'} -\cos \, [k\beta'S + k \, (\gamma'-ct)] \; |_0^{a'}$$

$$= \dfrac{a_y}{k\beta'} \; \{[\cos \, [-k\beta'a' + k(\gamma'-ct)] - \cos \, [k \, (\gamma'-ct)] \,]$$

$$+ \, [-\cos \, [k\beta'a' + k \, (\gamma'-ct)] + \cos \, [k \, (\gamma'-ct)] \,] \, \}$$

using the trigonometric identity: $\cos(a-b)-\cos(a+b) = 2 \sin(a) \cos(b)$, one obtains:

$$F_{1_y} = \frac{2a_y}{k\beta'} \sin (k\beta'a') \sin [k(\gamma'-ct)] \qquad (V-6)$$

Similarly, for hull No. 2:

$$F_{2_y} = \frac{-2a_y}{k\beta} \sin (k\beta'a') \sin [k(\gamma' + ct)] \qquad (V-7)$$

Combining F_{1_y} and F_{2_y}, the total horizontal inertia force on the hulls becomes:

$$F_y = \frac{-4a_y}{k\beta'} \sin (k\beta'a') \cos (k\gamma') \sin (kct) \qquad (V-8)$$

For the cross bracings (hulls No. 3 and No. 4),

$$\dot{u}_n = \dot{u} \cos \alpha ,$$

$$\dot{X} = \gamma'' - \beta'' S,$$

$$\gamma'' = a \cos \alpha ,$$

$$\beta'' = \sin \alpha .$$

Integrating in the y-direction yields:

$$F_x = \frac{-4a_x}{k\beta''} \sin (k\beta''b') \cos (k\gamma'') \sin (kct) \qquad (V-9)$$

where

$$a_x = \frac{\rho\pi^3 C_m d_3{}^2 H}{2T^2} \; e^{-k\overline{h}} \cos \alpha$$

d) Drag Forces on Hulls and Cross Bracings

The derivation of the drag forces on hulls and cross bracings is simi-
lar to that of inertia forces. For hull No. 1:

$$\overline{F}_{1_y} = (\overline{+}) \frac{\rho C_d D_1}{2} \int_{-a'}^{a'} [u_n \sin \alpha]^2 \, dS$$

$$= (\overline{+}) \frac{\rho C_d D_1}{2} \int_{-a'}^{a'} [\frac{\pi H}{T} e^{-k\overline{h}} \cos [k(\overline{x}-ct)] \sin\alpha]^2 dS$$

$$= (\overline{+}) \frac{\rho C_d D_1}{2} \frac{\pi^2 H^2}{T^2} e^{-2k\overline{h}} \sin^2 \alpha \int_{-a'}^{a'} \cos^2 [k(\overline{x}-ct)] \, dS$$

using the trigonometric identity: $\cos^2 a = \frac{1}{2} (\cos 2a + 1)$

$$\overline{F}_{1_y} = c_1 \int_{-a'}^{a'} (\cos [2k(\overline{x}-ct)]+1) \, dS$$

$$\overline{F}_{1_y} = c_1 \left\{ \int_{0}^{a'} (\cos [2k(\beta'S+\gamma'-ct)]+1) dS \right.$$

$$\left. + \int_{-a'}^{a'} (\cos[2k(-\beta'S+\gamma'-ct)]+ 1) \, dS \right\}$$

$$= \frac{c_1}{2k\beta'} [\sin [2k\beta'S + 2k(\gamma'-ct)] + S - \sin [-2k\beta'S + 2k(\gamma' - ct)] + S] \Big|_{0}^{a'}$$

$$= \frac{c_1}{2k\beta'} [\{\sin[2k\beta'a' + 2k(\gamma'-ct)] - \sin [2k(\gamma'-ct)]\}$$

$$- \{ \sin [-2k\beta'a' + 2k(\gamma'-ct)] - \sin [2k(\gamma'-ct)]\} +2a']$$

$$= \frac{c_1}{2k\beta'} [\sin[2k\beta'a' + 2k(\gamma'-ct)] - \sin [-2k\beta'a' + 2k(\gamma'-ct)] + 2a']$$

$$\overline{F}_{1_y} = \frac{c_1}{k\beta'} \sin (2k\beta'a') \cos [2k(\gamma'-ct)] +2c \, a' \qquad\qquad \text{(V-10)}$$

where $\quad c_1 = (\mp) \dfrac{\rho C_d D_1}{4} \dfrac{\pi^2 H^2}{T^2} e^{-2k\bar{h}} \sin^2 \alpha.$

Similarly, for hull No. 2:

$$\bar{F}_{2_y} = \dfrac{c_1}{k\beta} \sin (2k\beta'a') \cos [2k(\gamma'+ct)] + 2c_1 a' \tag{V-11}$$

Combining $\bar{F}_{1_y}$ and $\bar{F}_{2_y}$ gives the total horizontal drag force on the hulls in the y-direction as:

$$\bar{F}_y = \dfrac{2c_1}{k\beta'} \sin (2k\beta'a') \cos (2k\gamma') \cos (2kct) + 4c_1 a' \tag{V-12}$$

For the cross bracings (hulls No. 3 and No. 4),

$u_n = u \cos \alpha, \ \bar{x} = \beta'' -\beta''S, \ \gamma'' = a \cos \alpha, \ \beta'' = \sin \alpha.$

Through similar integration for hulls No. 1 and No. 2, one obtains:

$$\bar{F}_x = \dfrac{2c_2}{k\beta''} \sin (2k\beta''b') \cos (2k\gamma'') \cos (2kct) + 4c_2 b' \tag{V-13}$$

where $\quad c_2 = \mp \dfrac{\rho \pi^2 H^2 C_d D_3}{4T^2} e^{-2k\bar{h}} \cos^2 \alpha$

The total horizontal forces on the structure are:

For surge (x-direction):

$$F_{x_T} = \sum_{i=5}^{12} (F_{I_i} + F_{D_i}) \cos \alpha + (F_x + \bar{F}_x) \tag{V-14}$$

For sway (y-direction):

$$F_{y_T} = \sum_{i=5}^{12} (F_{I_i} + F_{D_i}) \sin \alpha + (F_y + \bar{F}_y) \tag{V-15}$$

where the corner columns are numbered 5-8, and the middle columns are numbered 9-12. The instantaneous heights of the water on each column are:

for i = 5-8:

$$h_i = h_0 + \dfrac{H}{2} \cos [k(\bar{x}-ct)] + (\ell - \sqrt{\ell^2 - x^2}) \tag{V-16}$$

and for i = 9-12

$$h_i = h_0 + \frac{H}{2} \cos [k(\overline{X}-ct)] + (\ell - \sqrt{\ell^2 - x^2}) - D_h \qquad (V-17)$$

2. Heave Forces

a) Vertical Inertia Force on Hulls

The vertical fluid acceleration at point p of Figure 16 is

$$\dot{v} = \frac{-2\pi^2 H}{T^2} e^{-k\overline{h}} \cos [k(\overline{x}-ct)] \qquad (V-18)$$

For hull No. 1: $X = \beta'S+\gamma'$ for O_1O_2, and $X = -\beta'S+\gamma'$ for O_1O_3. The vertical inertia force on hull No. 1 due to fluid acceleration is

$$F_{v_1} = \int_{-a'}^{a'} \frac{\rho\pi D_1^2}{4} C_m \left\{\frac{-2\pi^2 H}{T^2} e^{-k\overline{h}} \cos [k(\overline{x}-ct)]\right\} dS$$

$$= \frac{-\rho\pi^3 D_1^2 C_m H}{2T^2} e^{-k\overline{h}} \int_{-a'}^{a'} \cos [k(\overline{x}-ct)] dS$$

$$= \frac{-a_{v_1}}{2} \left\{\int_0^{a'} \cos [-k\beta'S + k(\gamma'-ct)] dS + \int_0^{a'} \cos [k\beta'S + k(\gamma'-ct)] dS\right\}$$

$$= \frac{-a_{v_1}}{2k\beta'} \left\{\left[-\sin [-k\beta'S + k(\gamma'-ct)]\right]_0^{a'} + \left[\sin [k\beta'S + k(\gamma'-ct)]\right]_0^{a'}\right\}$$

$$= \frac{-a_{v_1}}{2k\beta'} \left\{\left[-\sin[-k\beta'a' + k(\gamma'-ct)] + \sin [k(\gamma'-ct)]\right]\right.$$

$$+ \left.\left[\sin [k\beta'a' + k(\gamma'-ct)] - \sin [k(\gamma'-ct)]\right]\right\}$$

$$= \frac{-a_{v_1}}{2k\beta'} \left\{\sin [k\beta'a' + k(\gamma'-ct)] - \sin [-k\beta'a' + k(\gamma'-ct)]\right\}$$

$$= \frac{-a_{v_1}}{k\beta'} \sin (k\beta'a') \cos [k(\gamma'-ct)] \qquad (V-19)$$

Similarly, for hull No. 2

$$F_{V_2} = \frac{-a_{V_1}}{k\beta'} \sin(k\beta'a') \cos[k(\gamma'+ct)] \qquad (V\text{-}20)$$

For hulls No. 3 and 4:

$$F_{V_3} = \frac{-a_{V_2}}{k\beta''} \sin(k\beta''b') \cos[k(\gamma''+ct)] \qquad (V\text{-}21)$$

$$F_{V_4} = \frac{-a_{V_2}}{k\beta''} \sin(k\beta''b') \cos[k(\gamma''-ct)] \qquad (V\text{-}22)$$

where
$$a_{V_1} = \frac{\rho\pi^3 D_1^2 C_m H}{T^2} e^{-k\overline{h}}$$

and
$$a_{V_2} = \frac{\rho\pi^3 D_3^2 C_m H}{T^2} e^{-k\overline{h}}$$

Adding Equations (V-19) and (V-20) yields:

$$F_{V_{1,2}} = \frac{-a_{V_1}}{k\beta'} \sin(k\beta'a') \left[\cos[k\gamma' - kct] + \cos[k\gamma' + kct] \right]$$

$$= \frac{-2a_{V_1}}{k\beta'} \sin(k\beta'a') \cos(k\gamma') \cos(kct) \qquad (V\text{-}23)$$

Adding Equations (V-21) and (V-22) gives:

$$F_{V_{3,4}} = \frac{-2a_{V_2}}{k\beta''} \sin(k\beta''b') \cos(k\gamma'') \cos(kct) \qquad (V\text{-}24)$$

The total vertical inertia forces on the hulls is obtained by adding Equations (V-23) and (V-24):

$$F_v = F_{v_{1,2}} + F_{v_{3,4}}$$

$$= \frac{-2 \cos (kct)}{k} \left[\frac{a_{v_1}}{\beta'} \sin (k\beta'a') \cos (k\gamma') + \frac{a_{v_2}}{\beta''} \sin (k\beta''b') \cos (k\gamma'') \right]$$

$$\dots \text{(V-25)}$$

b) Vertical Drag Force on Hulls

The vertical fluid velocity at point p of Figure 16 is

$$v = \frac{\pi H}{T} e^{-k\overline{h}} \sin [k(x-ct)] \tag{V-26}$$

The vertical drag force on hull No. 1 due to fluid velocity is

$$\overline{F}_{v_1} = (\pm) \int_{-a'}^{a'} \rho \frac{C_d D_1}{2} \left\{ \frac{\pi H}{T} e^{-k\overline{h}} \sin [k(\overline{x}-ct)] \right\}^2 dS$$

$$= (\pm) \frac{\rho C_d D_1 \pi^2 H^2}{4T^2} e^{-2k\overline{h}} \int_{-a'}^{a'} \{1 - \cos [2k(\overline{x}-ct)] \} dS$$

$$= (\pm) \frac{\rho C_d D_1 \pi^2 H^2}{2T^2} e^{-2k\overline{h}} \int_{-a'}^{a'} \sin^2 [k(\overline{x}-ct)] dS$$

$$= c_3 \left\{ \int_0^{a'} \{1 - \cos [2k\beta'S + 2k(\gamma'-ct)] \} dS \right.$$

$$+ \int_0^{a'} \{1 - \cos [-2k\beta'S + k(\gamma'-ct)] \} dS$$

$$= c_3 \left\{ \left[S - \frac{1}{2k\beta'} \sin [2k\beta'S + 2k(\gamma'-ct)] \right]_0^{a'} \right.$$

$$+ \left. \left[S + \frac{1}{2k\beta'} \sin [-2k\beta'S + 2k(\gamma'-ct)] \right]_0^{a'} \right\}$$

$$= 2 c_3 a' + \frac{c_3}{2k\beta'} \{ \sin [-2k\beta'a' + 2k(\gamma'-ct)] - \sin [2k\beta'S + 2k(\gamma'-ct)] \}$$

$$\Rightarrow \overline{F}_{v_1} = 2 c_3 a' - \frac{c_3}{k\beta'} \sin (2k\beta'a') \cos [2k(\gamma' - ct)] \tag{V-27}$$

Similarly, for hull No. 2:

$$\overline{F}_{v_2} = 2 c_3 a' - \frac{c_3}{k\beta'} \sin (2k\beta'a') \cos [2k(\gamma' + ct)] \qquad (V-28)$$

For hulls No. 3 and 4:

$$\overline{F}_{v_3} = 2 c_4 b' - \frac{c_4}{k\beta''} \sin (2k\beta''b') \cos [2k(\gamma'' + ct)] \qquad (V-29)$$

$$\overline{F}_{v_4} = 2 c_4 b' - \frac{c_4}{k\beta''} \sin (2k\beta''b') \cos [2k(\gamma'' - ct)] \qquad (V-30)$$

where
$$c_3 = (\overline{+}) \frac{c_1}{\sin^2\alpha}$$

and
$$c_4 = (\overline{+}) \frac{c_2}{\cos^2\alpha}$$

Adding Equations (V-27), (V-28), (V-29), and (V-30) results in the total vertical drag force on the hulls:

$$\overline{F}_v = \overline{F}_{v_1} + \overline{F}_{v_2} + \overline{F}_{v_3} + \overline{F}_{v_4}$$

$$= 4 (c_3 a' + c_4 b') - \frac{2}{k} \cos (2kct) [\frac{c_3}{\beta'} \sin (2k\beta'a') \cos (2k\gamma')$$

$$+ \frac{c_4}{\beta''} \sin (2k\beta''b') \cos (2k\gamma'')] \qquad \dots (V-31)$$

c) Dynamic Pressure on Corner Column Bases

The dynamic pressure in the fluid is given by:

$$p_i = \frac{\rho g H}{2} e^{-kh_i} \cos [k(\overline{X} - ct)] \tag{V-32}$$

The total dynamic pressure on all corner columns is

$$F_{cv} = \sum_{i=5}^{8} p_i \left(\frac{\pi D_i^2}{4}\right) = \frac{\pi \rho g H}{8} \sum_{i=5}^{8} d_i^2 e^{-kh_i} \cos [k(\overline{X} - ct)] \tag{V-33}$$

The total vertical force on the structure becomes:

$$F_{z_T} = F_v + \overline{F}_v + F_{cv} \tag{V-34}$$

3. Forces Producing Pitch and Roll

a) Moments Due to Inertia Force on Columns

In this analysis, it is assumed that pitch and roll take place about horizontal axes passing through the center of gravity of the structure.

The moment about G of the inertia force on column i is

$$M_{I_i} = -\frac{\rho \pi D_i^2}{4} \int_0^{h_i} (z - \overline{z}) [C_m \dot{u}_i - (C_m-1) [\ddot{x} - (z - \overline{z})\ddot{\alpha} + x_i \dot{\alpha}^2]]dz$$

$$= \overline{z} F_{I_i} - \frac{\rho \pi D_i^2}{4} \{2c_m \pi^2 H \sin [k(\overline{X} - ct)] \frac{1}{T^2} \int_0^{h_i} z e^{-kz} dz$$

$$- (C_m -1) \int_0^{h_i} z[(\ddot{x} + z\ddot{\alpha} + x_i \frac{\dot{\alpha}^2}{2}) - z\ddot{\alpha}] dz\}$$

$$= \overline{z} F_{I_i} - a_1 D_i^2 (\frac{1}{k} - e^{-kh_i} - h_i e^{-kh_i}) \sin [k(\overline{X} - ct)]$$

$$+ a_2 D_i [(\ddot{x} + z\ddot{\alpha} + x_i \dot{\alpha}^2)\frac{h_i^2}{2} - \frac{h_i^2}{2} - \frac{h_i^3 \ddot{\alpha}}{3}] \tag{V-35}$$

b. Moments Due to Drag Force on Columns

$$M_{D_i} = (\overline{+}) \ -\frac{\rho c_d D_i}{2} \int_0^{h_i} (z - \overline{z}) \ \{u_i - [\dot{x} - (z - \overline{z})\dot{\alpha} + \frac{X_i \ddot{\alpha}^2}{2}]\}^2 dz$$

$$= (\overline{+}) \ -\frac{\rho C_d D_i}{2} \left\{ \left[\int_0^{h_i} z\{\frac{\pi^2 H^2}{T^2} e^{-2kz} \cos^2 [k(\overline{X} - ct)]\} \ dz \right] \right.$$

$$+ [\int_0^{h_i} -2z \ [(\dot{x} + \overline{z}\dot{\alpha} + \frac{x_i \dot{\alpha}^2}{2}) - z\dot{\alpha}](\frac{\pi H}{T} e^{-kz} \cos [k(\overline{X} - ct)]) \ dz$$

$$+ [\int_0^{h_i} z[(\dot{x} + \overline{z}\dot{\alpha} + \frac{x_i \dot{\alpha}^2}{2}) - z\dot{\alpha}]^2 \ dz] \right\} + \overline{z} \ F_{D_i}$$

$$= (\overline{+}) \ -\rho C_d D_i \ [1] + [2] + [3] \ + \overline{z} \ F_{D_i}$$

Evaluate 1 , 2 , 3 separately as follows:

$$[1] = \int_0^{h_i} \frac{\pi^2 H^2}{T^2} \cos^2 [k(\overline{X} - ct)] z e^{-2kz} \ dz$$

$$= \frac{\pi^2 H^2}{2kT^2} \cos^2 [k(\overline{X} - ct)] \ (\frac{1}{2K} - \frac{e^{-2kh_i}}{2k} - h_i \ e^{-2kh_i})$$

$$[2] = \int_0^{h_i} -2z \left\{ [(\dot{x} + \overline{z}\dot{\alpha} + \frac{X_i \dot{\alpha}^2}{2}) - z\dot{\alpha}] \ (\frac{\pi H}{T} e^{-kz} \cos [k(\overline{X} - ct)]) \right\} \ dz$$

$$= \frac{-2\pi H}{T} \cos[k(\overline{X} - ct)] \left\{ (\dot{x} + z\dot{\alpha} + \frac{X_i \dot{\alpha}^2}{2}) \int_0^{h_i} z\, e^{-kz}\, dz - \dot{\alpha} \int_0^{h_i} z^2\, e^{-kz}\, dz \right\}$$

$$= \frac{-2\pi H}{T} \cos[k(\overline{X} - ct)] \left\{ b_{2_i} \frac{(1)}{k} \frac{1}{K}(\frac{1}{K} - \frac{e^{-kh_i}}{k} - h_i\, e^{-kh_i}) \right.$$

$$\left. + h_i^2\, e^{-kh_i} - \frac{2}{K} \frac{1}{k}(\frac{1}{k} - \frac{e^{-kh_i}}{k} h_i\, e^{-kh_i}) \right\}$$

$$= \frac{2\pi H}{kT} \cos[k(\overline{X} - ct)] \left\{ (\frac{2\dot{\alpha}}{k} - b_{2_i})(\frac{1}{k} - \frac{e^{-kh_i}}{k} h_i\, e^{-kh_i}) - \dot{\alpha} h_i^2\, e^{-kh_i} \right\}$$

$$[3] = \int_0^{h_i} [(\dot{x} + \overline{z}\dot{\alpha} + \frac{X_i \dot{\alpha}^2}{2})^2 z\, dz - \int_0^{h_i} 2(\dot{x} + \overline{z}\dot{\alpha} + \frac{X_i \dot{\alpha}^2}{2})\dot{\alpha} z^2\, dz + \int_0^{h_i} \dot{\alpha}^2 z^3\, dz$$

$$= (b_{2_i})^2 \frac{h_i^2}{2} - 2 b_{2_i} \dot{\alpha} \frac{h_i^3}{3} + \dot{\alpha} \frac{h_i^4}{4}$$

$$\Rightarrow M_{D_i} = (\overline{+}) - D_i \left\{ b_1 \cos^2[k(\overline{X} - ct)] (\frac{1}{2k} - \frac{e^{-2kh_i}}{2k} - h_i\, e^{-2kh_i}) \right.$$

$$+ b_3 \cos[k(\overline{X} - ct)] [(\frac{2\dot{\alpha}}{k} - b_{2_i})(\frac{1}{k} - \frac{e^{-kh_i}}{k} - h_i\, e^{-kh_i}) - \dot{\alpha} h_i\, e^{-kh_i}]$$

$$\left. + (b_{2_i})^2 \frac{h_i^2}{2} - 2 b_{2_i} \dot{\alpha} \frac{h_i^3}{3} + \dot{\alpha} \frac{h_i^4}{3} \right\} + \overline{z}\, F_{D_i} \qquad \text{(V-36)}$$

A positive rotational moment about the y-axis produces a positive y-component (pitch), and a negative x-component (roll), see Figure 16. Hence, from Equations (V-35) and (V-36),

$$M_y = \sum_{i=5}^{12} (M_{D_i} + M_{I_i}) \cos\alpha \qquad \text{(V-37)}$$

and

$$M_x = \sum_{i=5}^{12} (M_{D_i} + M_{I_i}) \sin\alpha \qquad \text{(V-38)}$$

c) and d) Moments Due to Horizontal Inertia and Drag on Hulls

As shown in Figure 18, only hulls No. 3 and 4 have pitching effects:

$$M_{3,4_{y_h}} = - (F_x + \overline{F}_x) (\overline{h} - \frac{D_3}{2}) \tag{V-39}$$

where F_x and $\overline{F}_x$ are given in Equations (V-9) and (V-13), respectively.

Roll Moments

As shown in Figure 17, only hulls No. 1 and 2 have rolling effects:

$$M_{1,2_{x_h}} = (F_y + \overline{F}_y) (\overline{h} - \frac{D_1}{2}) \tag{V-40}$$

where F_y and $\overline{F}_y$ are given in Equations (V-8) and (V-12), respectively.

e) and f) Moments Due to Vertical Inertia Forces on Hulls

Pitch Moments

The pitching moments caused by forces on hulls No. 3 and 4 have a constant moment arm, a: (See Figure 18)

$$M_{3,4_y} = [(F_{v_3} + \overline{F}_{v_3}) - (F_{v_4} + \overline{F}_{v_4})]a \tag{V-41}$$

where $F_{v_3}, \overline{F}_{v_3}, F_{v_4}, \overline{F}_{v_4}$ are as given in Equations (V-21), (V-29), (V-22), and (V-30), respectively.

The pitching moments arising from vertical forces on hulls No. 1 and 2 have a variable moment arm S. Therefore, for hull No. 1, the moment about the y-axis of the vertical _inertia_ force is

$$\Rightarrow M_{1_y} = \int_{-a'}^{a'} \frac{\rho \pi D_1^2}{4} \ c_m \ (\frac{-2\pi^2 H}{T} \ e^{-k\overline{h}} \cos [k(\overline{x} - ct)]) \ S \ d \ S$$

$$= (\frac{\rho\pi D_1^2}{4} c_m)(\frac{-2\pi^2 H}{T} e^{-k\overline{h}}) \{+\int_0^{a'} S \cos [-k\beta'S + k(\gamma' - ct)] \, dS$$

$$- \int_0^{a'} S \cos [k\beta'S + k(\gamma' - ct)] \, dS \}$$

$$= \frac{a_{v_1}}{2k\beta'} \{[S \sin [k\beta'S + k(\gamma' - ct)] + \frac{1}{k\beta'} \cos [k\beta'S + k(\gamma' - ct)]]_0^{a'}$$

$$- [-S \sin [-k\beta'S + k(\gamma' - ct)] + \frac{1}{k\beta'} \cos [-k\beta'S + k(\gamma' - ct)]]_0^{a'} \}$$

$$= \frac{a_{v_1}}{2k\beta'} \{[a' \sin [k\beta'a' + k(\gamma' - ct)] + \frac{1}{k\beta'} \cos [k\beta'a' + k(\gamma' - ct)]$$

$$- \frac{1}{k\beta'} \cos [k(\gamma' - ct)]] - [-a' \sin [-k\beta'a' + k(\gamma' - ct)] + \frac{1}{k\beta'} \cos [-k\beta'a'$$

$$+ k(\gamma' - ct)] - \frac{1}{k\beta'} \cos [k(\gamma' - ct)]] \}$$

$$= \frac{a_{v_1}}{k\beta'} \{ [a' \cos (k\beta'a') \sin [k(\gamma' - ct)] - \frac{1}{k\beta} [\sin (k\beta'a') \sin [k(\gamma' - ct)]]\}$$

$$\Rightarrow M_{1_y} = \frac{-a_{v_1}}{k\beta'} \sin [k(\gamma' - ct)] [\frac{\sin (k\beta'a')}{k\beta'} - a' \cos (k\beta'a')] \qquad (V-42)$$

Similarly, for hull No. 2:

$$M_{2_y} = \frac{a_{v_1}}{k\beta'} \sin [k(\gamma' + ct)] [\frac{\sin(k\beta'a')}{k\beta'} - a' \cos (k\beta'a')] \qquad (V-43)$$

Now, the moment about the y-axis of the vertical drag force for hull No. 1
is

$$\overline{M}_{1_y} = (\mp) \int_{-a'}^{a'} \frac{\rho C_d D_1}{2} [\frac{\pi H}{T} e^{-k\overline{h}} \sin [k(\overline{x} - ct)]]^2 \, S \, dS$$

$$= (\overline{\mp}) \frac{\pi C_d D_i}{2} \frac{\pi^2 H^2}{T^2} e^{-2k\overline{h}} \int_{-a'}^{a'} S \sin^2 [k(x - ct)] \, dS$$

$$= c_3 \left\{ \int_0^{a'} - S (1 - \cos [2k\beta'S + 2k(\gamma' - ct)]) \, dS \right.$$

$$+ \int_0^{a'} S (1 - \cos [-2k\beta'S + 2k(\gamma' - ct)]) \, dS$$

$$= c_3 \left\{ \left[\frac{S}{2k\beta'} \sin [2k\beta'S + 2k(\gamma' - ct)] + \frac{1}{(2k\beta')} \cos [2k\beta'S' + 2k(\gamma' - ct)] \right]_0^{a'} \right.$$

$$- \left[\frac{-S}{2k\beta'} \sin [-2k\beta'S + 2k(\gamma' - ct)] + \frac{1}{(2k\beta')} \cos [-2k\beta'S + 2k(\gamma' - ct)] \right]_0^{a'} \right\}$$

$$= \frac{c_3}{2k\beta'} \left\{ [a' \sin [2k\beta'a' + 2k(\gamma' - ct)] + \frac{1}{2k\beta'} \cos [2k\beta'a' + 2k(\gamma' - ct)] \right.$$

$$- \frac{1}{2k\beta'} \cos [2k(\gamma' - ct)]] - [-a' \sin [-2k\beta'a' + 2k(\gamma' - ct)]$$

$$+ \frac{1}{2k\beta'} \cos [-2k\beta'a' + 2k(\gamma' - ct)] - \frac{1}{2k\beta'} \cos [2k(\gamma' - ct)]] \right\}$$

$$= \frac{c_3}{2k\beta'} \left\{ 2a' \cos (2k\beta'a') \sin [2k(\gamma' - ct)] - \frac{1}{k\beta'} \sin (2k\beta'a') \sin [2k(\gamma' - ct)] \right\}$$

$$\Rightarrow \overline{M}_{1_y} = \frac{c_3}{k\beta'} \sin [2k(\gamma' - ct)] [a' \cos (2k\beta'a') - \frac{1}{2k\beta'} \sin (2k\beta'a')] \qquad (V-44)$$

Similarly, for hull No. 2:

$$\overline{M}_{2_y} = \frac{-c_3}{k\beta'} \sin [2k(\gamma' + ct)] [a' \cos (2k\beta'a') - \frac{1}{2k\beta'} \sin (2k\beta'a')] \qquad (V-45)$$

The total pitching moment due to vertical drag and inertia forces on all hulls is

$$M_{v_y} = \dot{M}_{3,4_y} + M_{1_y} + M_{2_y} + \overline{M}_{1_y} + \overline{M}_{2_y} \qquad (V-46)$$

where $M_{3,4_y}$, M_{1_y} , M_{2_y} , $\overline{M}_{1_y}$, $\overline{M}_{2_y}$ are as given in Equations (V-41), V-42), (V-43), (V-44), and (V-45), respectively.

Roll Moments

As seen in Figure 13, the rolling moments due to hulls No. 1 and 2 have a constant moment arm, b.

$$\Rightarrow M_{1,2_x} = [(F_{v_1} - F_{v_2}) + (\overline{F}_{v_1} - \overline{F}_{v_2})] \ b \qquad (V-47)$$

where F_{v_1} , F_{v_2} , $\overline{F}_{v_1}$, $\overline{F}_{v_2}$ are as given in Equations (V-19), (V-20), (V-27), (V-28), respectively.

The rolling moments due to vertical forces on hulls No. 3 and 4 are derived by integration, in a similar way to the pitching moment.

$$\Rightarrow M_{3_x} = \frac{-a_{v_2}}{k\beta''} \sin [k(\gamma'' + ct)] \ [\frac{\sin(k\beta''b')}{k\beta'} - b' \cos (k\beta''b')] \qquad (V-48)$$

$$M_{4_x} = \frac{a_{v_2}}{k\beta''} \sin [k(\gamma'' - ct)] \ [\frac{\sin(k\beta''b')}{k\beta''} - b' \cos (k\beta''b')] \qquad (V-49)$$

Similarly, for drag:

$$\overline{M}_{3_x} = \frac{c_3}{k\beta''} \sin [2k(\gamma'' + ct)] \ [b' \cos (2k\beta''b') - \frac{1}{2k\beta''} \sin (2k\beta''b')] \qquad (V-50)$$

$$\overline{M}_{4_x} = \frac{-c_3}{k\beta''} \sin [2k(\gamma'' - ct)] \ [b' \cos (2k\beta''b') \frac{-1}{2k\beta''} \sin (2k\beta''b')] \qquad (V-51)$$

Finally, the total rolling moment due to vertical drag and inertia forces on all hulls is

$$M_{v_x} = M_{1,2_x} + M_{3_x} + M_{4_x} + \overline{M}_{3_x} + \overline{M}_{4_x} \qquad (V-52)$$

where $M_{1,2_x}$, M_{3_x}, M_{4_x}, $\overline{M}_{3_x}$, and $\overline{M}_{4_x}$ are as given in Equations (V-47), (V-48), (V-49), (V-50), and (V-51), respectively.

g) Moments Due to Dynamic Pressure

Pitching Moment

The moment about the y-axis due to the dynamic pressure on the base of the corner columns (5,6,7,8) is:

$$M_{p_y} = -\rho \pi g H \frac{}{8} a \sum_{i=5}^{8} (-1)^i D_i^2 e^{-kh_i} \cos [k(x - ct)] \qquad (V-53)$$

Rolling Moment

Similarly, the rolling moment (about x-axis) is:

$$M_{p_x} = \rho g \pi H \frac{}{8} b \left\{ \left[\sum_{i=5}^{6} D_i^2 e^{-kh_i} \cos [k(x - ct)] \right] \right.$$

$$\left. - \sum_{i=7}^{8} D_i^2 e^{-kh_i} \cos [k(x - ct)] \right\} \qquad (V-54)$$

4. Yaw Moments

The forces causing rotation about the vertical axis are those from horizontal drag and inertia acting on the columns. The moment produced by these forces is:

$$M_z = \sum_{i=5}^{12} (F_{I_i} + F_{D_i}) Y_i \qquad (V-55)$$

where: $Y_5 = a \sin \alpha + b \cos \alpha$

$Y_6 = b \cos \alpha - a \sin \alpha$

$Y_7 = -Y_6$

$Y_8 = -Y_5$

$Y_9 = b \cos \alpha$

$Y_{10} = -Y_9$

$Y_{11} = a \sin \alpha$

$Y_{12} = -Y_{11}$

5. Limits for $\alpha = 0^0$ and $\alpha = 90^0$

The derived hull forces and moments contain the terms β and β' in the numerators and denominators, and γ and γ' in their numerators. These terms are related to the wave direction (α) as follows:

$\beta' = \cos \alpha$

$\beta'' = \sin \alpha$

$\gamma' = b \sin \alpha$

$\gamma'' = a \cos \alpha$

As the wave direction (α) approaches 0^0 or $\frac{\pi}{2}$, a limiting case exists where L'Hospital's rule must be applied to find the forces and moments associated with these extreme values of α.

a) Limits of Hull Forces for $\alpha = 0^0$

As $\alpha \rightarrow 0$, Equation (V-56) becomes

$\beta' = 1$

$\beta'' = 0$

$\gamma' = 0$

$\gamma'' = a$
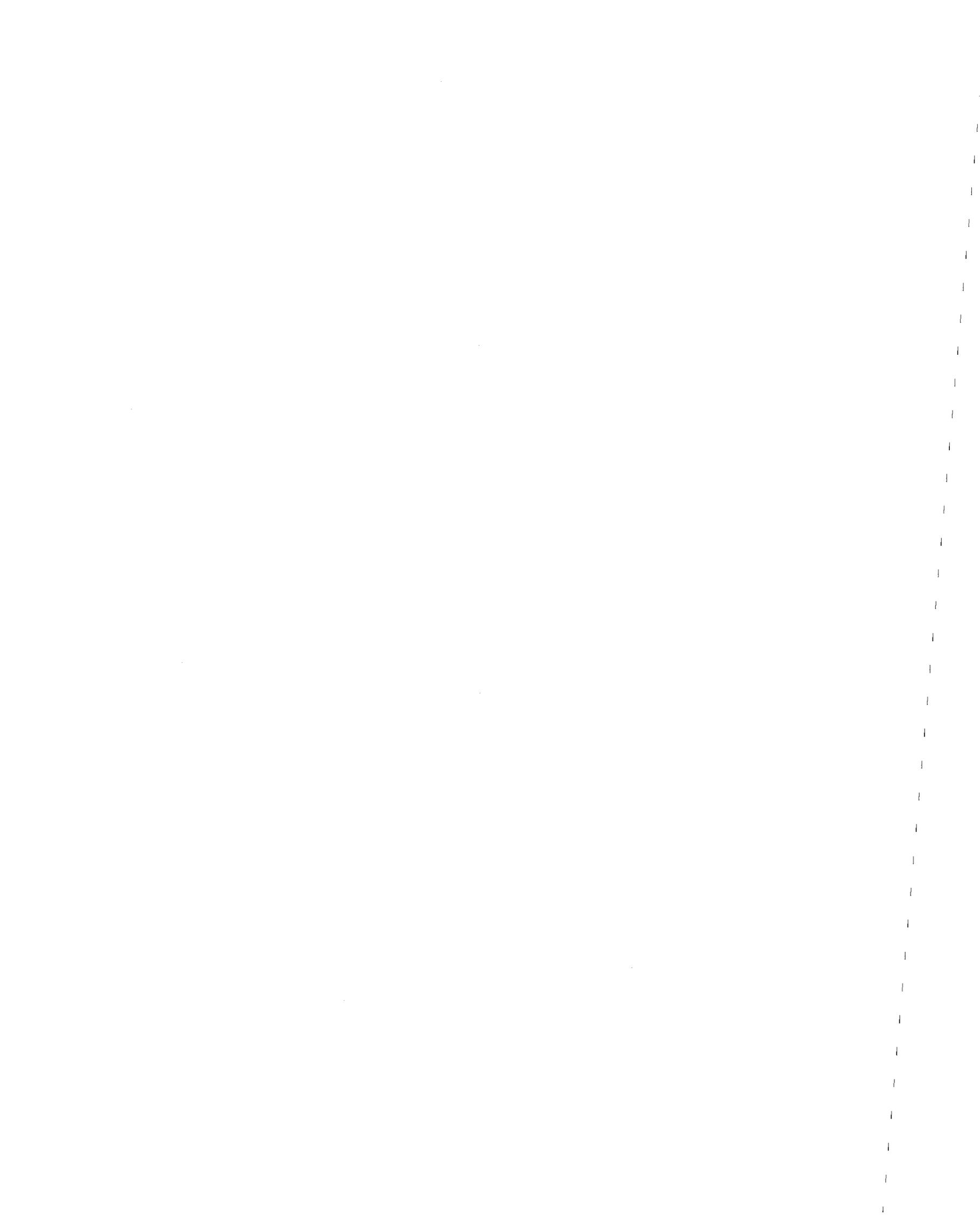
Recalling Equations (V-8), (V-9), (V-12), (V-13), (V-25), and (V-31) and rewriting them gives:

$$F_y = \frac{-4a_y}{k\beta'} \sin(k\beta'a') \cos(k\gamma') \sin(kct)$$

$$F_x = \frac{-4a_x}{k\beta''} \sin(k\beta''b') \cos(k\gamma'') \sin(kct)$$

$$\overline{F}_y = \frac{2c_1}{k\beta'} \sin(2k\beta'a') \cos(2k\gamma') \cos(2kct) + 4c_1a'$$

$$\overline{F}_x = \frac{2c_2}{k\beta''} \sin(2k\beta''b') \cos(2k\gamma'') \cos(2kct) + 4c_2b'$$

$$F_v = \frac{-2\cos(kct)}{k} \left[\frac{a_{v_1}}{\beta'} \sin(k\beta'a') \cos(k\gamma') + \frac{a_{v_2}}{\beta''} \sin(k\beta''b') \cos(k\gamma'') \right]$$

$$\overline{F}_v = 4(c_3a' + c_4b') - \frac{2}{k}\cos(2kct) \left[\frac{c_3}{\beta'} \sin(2k\beta'a') \cos(2k\gamma') \right.$$

$$\left. + \frac{c_4}{\beta''} \sin(2k\beta''b') \cos(2k\gamma'') \right]$$

For $\alpha = 0$:

$\Rightarrow \qquad a_y = 0$

and $\qquad c_1 = 0$

For $\gamma' = 0$, $\cos(k_\gamma) = 1$

For $\beta = 0$, $\quad \dfrac{\sin(k_\beta''b')}{k_\beta''} = b' \qquad$ (by L'Hospital's rule)

Thus, the above equations become:

$$F_y = 0$$

$$\overline{F}_y = 0$$

$$F_x = -4a_x b' \cos(ka) \sin(kct)$$

$$\overline{F}_x = 4c_2 b' [\cos(2ka) \cos(2kct) + 1]$$

$$F_v = -2 \cos(kct) \left[\frac{a_{v_1}}{k} \sin(ka') + a_{v_2} b' \cos(ka) \right]$$

$$\overline{F}_v = 4(c_3 a' + c_4 b') - 2 \cos(2kct) \frac{[c_3 \sin(2ka') + 2c_4 b' \cos(2ka)]}{k}$$

Recalling Equations (V-41), (V-42), (V-43), (V-44), and (V-45), and performing similar operations with the above equations yields:

$$M_{3,4_y} = 2ab' [a_{v_2} \sin(ka)\sin(kct) + 2c_4 \sin(2ka)\sin(2kct)]$$

$$M_{1_y} = \frac{a_{v_1}}{k} \sin(kct) \left[\frac{\sin(ka')}{k} - a' \cos(ka') \right]$$

$$M_{2_y} = \frac{a_{v_1}}{k} \sin(kct) [\sin(ka') - a' \cos(ka')]$$
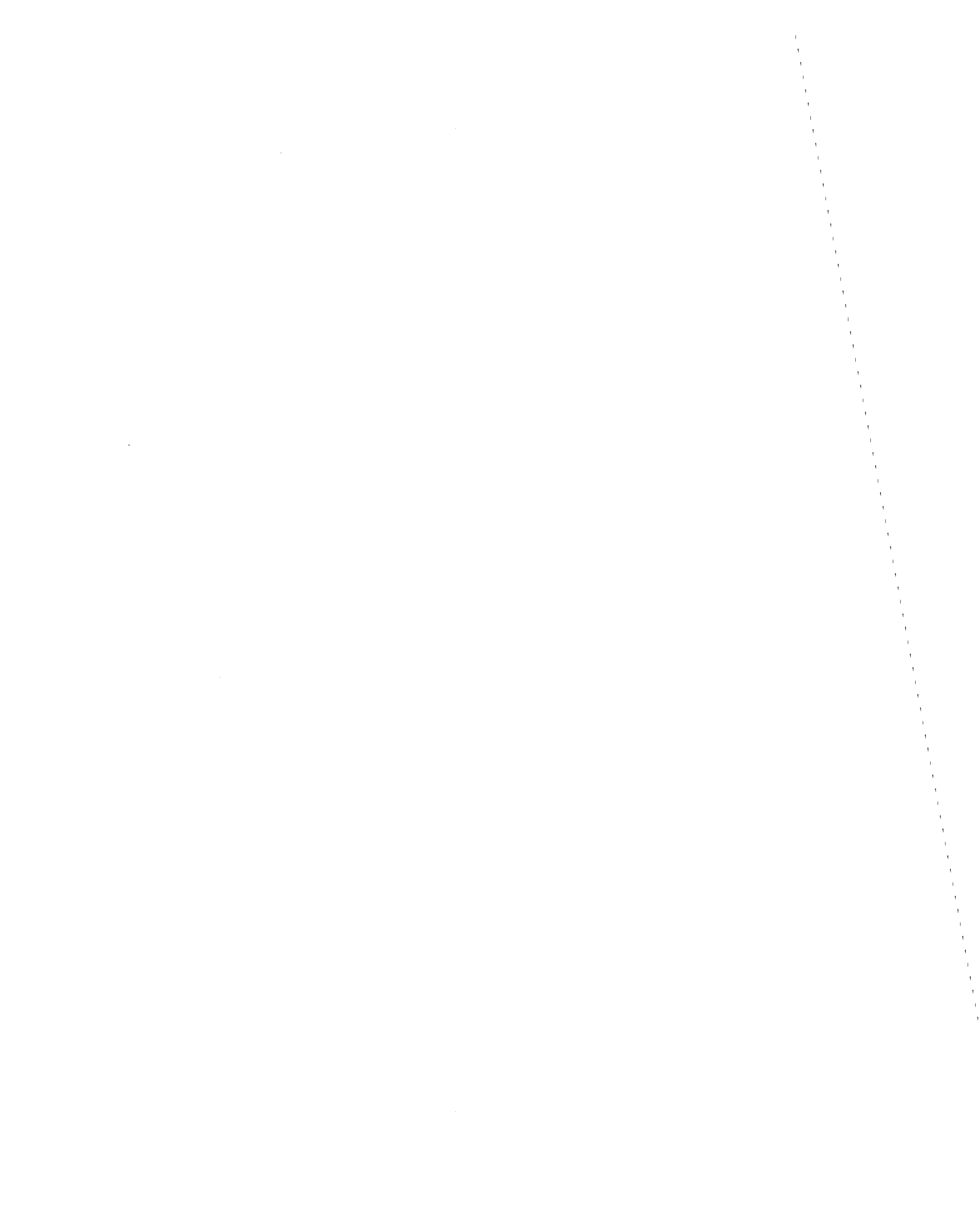
$$\overline{M}_{1_y} = \frac{-c_3}{k} \sin(2kct) \left[a' \cos(2ka') - \frac{1}{2K} \sin(2ka') \right]$$

$$\overline{M}_{2_y} = \overline{M}_{1_y}$$

b) Limits of Hull Forces for $\alpha = 90^0$

As $\alpha \to 90^0$, Equation (V-56) becomes

$$\beta' = 0$$

$$\beta'' = 1$$

$$\gamma' = 6$$

$$\gamma'' = 0$$

Similar manipulations to those for $\alpha = 0$, convert Equations (V-8), (V-9), (V-12), (V-13), (V-25), and (V-31) to:

$$F_y = -4a_y \, a' \cos(kb) \sin(kct)$$

$$\overline{F}_y = 4c_1 \, a' \left[\cos(2kb) \cos(2kct) + 1 \right]$$

$$F_x = 0$$

$$\overline{F}_x = 0$$

$$F_v = -2 \cos(kct) \left[a' \, a_{v_1} \cos(kb) + \frac{a_{v_2}}{k} \sin(kb') \right]$$

$$\overline{F}_v = 4(c_3 a' + c_4 b') - 2 \cos(2kct) \left[\frac{c_4}{k} \sin(2kb') + 2c_3 a' \cos(2kb) \right]$$
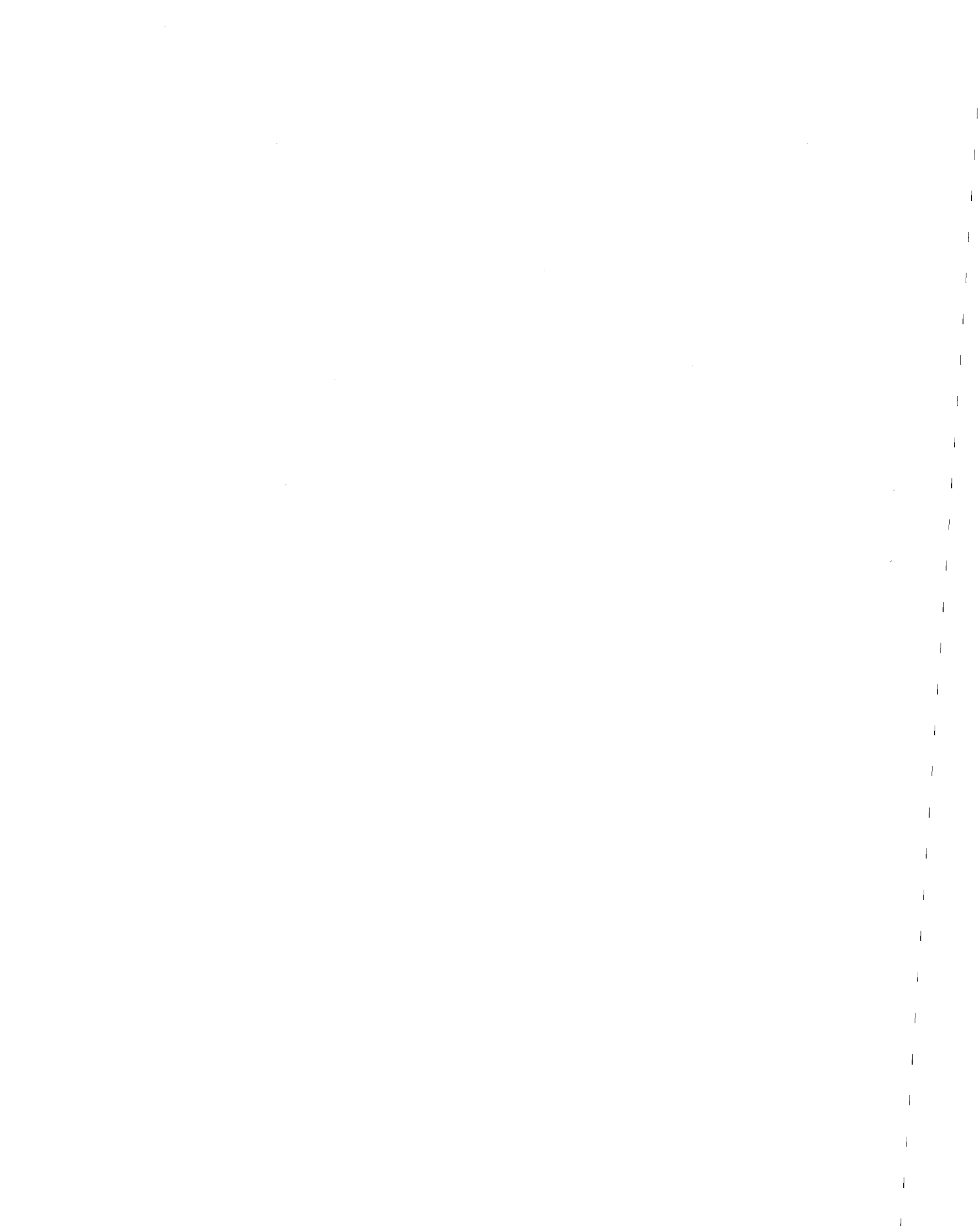
Similarly, the roll moments become:

$$M_{1,2_x} = -2 \, a'b \, [a_{v_1} \sin(kb) \sin(kct) + 2c_3 \sin(2kb) \sin(2kct)]$$

$$M_{3_x} = - \frac{a_{v_2}}{k} \sin(kct) \left[\frac{\sin(kb')}{k} - b' \cos(kb')\right]$$

$$M_{4_x} = M_{3_x}$$

$$\overline{M}_{3_x} = \frac{c_4}{k} \sin(2kct) \left[b' \cos(2kb') - \frac{1}{2k} \sin(2kb')\right]$$

$$\overline{M}_{4_x} = \overline{M}_{3_x}$$

APPENDIX II: DERIVATION OF EARTHQUAKE FORCES

1. Fluid Inertia and Drag Forces Due to Interaction

a) Inertia Forces on Columns

Assuming calm water (no waves), the inertia force from structural motion can be calculated with Morison's equation as:

$$F_{I_i} = \frac{\rho \pi D_i^2}{4} \int_0^{h_i} \{0 - (C_m - 1)[\ddot{x} - (z - \bar{z})\ddot{\alpha}]\}\, dz$$

$$= -\frac{\rho \pi D_i^2}{4}(C_m - 1)[\ddot{x}h_i + \bar{z}\ddot{\alpha}h_i - \ddot{\alpha}\frac{h_i^2}{2}] \tag{V-59}$$

and the moment caused by this force is:

$$M_{I_i} = -\frac{\rho \pi D_i^2}{4} \int_0^{h_i} (z - \bar{z})\{0 - (C_m - 1)[\ddot{x} - (z - \bar{z})\ddot{\alpha}]\}\, dz$$

$$= \frac{\rho \pi D_i^2}{4}(C_m - 1)[\frac{\ddot{x}h_i^2}{2} + \frac{\bar{z}h_i^2\ddot{\alpha}}{2} - \frac{\ddot{\alpha}h_i^3}{3}] + \bar{z}F_{I_i} \tag{V-60}$$

The total fluid inertia force on columns is:

$$F_I = \sum_{i=5}^{12} (F_{I_i}) \tag{V-61}$$
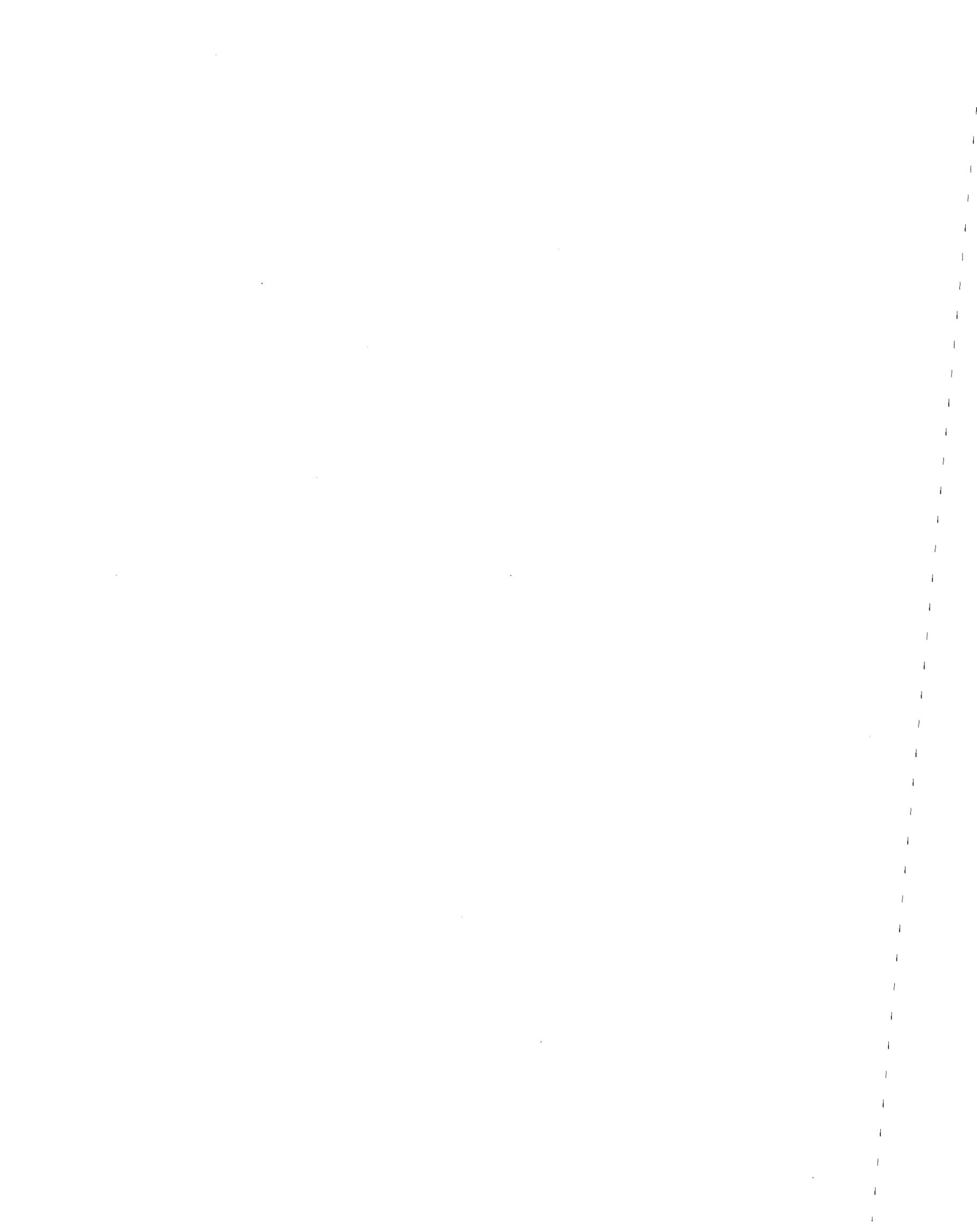
and the total fluid inertia moment on columns is:

$$M_I = \sum_{i=5}^{12} (M_{I_i})$$

(V-62)

b) Drag Forces on Columns

An application of Morison's equation for drag forces on the columns yields:

$$F_{D_i} = (\text{sgn})\rho \, \frac{C_d D_i}{2} \int_0^{h_i} \{0 - [\dot{x} - (z - \bar{z})\dot{\alpha}\,]\}^2 \, dz$$

$$= (\text{sgn})\rho \, \frac{C_d D_i}{2} \int_0^{h_i} [(\dot{x} + \bar{z}\,\dot{\alpha})^2 - 2(\dot{x} + \bar{z})\dot{\alpha}\,z + z^2\dot{\alpha}^2] \, dz$$

$$= (\text{sgn}) \, \frac{\rho C_d D_i}{2} [(\dot{x} + \bar{z}\,\dot{\alpha})^2 h_i - (\dot{x} + \bar{z}\,\dot{\alpha})\dot{\alpha}h_i^2 + \frac{\dot{\alpha}^2 h_i^3}{3}]$$

(V-63)

The moment caused by the drag force is:

$$M_{D_i} = (\text{sgn}) \, \frac{(-\rho c_d D_i)}{2} \int_0^{h_i} (z - \bar{z}) [(\dot{x} + \bar{z}\dot{\alpha}) - z\dot{\alpha}\,]^2 \, dz$$

$$= (\text{sgn}) \, \frac{(-\rho c_d D_i)}{2} \int_0^{h_i} [z(\dot{x} + \bar{z}\,\dot{\alpha})^2 - 2z^2(\dot{x} + \bar{z}\dot{\alpha}) + z^3\dot{\alpha}^2] \, dz + \bar{z}\, F_{D_i}$$

$$= (\text{sgn}) \, \frac{(-\rho c_d D_i)}{2} [(\dot{x} + \bar{z}\,\dot{\alpha})\frac{h_i^2}{2} - \frac{2}{3}(\dot{x} + \bar{z}\dot{\alpha}\,)h_i^3 + \frac{1}{4}\,\dot{\alpha}^2 h_i^4] + \bar{z}\, F_{D_i}$$

(V-64)

where $\qquad$ $(sgn) = +1$ if $(\dot{x} + \overline{z}\dot{\alpha}) < 0$ and $(\dot{x} + \overline{z}\dot{\alpha} - h_i\dot{\alpha}) < 0$ $\qquad$ (case 1)

and $\qquad$ $= -1$ if $(\dot{x} + \overline{z}) > 0$ and $(\dot{x} + \overline{z}\dot{\alpha} - h_i\dot{\alpha}) > 0$ $\qquad$ (case 2)

If neither case 1 nor case 2 applies,

$$a_i = h_i \frac{\left|\dfrac{\dot{x} + \overline{z}\dot{\alpha} - h_i\dot{\alpha}}{x + \overline{z}\dot{\alpha}}\right|}{1 + \left|\dfrac{x + \overline{z}\dot{\alpha} - h_i\dot{\alpha}}{x + \overline{z}\dot{\alpha}}\right|}$$

and

$$F_{D_i} = \mp \frac{\rho c_d D}{2} \left\{ \int_0^{h_i - a_i} [(\dot{x} + \overline{z}\,\dot{\alpha}) - z\,\dot{\alpha}]^2\, dz - \int_{h_i - a_i}^{h_i} [(\dot{x} + \overline{z}\dot{\alpha}) - z\,\dot{\alpha}]^2\, dz \right\}$$

$$= \mp \frac{\rho c_d D}{2} \left\{ 2[(\dot{x} + \overline{z}\,\dot{\alpha})^2 (h_i - a_i) - (\dot{x} + \overline{z}\dot{\alpha})(h_i - a_i)^2\,\dot{\alpha} + \frac{\dot{\alpha}^2}{3}(h_i - a_i)^3] \right.$$

$$\left. - [(\dot{x} + \overline{z}\,\dot{\alpha})h_i - (\dot{x} + \overline{z}\,\dot{\alpha})h_i^2\,\dot{\alpha} + \frac{\dot{\alpha}^2}{3} h_i^3] \right\}$$

If case 1 or case 2 does not apply, M_{D_i} becomes:

$$M_{D_i} = \mp \left(\frac{-\rho C_d D}{2}\right) \quad 2\left[(\dot{x} + \overline{z}\,\dot{\alpha})^2 \frac{(h_i - a_i)^2}{2} - \frac{2}{3}(\dot{x} + \overline{z}\,\dot{\alpha})\dot{\alpha}(h_i - a_i)^3\right.$$

$$\left. + \frac{1}{4}(h_i - a_i)^4 \dot{\alpha}^2\right] - \left[(\dot{x} + \overline{z\dot{\alpha}})\frac{h_i^2}{2} - \frac{2}{3}(\dot{x} + \overline{z}\,\dot{\alpha})\dot{\alpha}\, h_i^3 + \frac{1}{4}h_i^4 \dot{\alpha}^2\right]$$

$$+ \overline{z}\, F_{D_i} \qquad\qquad\qquad\qquad ....(V\text{-}66)$$

where

$$(\mp) = +1 \text{ if } (x + \overline{z}\,\dot{\alpha}) < 0$$

and

$$= -1 \text{ if } (\dot{x} + \overline{z}\,\dot{\alpha}) > 0$$

c) Inertia Forces on Hulls

<u>For Hulls No. 1 and 2:</u>

$$F_{y_1} = \frac{-\rho \pi D_1^2}{4}(C_m - 1)[2a'\ddot{y}] = -\frac{\rho \pi D_1^2}{2}(C_m - 1)\, a'\,\ddot{x}\,\sin \alpha \qquad (V\text{-}67)$$

$$F_{y_2} = F_{y_1}$$

<u>For Hulls No. 3 and 4:</u>

$$F_{x_3} = -\frac{\rho \pi D_3^2}{2}(C_m - 1)\, a'\,\ddot{x}\,\cos \alpha \qquad\qquad (V\text{-}68)$$

$$F_{x_4} = F_{x_3}$$

<u>Moments Due to Inertia Forces on Hulls</u>

$$M_{1,2_x} = (F_{y_1} + F_{y_2})\left(\overline{h} - \frac{D_1}{2}\right) \qquad\qquad (V\text{-}69)$$

$$M_{3,4_y} = (F_{x_3} + F_{x_4})\left(\overline{h} - \frac{D_3}{2}\right) \qquad\qquad (V\text{-}70)$$
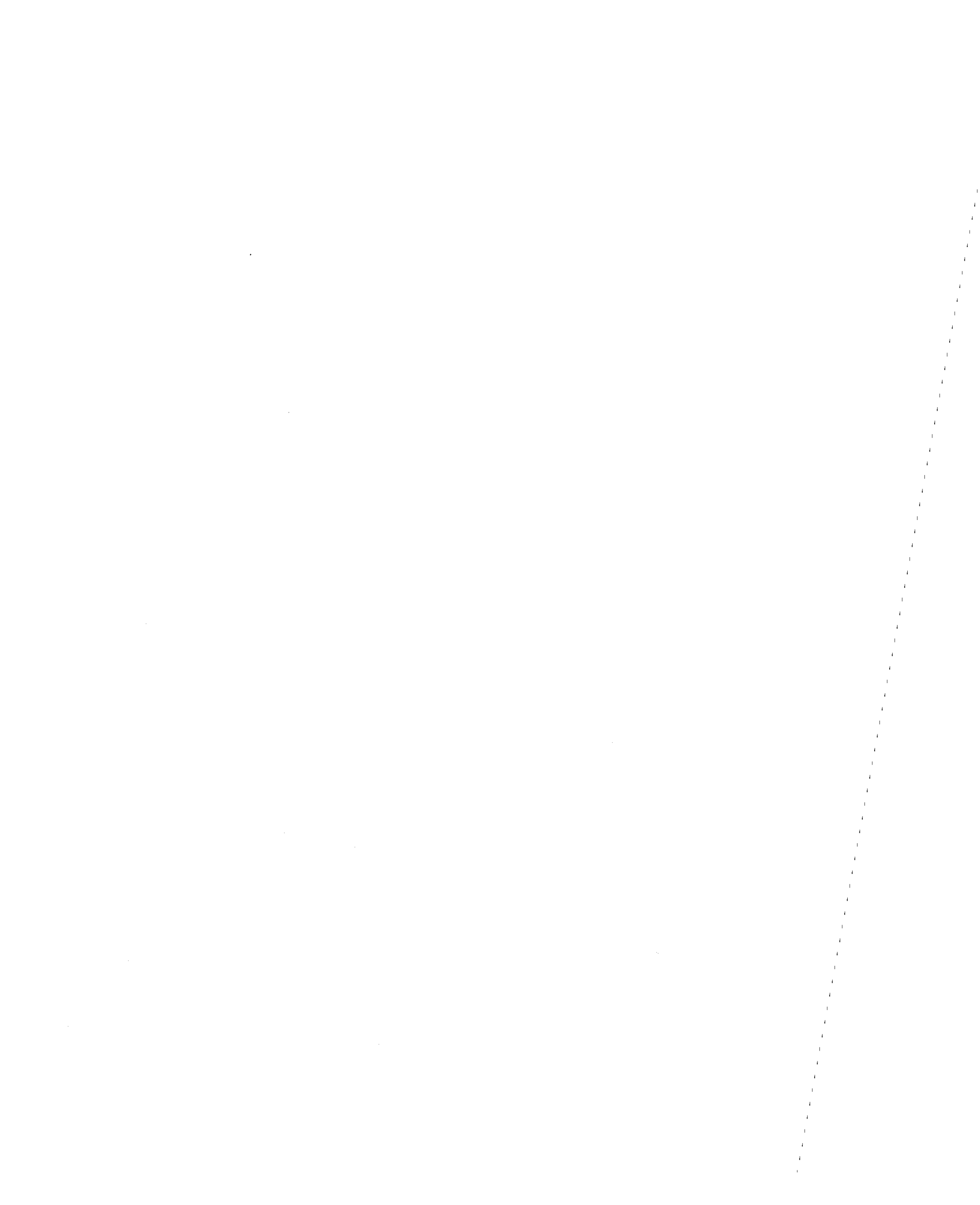
d) Drag Forces on Hulls

For Hulls No. 1 and 2:

$$\overline{F}_{y_1} = (\text{sgn}) \frac{\rho C_d D_1}{2} [\dot{x} \sin \alpha]^2 (2a') = (\text{sgn}) \rho C_d D_1 a' \dot{x}^2 \sin^2 \alpha \qquad (V\text{-}71)$$

$$\overline{F}_{y_2} = \overline{F}_{y_1}$$

For Hulls No. 3 and 4:

$$\overline{F}_{x_3} = (\text{sgn}) \rho C_d D_3 b' \dot{x}^2 \cos^2 \alpha \qquad (V\text{-}72)$$

$$\overline{F}_{x_4} = \overline{F}_{x_3}$$

Moments Due to Drag Forces on Hulls:

$$M_{1,2_x} = (\overline{F}_{y_1} + \overline{F}_{y_2}) (\overline{h} - \frac{D_1}{2}) \qquad (V\text{-}73)$$

$$M_{3,4_y} = (\overline{F}_{x_3} + \overline{F}_{x_4}) (\overline{h} - \frac{D_3}{2}) \qquad (V\text{-}74)$$

$$(\text{sgn}) = +1 \text{ if } \dot{x}_{h_o} < 0 \qquad = -1 \text{ if } \dot{x}_{h_o} > 0$$

e) Yaw Moments

$$M_z = \sum_{i=5}^{12} (F_{I_i} + F_{D_i}) Y_i \qquad (V\text{-}75)$$